UNIVERSITY OF CAPE COAST

MODELLING THE VARIABILITY OF FUVEME BEACH IN THE

LOWER VOLTA DELTA, GHANA

NANABANYIN KWAME OKWENTSIE EKUMAH

2022

© Nanabanyin Kwame Okwentsie Ekumah

University of Cape Coast

UNIVERSITY OF CAPE COAST

MODELLING THE VARIABILITY OF FUVEME BEACH IN THE

LOWER VOLTA DELTA, GHANA

BY

NANABANYIN KWAME OKWENTSIE EKUMAH

Thesis submitted to the Department of Fisheries and Aquatic Sciences of the

School of Biological Sciences, College of Agriculture and Natural Sciences,

University of Cape Coast, in partial fulfilment of the requirements for the

award of Master of Philosophy degree in Oceanography and Limnology

DECEMBER 2022

DECLARATION

Candidate's Declaration

I hereby declare that this thesis is the result of my own original research and that no part of it has been presented for another degree in this university or elsewhere.

Candidate's Signature...……………………… Date …………..……………

Name: …………………………………………………………………………

Supervisors' Declaration

We hereby declare that the preparation and presentation of the thesis were supervised in accordance with the guidelines on supervision of thesis laid down by the University of Cape Coast.

Principal Supervisor's Signature…………………………. Date….…………

Name: ………………………………………………………………………

Co-Supervisor's Signature …………………….…. Date ……………….…

Name: …………………………………………………………………………

ii

ABSTRACT

Issues of coastal erosion have been on the rise globally due to climate change and anthropogenic activities such as the construction of dams, harbours and coastal defences. According to multiple reports, the Fuveme coastline in eastern Ghana, West Africa, has been experiencing regular flooding and erosion since the mid-1880s. The intense erosion and flooding at Fuveme have been attributed to reduced fluvial sediment transport to the area. Recently, the sea breached a nearshore sandbar on the coast creating a 'new estuary' where tidal waves now move water and sediment between the sea and the estuary. This seems to be exacerbating erosion and flooding. The aim of this research was to assess the geomorphic variabilities surrounding the 'new estuary'. Hydrodynamic conditions (wave heights, tides and currents) off the coast of Fuveme were retrieved from ERA 5 website and aerial photographs of the beach were collected from October 2021 to October 2022. Sediment dynamics were assessed using MIKE 21 software to predict the trend of sediment movement along the coast of Fuveme. The results showed significant sediment exchange with -18.02 ± 0.25 m/yr shoreline erosion, 126, 979 m^3 and -35,359 m^3 sediment volume changes over the period as a consequence of the overtopping/flooding and the hydrodynamic conditions that are resident on the Fuveme Beach. The magnitude and direction of sediment total load were simulated with results showing higher sediment rates on the eastern stretch of the area. At the end of the study, wave action was found to be the principal hydrodynamic condition that affected the coast of Fuveme. Further studies are recommended to ensure a deeper understanding of the area's beach dynamics and for better coastal management purposes in the Volta Delta as a whole.

KEYWORDS

Accretion

Coastal Zone

Erosion

MIKE 21 model

Modelling

Sediment Transport

ACKNOWLEDGEMENTS

DEDICATION

To the loving memory of my father, Daniel Kodjo Effesah Ekumah.

TABLE OF CONTENTS

LIST OF TABLES

LIST OF FIGURES

LIST OF ACRONYMS

AMP	Agisoft Metashape PhotoScan
CMEMS	Copernicus Marine and Environmental Monitoring Services
DGPS	Differential Global Positioning System
DoD	Digital Elevation Model of Difference
EPR	End Point Rate
FM	Flexible Mesh
GCD	Geomorphic Change Detection
GCP	Ground Control Point
HD	Hydrodynamic
HWL	High Water Line
MWD	Mean Wave Direction
NSM	Net Shoreline Movement
PWP	Peak Wave Period
RSLR	Relative Sea Level Rise
ST	Sediment Transport
STD	Standard Deviation
SW	Spectral Wave
SWH	Significant Wave Height
UAV	Unmanned Aerial Vehicle

xiv

CHAPTER ONE

INTRODUCTION

1.1 Background to the Study

Coastal areas are home to around 40 % of the world's population (Badru et al., 2022). They are vital areas that form the region between the land and sea (Mentaschi et al., 2018). Areas including intertidal mudflats, beaches, bays, estuaries, lagoons, deltas and others are found within coastal areas. Coastal deltas are one of the most inhabited coastal areas in the world (United Nations Ocean Conference, 2017). All over the world, about half a billion people are estimated to reside within these areas (Living Deltas, 2022) with significant concentrations in Africa and Asia (Appeaning Addo, 2015). Deltaic areas are generally described by Bhattacharya (2003) as the 'discrete bulge of shoreline formed at the point where a river enters an ocean, sea, lake, lagoon or other standing body of water'. These areas serve with significant ecological and economic importance due to their productivity, abundant biodiversity and waterway transportation (Jayson-Quashigah, 2019).

There are many recognized deltas including; Ganges-Brahmaputra-Meghna, Mekong Delta, Mississippi Delta, Nile Delta and the Volta Delta across the globe. The Ganges–Brahmaputra-Meghna (GBM) Delta has more than 1200 people per km² and is the most populated delta in the world (FAO, 2011). It is also estimated that numerous Vietnamese and Cambodians reside within the Mekong Delta (Buschmann et al., 2008). The Volta Delta in Ghana also hosts about 3.5 % of the nation's population (Codjoe et al., 2020).

Deltas are highly vulnerable coastal environments due to their physical and socio-economic characteristics and are often threatened by the dynamics

1

in the shoreline position. Coastal erosion and flooding have occurred due to changes in coastal positions in most cases, rendering low elevation deltas more sensitive to changing climatic conditions (Appeaning Addo, 2015a). The Volta Delta is no exception, as it has seen tremendous changes since the 1960s. There have been numerous studies done in the region covering coastal degradation, steps in curbing coastal degradation and various coastal management plan effective for the area including; Boateng (2009), Angnuureng et al. (2013); Jayson-Quashigah et al. (2013); Appeaning Addo (2015a); Jayson-Quashigah et al. (2021); Brempong et al. (2021) all within Ada, Ningo, Dzita, Fuveme, Atorkor, Keta and other areas. This study also seeks to assess the variabilities surrounding the newly created estuary in Fuveme, an area in the Volta Delta.

Sediments from rivers, nearshore currents and waves cause morphological changes along a coast due to regular sediment deposits within the nearshore zone. These morphological changes intensify coastal erosion due to both natural and human activities (Appeaning Addo, 2015b). Coastal areas are changing as a result of human activities, both the purposeful exploitation of coastal resources and the unintended consequences of actions. Additionally, due to complex morphological adaptation and greater susceptibility to other morphodynamic processes, Relative Sea Level Rise (RSLR) also contributes to coastal erosion, particularly in low-lying locations (Mentaschi et al., 2018).

Globally, sandy beaches cover one-third of the world's coast (Luijendijk et al., 2018) and it is known that a large percentage of these areas are eroding (Mentaschi et al., 2018), an unfortunate situation that is being compounded by climate change (Ranasinghe, 2016). Similar to the trend

2

happening globally, the entire coast of West Africa is also undergoing changes due to climate change with various levels of severity (Alves et al., 2020). The coasts which are made up mainly of sandy beaches have been rapidly eroding as a result of harbour expansion, building of hydroelectric dams, irrigation dams, dredging and coastal defence systems since the mid-20th century (Angnuureng et al., 2013). These constructions and systems have caused sediment imbalance and starvation, therefore, reducing sediment transported to coastal areas, causing erosion and persistent flooding (Angnuureng et al., 2019). Since beaches are intrinsically dynamic, these factors influence them over time (Appeaning Addo et al., 2020). As a result, understanding the dynamics of beaches' evolution over time and how it affects beaches require monitoring their morphology (Oyedotun, 2014; Appeaning Addo, 2015).

The evolution of a beach depends on the overall understanding of the cross-shore and the longshore sediment contributions (Angnuureng et al., 2019). In recent decades, several studies have increased the understanding of beach morphodynamics, but these have not been used to forecast morphological evolution because most data available are poor or not fit for purpose, which has necessitated modelling as an alternative (Luan et al., 2017).

For any interval, the hydrodynamics and morphodynamics of a coastal waterbody can be modelled using simulations. Simulation models resolve precise hydrodynamics, wave and sediment parameters in time and space (Murray, 2003) and allow for more predictions which are more accurate than the simpler ones. Simulation models have successfully simulated deltas, inlets, and small portions of salt marshes (Temmerman et al., 2005; Edmonds &

3

Slingerland, 2010; Nienhuis et al., 2016; Belliard et al., 2015; Mariotti & Canestrelli, 2017). Fully linked morphodynamics models, which update the morphology of coastal ecosystems as a result of sediment movement and modify the hydrodynamics correspondingly, are particularly effective for the simulation of medium to long-term evolution of coastal systems (Mariotti & Canestrelli, 2017).

The Volta Delta is a significant geomorphic and coastal feature located on Ghana's eastern stretch. Mangroves, lagoons, and marshes are among the diverse and abundant ecosystems found in this area. It also acts as a key fishing and farming hub (Appeaning Addo et al., 2018b). However, this area is at risk from continual exposure to coastal erosion, salinization, subsidence, storm surge, flooding and sea-level rise (Tessler et al., 2015). As ecologically and economically important as deltas are, there is a need for concern due to their environmental and geomorphological changes (Woodroffe et al., 2006). Investigations concerning these changes must be conducted so that relevant information will help policymakers in decision-making concerning coastal management. As such this study aims to assess the geomorphic variabilities along Fuveme Beach using Unmanned Aerial Vehicle (UAV), simulate the evolution of sediment movement and finally determine the prevalent hydrodynamic condition that affects the area.

1.2 Statement of the Problem

Historically, moderate erosion has occurred along the frontage of Ghana's eastern coast and research done in the Volta Delta shows that there has been a gradual erosion since the mid-1880s with major erosion being recorded in 1929, particularly in Keta (Nairn et al. 1999). The constructions of

4

Tema Port in 1955 and Akosombo Dam for hydroelectric power in 1965 have had major impacts on Ghana's eastern coast (Ly, 1980). The construction of the hydroelectric dam particularly, on the Volta River, has reduced fluvial sediment distribution which has significantly impacted the sediment budget (Anthony et al., 2016). All these factors have caused the front shoreline of the delta to be undergoing massive changes over time (Appeaning Addo, 2015a).

The Volta Delta shorelines are very dynamic, periodically undergoing changes (Dada et al., 2016) and even though numerous control measures such as revetments and groynes have been built along its shorelines, the issues of erosion persist (Angnuureng et al., 2019). The erosion rates along the shorelines were 4 m/yr (1923 - 1949), 6 m/yr (1959 – 1975), and 8 m/yr – 10 m/yr rise after 1964, after the dam construction (Ly, 1980). The constructions of sea defence structures at Keta and Ada in 2001 and 2013 respectively have helped stabilize the situation over the years but a report by Angnuureng et al. (2013), showed an erosion rate of 17.00 ± 0.3 m/yr downdrift the sea defence structures aimed to prevent longshore transport particularly at Keta. Jayson-Quashigah (2019), also reported average erosion rate at Fuveme from 2005 to 2013 (before the Ada Sea defence was put up) as 4.4 m/yr with the updrift and downdrift corners averaging, 12 ± 0.62 m/yr. After the Ada Sea defence was built, the erosion rate (2013 - 2017) increased to 31 ± 0.62 m/yr. This indicates the challenges posed by the Ada Sea defence, Keta Sea defence structures and quite recently the Atorkor Sea defence structures to the coast of Fuveme.

Aside from the increment in the erosion rate, there have also been multiple flooding at Fuveme which have displaced thousands of people and destroyed properties over the years (Appeaning Addo et al., 2018a).

According to residents of Fuveme, the sea breached a nearshore sandbar on the coast in May 2021, creating a 'new estuary' where tidal waves now move water and sediment between the sea and the estuary. This seems to be exacerbating erosion and flooding. This newly created 'bridged estuary', whose hydrodynamics and morphodynamics are not known, compounds the existing issues. The diversion of sediment load away from the Volta Delta poses a new challenge that researchers and policymakers do not know about. For this reason, it is vital to assess the geomorphic variabilities of this 'newly bridged estuary' and the entire coast, to ascertain its sediment dynamics and predict its effects on the entire coast of Fuveme.

1.3 Purpose of the Study

The Volta Delta is undergoing persistent morphological changes along its frontal shorelines due to climate change and anthropogenic activities (Appeaning Addo et al., 2018a). The Fuveme beach, which is the closest area downdrift of the Volta Estuary is facing unprecedented erosion over the years. The creation of a 'new estuary' along Fuveme's coast compounds the issues faced in that area. Additionally, this is the first bridge to occur in the Volta Delta which means that policy makers know nothing about its effects on the area and the delta as a whole.

Therefore, the purpose of the study is to estimate beach morphodynamics (beach profile, sediment volume and shoreline changes) of Fuveme Beach. In addition, sediment movement of the area will be assessed. Finally, the prevalent hydrodynamic condition affecting sediment movement in Fuveme Beach will also be assessed as well. The results for this research will provide information on shoreline changes, sediment volume changes,

beach profiles and sediment evolution. The outcome of the study would inform coastal dwellers as well as policy makers on the beach morphodynamics of Fuveme Beach.

1.4 Research Objectives

This research aims to assess the geomorphic variabilities along the coast of Fuveme. The objectives of this research are:

1. to assess sediment dynamics on the coast of Fuveme.

2. to simulate the trend of sediment movement along the coast of Fuveme.

3. to determine the predominant hydrodynamic parameter affecting the coast of Fuveme.

1.5 Hypothesis

The following hypothesis were formulated to guide this research:

Hypothesis 1

H_{01}: Sediment dynamics on the coast of Fuveme do not change over the year.

H_{A1}: Sediment dynamics on the coast of Fuveme changes over the year.

Hypothesis 2

H_{02}: The trend of sediment movement does not have any significant influence on Fuveme Beach.

H_{A2}: The trend of sediment movement significantly influences Fuveme Beach.

Hypothesis 3

H_{03}: Hydrodynamic parameters do not affect the coast of Fuveme.

H_{A3}: Hydrodynamic parameters affect the coast of Fuveme.

7

1.6 Significance of the Study

The study is the premier research done on the 'newly created estuary' off the coast of Fuveme in the Volta Delta. This study will give results on the sediment changes over the course of the study and give a better understanding of the sediment dynamics in the area that is resulting in periodic flooding and erosion.

It focuses mainly on using a numerical model to simulate the evolution of sediment within Fuveme area coupled with topographic data from monthly UAV flights to assess sediment volume changes, shoreline changes, beach profile changes and finally, predicting the predominant hydrodynamic condition affecting sediment transport along Fuveme Beach. This research also serves as a baseline for future studies on any newly created bridged estuary along the coast of Ghana. This study also fits one of the Africa Centre of Excellence in Coastal Resilience research objectives in Coastal Geomorphology and Engineering.

1.7 Delimitations

The water logger should have been left in the river Volta to accumulate data for three months but due to the nature of fishermen who normally take them and keep them for themselves, the water logger was deployed anytime I went to the field so that water level data obtained was for a month but interpolated to suit the simulation period (three months).

1.8 Limitations

The drone data was to be collected monthly after the very first month (October 2021) but due to insufficient funds, the next batch of data collection was from March 2022 to October 2022.

8

In addition, the validation for all three wave parameters (significant wave height, mean wave period and peak wave period) was not duly done as only the significant wave height was validated. The validation of the significant wave height was used as the validation for the MIKE 21 Spectral Wave simulation.

Finally, due to the unavailability of sediment transport data for Fuveme area, results from the MIKE 21 Sediment Transport (ST) module were also not validated. Instead, sediment deposition results from Geomorphic Change Detection (GCD) software were compared with results from the MIKE 21 ST module.

1.9 Definition of Terms

Mean Wave Period: An average of all individual wave directions in a time series that represents a sea state at a particular time.

Model Calibration: The iterative process of comparing the model with real system and revising the model until results from the model are accepted.

Model Validation: A process of comparing the model and its behaviour to a real system and its behaviour.

Sediment Accretion: The accumulation of sediment, deposited by natural fluid flow process.

Sediment Erosion: The detachment and movement of sediment by waves, wind, and currents.

Significant Wave Height: The average of the highest one-third of all waves in a wave train.

Peak Wave Period: The highest wave period with the greatest wave energy in a wave series.

9

1.10 Organization of the Study

This thesis is in six chapters whereby Chapter One introduces the study, covers the problem statement, the aim and specific objectives set out for the research together with the purpose of the research. An extensive review of literature is covered in the second chapter. The Conceptual framework of the study, coastal areas, including beaches and estuaries, sediment and sediment transport, modelling and a review of the coastal zone of Ghana and the Volta Delta are covered in Chapter Two. The research methodology, research design, equipment used for data collection procedures and analyses are captured in the third chapter. The results of the research together with brief interpretations of the results are covered in the fourth chapter. The discussions of the results of the study are done extensively in Chapter Five. The sixth chapter covers the summary of the research, conclusions of the objectives achieved and recommendations. Ground Control Points (GCPs) readings for the site, sample GCP markers, Net Shoreline Movement and End Point Rates for the study period and some field pictures are captured under Appendices A, B, C and D.

CHAPTER TWO

LITERATURE REVIEW

2.1 Introduction

Beach erosion problems have been getting worse for years. They have been attributed to climate change and anthropogenic activities which continuously threatens coastal areas. This part of the thesis reviews relevant literature that supports the research including coastal areas, beaches, estuaries, sediment transport, review of the Volta Delta and coastal management.

2.2 Conceptual Framework of the Study

This study was guided by a conceptual framework (Figure 1) used by Jayson-Quashigah (2019). In this framework, Unmanned Aerial Vehicle (UAV) was primarily used to capture aerial images of Fuveme Beach which were processed and specifically used for shoreline, sediment volume and beach profile analyses. In this conceptual framework, the arrows indicate the direction and link between each section.

The first objective estimates beach morphodynamics using Digital Elevations Models (DEMs) generated from images of the UAV surveys. The results from this objective provide sediment variations of Fuveme Beach in the successive months. These then feed into the second objective which provide georeferenced shorelines for land boundary generation in MIKE 21 model. Additionally, waves, tides and wind forcing are fed into the model to simulate sediment evolution. This generates the sediment transport rates for Fuveme area. Some parameters (waves, current and tides) of the model are unchecked to determine the predominant hydrodynamic condition affecting sediment transport in the area for the third objective.

11

The results from this study will provide shoreline changes, sediment volume changes, beach profile changes over the study period, sediment evolution, direction as well as the prevalent hydrodynamic condition affecting Fuveme Beach. This would inform the residents of Fuveme and policy makers of the happenings of the area and support coastal management policy for the area.
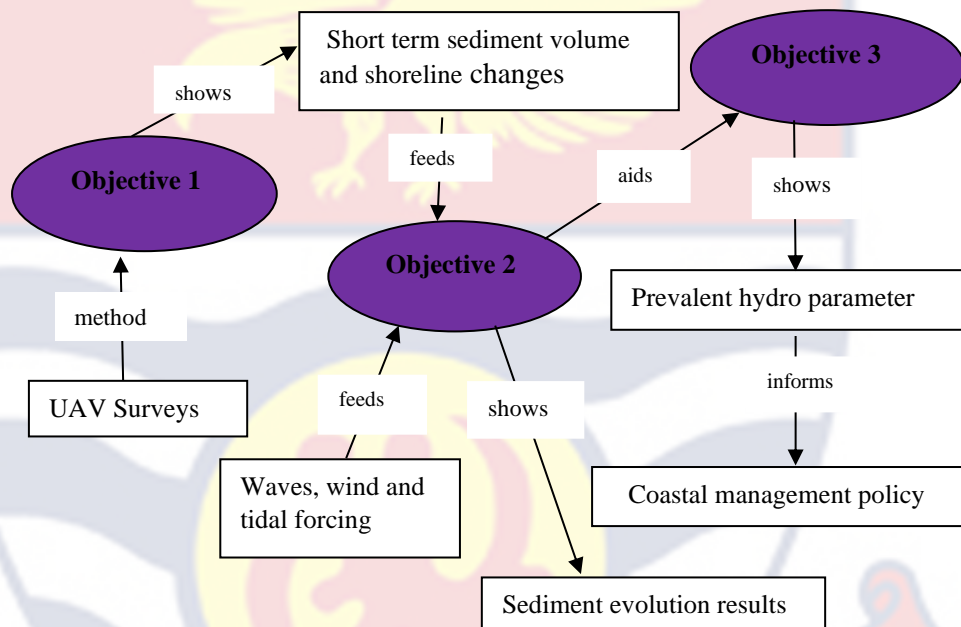
Figure 1: Conceptual framework of the study

2.3 Coastal Areas

One of the most inhabited areas in the world are coastal areas. Many people inhabit these areas with an estimated 40 % of the population of the world residing in coastal areas (United Nations Ocean Conference, 2017). Again, most of the world's largest cities, which house more people, are located in coastal areas. A coastal area is an area that is located 100 km inland from the coastline (United Nations Ocean Conference, 2017). All coastal areas experience unique influences from the sea, land, atmosphere, and general coastal processes. These processes include creation, breaking up and the

12

movement of sediment in the coastal areas (Gregory, 2011). These processes are vital for shaping the morphology of the area. Many divisions within coastal areas are known as coastal partitions or zones and the land-ocean transition zones, which include shoreline ecosystems and nearby coastal waters (Webb, 2022a). Many features are found in coastal areas, including beaches, dunes, barrier islands and deltas, which are greatly affected by physical factors such as waves, wind, currents and tides. This next section reviews waves, tides and currents as coastal processes.

2.3.1 Coastal processes

Coastal processes work in the coastal zones to change their landscapes and they refer to processes working along a coast to move sediment either by deposition or erosion (Allaby & Allaby, 2018). Currents, tides and waves influence the movement of sediment along and across a coast from a small to a large scale (Aagaard, 2002). These processes are monitored regularly with researchers often looking for physical signs of deposition or erosion to understand what physical process a coastal area is undergoing (Coastal Processes, 2022). According to Aagaard (2002), understanding of the coastal processes will ensure the understanding of morphodynamics in coastal areas.

2.3.2 Physical forces influencing coastal processes

One of the crucial physical forces that influence coastal processes is waves. A wave moves ocean energy from offshore to the coast thereby actively shaping its morphology (Reeve et al., 2004). When wind blows over the ocean's surface, it causes little ripples that gradually grow into waves with passing time and distance (Blanchette et al., 2008). The magnitude of waves depends on the wind's force and the area of open water it hovers over (Cohn et

13

al., 2021). A wave's period, wavelength, height, and direction of propagation are all terms used to characterize waves. Seas are locally produced waves closer to the shores and swells are waves from distance offshore such as a far-off storm (Xorse, 2013).

Ocean waves play a major role in open beach geomorphic changes over time and space due to their high energy dissipation after breaking (Morton, Miller & Moore, 2005; Hapke et al., 2006). Waves with intense energy impact the shore by breaking sediments and moving them downdrift through longshore currents. In wave formation, wave energy is accumulated until 1/7 of wave height is attained which causes them to recede resulting in the formation of white caps (Garrison, 2013). Large waves formed far from the shore break gradually as they get closer to the beach in a process called shoaling (Thornton & Guza, 1983). As they progress, they draw nearer to the shore and break down in magnitude and velocity. Wave breaking stimulates nearshore circulation and moves sediment, causing a coast's morphological development (Cohn et al., 2021). Thus, wave-breaking conditions affect sediment transport along beaches (Masselink et al., 2014). The impact of the wave-breaking influences the movement of sediment such that a greater wave-breaking moves more sediment and vice-versa (Reeve et al., 2004). The impact of ocean waves is predominant on the sea and the adjourning coast by causing disturbances at sea and on the coast. Among the physical forces, waves are the primary factors that influence changes in shoreline positions the most (Dawson, 2003; Vassie et al., 2004).

Tides, just like waves, are vital physical coastal processes. Its generation involves the sun and the moon. The Moon and Sun's gravitational

14

pull on the ocean water causes the vertical rise and fall of the water mass and these are referred to as tides (Short, 2012). This important phenomenon occurs as the moon rotates about the earth and concurrently as the earth rotates the sun around their barycentre. The highest of tides occur when all three celestial bodies (earth, sun and moon) are all in a 180 ° position normally called a spring tide. The lowest of tides, the neap tide, occurs when the earth is at right angles with the other celestial bodies (Pinet, 2009). Normally, different coasts respond to a different number of tides depending on the geographic location of the celestial bodies to the earth as well as the coastline (Pinet, 2009; Brempong, 2019).

A beach can be described according to the range of tide that approaches its shore. It can be described as a microtidal beach when it has less than a 2 m tidal range, a mesotidal beach with a range between 2 m – 4 m and a macrotidal beach with tides above 4 m and below 6 m. Amongst the various descriptions of tidal beaches, microtidal beaches are characterized by low tide and greatly dominated by high wave conditions both of which shape beach morphology. Macrotidal beaches form numerous sand bars and swash processes due to their tidal range (Pugh, 2019).

Currents refer to the vertical or horizontal movement of both surface and deep-water masses (Balasubramanian, 2014). It can also be described as the back-and-forth movement of water molecules (Drishtiias, 2022). Currents put the ocean into motion and are driven either by primary or secondary forces (Drishtiias, 2022). These fundamental forces are Coriolis force, heating by solar energy, wind and gravity (Study page, 2022). Differences in water density and temperature make up the secondary forces. Some examples of

15

ocean currents include Guinea current, Equatorial current, Benguela current and Canary current. Ocean currents transport heat from one latitude to the other like the general circulation in the atmosphere. They are also responsible for upwelling and downwelling which feeds the various sections of the ocean with cold, nutrient water from below to the upper part of the ocean (Drishtiias, 2022). Based on temperature, currents can be classified as either cold or warm ocean currents (GK Today, 2016). The cold ones are mainly responsible for transporting cold water to warm areas whilst warm currents transport warm water to cold waters. Cold currents are found in the western regions of low and middle latitudes continents in the north and the south hemispheres and also on the eastern coast of higher latitudes continents only in the northern hemisphere. Warm currents are also found in both hemispheres at the low and middle latitudes and on the western ends of continents in higher latitudes (Drishtiias, 2022). Surface currents and Deep currents (Figure 2) constitute the two types of ocean currents (Heaslip, 2022).

Currents driven by global wind systems that are fuelled by the energy of the sun are the surface ocean currents (NOAA, 2011). They are primarily initiated by gravity acting on the surface of the ocean. They aid in transporting heat from the tropical regions to the polar regions thereby influencing local, regional and global climate. They make up about 10 % of the total volume of water, from the surface to about 400 m depth. Deep ocean currents are currents formed as a result of differences in water density (NOAA, 2011). The density differences result from the ocean's temperature and salinity water masses (Drishtiias, 2022). They are found about 400 m below the surface of

16

the ocean and they make up about 90 % of the ocean. Rip currents, undertow currents and longshore currents constitute other forms of ocean currents.

Rip currents are defined as small currents that flow from the coastline towards the ocean (Earth Networks, 2018). They are dangerous currents seen closer to the beach when waves carry water towards the coast. A current that runs parallel to the shore as a result of the refraction of waves is the longshore current (Holt, 2022). It is responsible for longshore drift which moves sediment along the shore due to wave action. During wave breaking, the swash moves sediment up and backwash carries the materials down to the ocean at right angles due to gravitational forces. This process slowly moves materials up, down and along a beach (Dean & Dalrymple, 2004). This contributes to sediment deposition and sediment loss.

Undertow currents also carry sand near the shallow ocean floor and influence the formation and activity of waves located closer to the surface, usually breaking on the outer bars of a beach before coming too close to shore (Reeve at al., 2014).
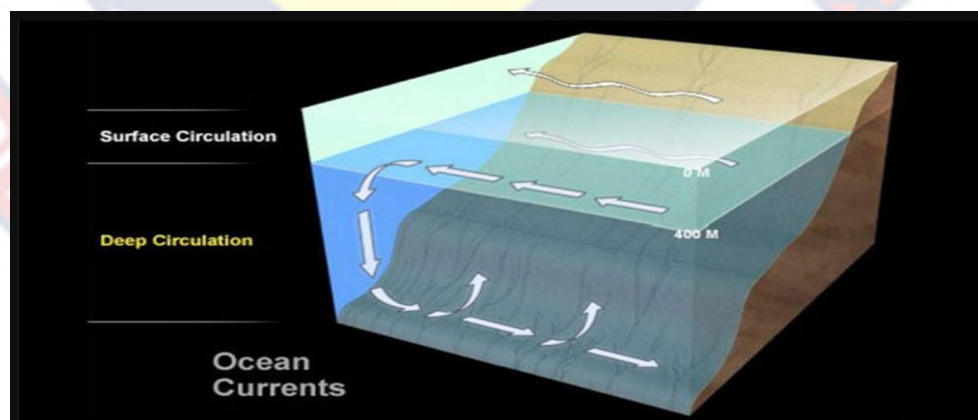
Figure 2: Deep and Surface Ocean currents (NOAA, 2011)

2.3.3 Beaches

Beaches were traditionally defined by Shepard (1973) as a 'shore with a covering of sand or gravel'. Over time, the definition has evolved to a 'coastal accumulation of non-cohesive sediment along an orthogonal path, the form and texture of which is controlled by wave-dominated processes' (Hardisty, 1990). A beach is therefore a sediment-accumulated area caused by wave action closer to the sea (Short, 2012). Sand, mud, boulders, gravel, rocks and pebbles mostly cover beaches. Sediments found along the beaches are products of weathering and erosion. They are carried by wind, currents, waves and tides over a long distance. Most beach systems have various zones that characterize them. They include: the nearshore, backshore, intertidal, offshore, littoral, swash, surf and other zones as shown in Figure 3.

The area of the beach above the high tide line and submerged under high wave conditions is the backshore. It is also the portion of the beach that is subject to wave action only during storms. The foreshore is the zone between high tide and low tide. This zone is always subject to wave action. The berm is above the sea and includes the intertidal area. It may include vegetation such as grasses, shrubs or trees. The nearshore zone extends from the low tide line to the depth where the bottom no longer influences wave action (Dean & Dalrymple, 2004). In the offshore zone, there is no sediment transport by any coastal process. The zone where there is significant sediment movement by wave action is the littoral zone and the zone where backwash moves back (wave run-up) into the ocean is the swash zone. The surf zone is the zone that extends from the breaker zone to the foreshore zone (McGlashan et al., 2005). There are various types of beaches depending on the materials that make up

18

the beach but based on beach composition, they are grouped into rocky, sandy, pebble and others. Only sandy beaches will be reviewed for this section.
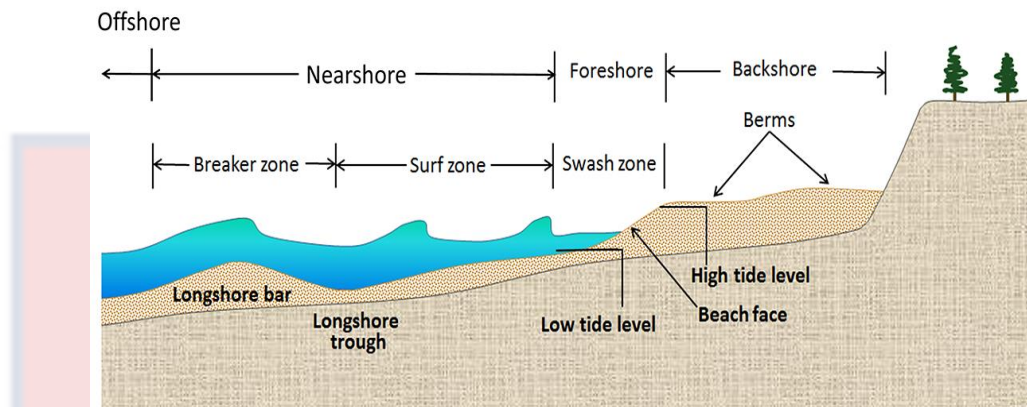
Figure 3: The zonation of a beach (Webb, 2022a)

A beach is described as sandy when it is made up of loose sediment (< 2.0 mm in size) on its shore (Vousdoukas et al., 2020). Sandy beaches (Figure 4) occur on coasts that experience low-energy waves which gradually deposit the sand on the beach. They are geomorphologically complex beaches with constantly changing shorelines due to the constant interactions between coastal processes and the coast (Mentaschi et al., 2018; Vousdoukas et al., 2020). Naturally, the accumulation of sand transported from rivers, waves and currents build sandy beaches (Ecoshape, 2022). Sandy beaches are classified as reflective or dissipative (Short,1999; Finkl, 2004). They are termed dissipative when they are wide, flat with low energy and reflective when they are narrow and steep with high energy (Finkl, 2004).

Sand movement occurs due to wave action in wet areas and wind in dry areas, and it is most significant in open surf zones. On the other hand, well-developed dunes tend to store large amounts of sand. During storms, sand is swiftly transported towards the sea across the beach and surf zone, but during calmer periods, it gradually moves back landwards (Short, 1999; Nordstrom, 2000).

19

Figure 4: A sandy beach at Fuveme

Sandy beaches are characterized by sandy profiles from the backshore to the nearshore dominated heavily by aeolian processes (Ecoshape, 2022). Sandy beaches are tourist attraction sites with huge socio-economic significance as well. They support rich biodiversity and while biodiversity is high, species diversity varies across the coastal profile and increases from the high to low water lines (Schlacher et al., 2007). They are geomorphic systems with rapid shoreline changes (Del Rio et al., 2012) and serve as a substrate that exposes organisms to severe conditions (Ecoshape, 2022). They serve as nurseries and foraging regions for some fishes. Sandy beaches are important nesting areas for marine turtles and shorebirds (Schlacher et al., 2007). Sensitive features of sandy coastlines offer numerous ecosystem services, which are advantageous to humans. These services encompass sediment storage and transport, wave reduction, and protection against extreme events such as storms and tsunamis. Additionally, they contribute to nutrient mineralization and recycling (Defeo et al., 2009).

2.4 Estuaries

An estuary is a 'semi-enclosed coastal body of water with free connectivity to the open sea and within which seawater is significantly diluted

20

with fresh water generated from land drainage' (Cameron & Pritchard, 1963; Cochran, 2014). Most estuaries share several characteristics that make them unique habitats. Estuarine salinities can go from extremely low values typical of the majority of rivers to high values seen in the open ocean. Estuarine areas are usually < 100 m in depth and thus allows for an interaction between the bed and the water mass in a process called 'benthic-pelagic coupling'. This in turn creates a tidal effect that is generated by the physical configuration and the half-enclosed nature of the estuary (Cochran, 2014).

2.4.1 Classification of estuaries

The classification of estuaries can be in terms of the vertical structure of salinity (stratification), water balance, hydrodynamics or geomorphology (Ville-Levinson, 2010).

The classification of estuaries (Figure 5) based on water balance is grouped into low-inflow, inverse and positive estuaries. Estuaries that occur in areas of bigger evaporation rates with a relatively minute river discharge influence are called low inflow. They are found in regions that are partially hot and dry (Devlin & Pan, 2020). An inverse estuary is predominantly found in hot and dry regions and it is where high evaporation of freshwater does not exceed rainfall additions of freshwater. Inverse estuaries are so named because of the longitudinal density gradient that is opposite the sign of positive estuaries (Ville-Levinson, 2010). A positive estuary on the other hand has freshwater additions exceeding evaporation losses thereby establishing a longitudinal density gradient. This longitudinal density gradient moves volume outflow to the ocean which induces circulation called estuarine or gravitational circulation (Devlin & Pan, 2020).

21
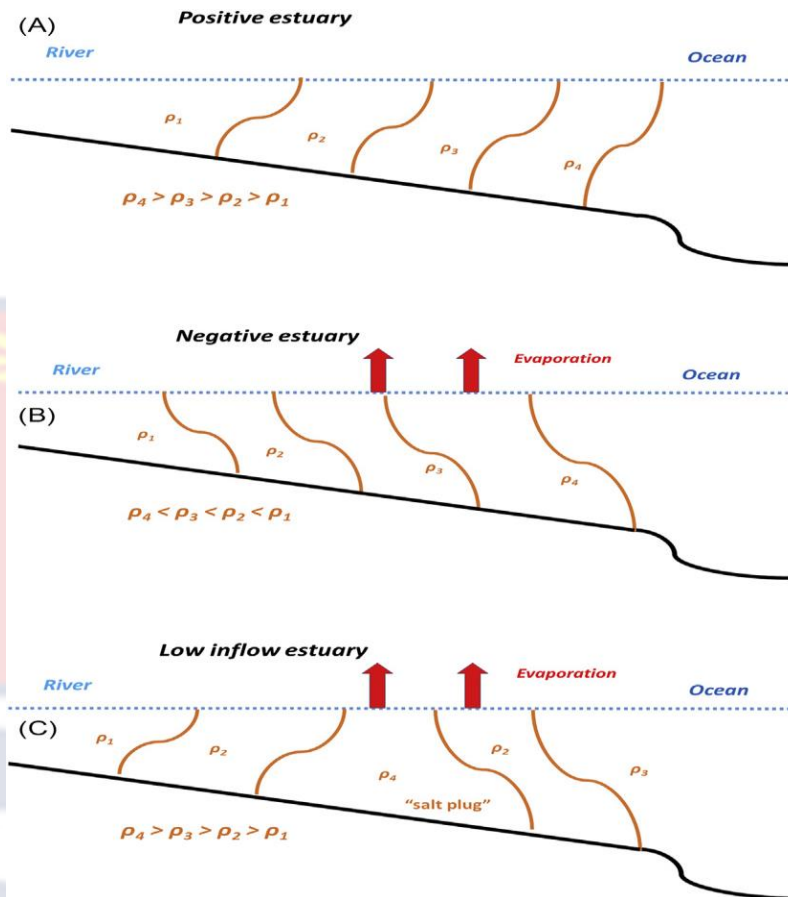
Figure 5: Classification of Estuaries; a) Positive estuary b) Negative estuary c) Low inflow estuary (Devlin & Pan, 2020)

Fjord, bar built, coastal plain, and tectonic estuary represent geomorphological classifications of estuaries. A coastal plain is a wide estuary and very shallow with large width/depth ratios. A fjord estuary is an elongated, deep waterway with a sill (Ville-Levinson, 2010). They are only found in extremely cold areas. A glacial fjord (a subgroup of fjord) is associated with an active glacier, whilst a riverine fjord (a subgroup of fjord) is an extinct glacier where freshwater supply is primarily generated by mainly river flow. Fjords are steep and possess low width/depth aspect ratios and are deep and narrow as well. An example of a fjord estuary is Glacier Bay in Alaska. A bar built is formed from an embayment that is semi-enclosed as a result of sand pit formation between the sea and the adjourning littoral drift

22

(Ville-Levinson, 2010). An estuary created by earthquakes or cracks in the crust of the Earth that cause faults to emerge near the ocean is described as a tectonic estuary. These faults create a basin which is filled by the ocean. A typical example is the San Francisco Bay (NOAA, 2022b).

The classification of estuaries based on vertical mixing or stratification is very important. This form of classification takes into account the competing forces of mixing caused by tidal forcing at the ocean's edge and buoyant forcing from upstream river flow (Devlin & Pan, 2020). The amount of marine water that enters each tidal cycle (tidal prism), determines how much mixing occurs as a result of the tides. In this way, many estuaries are polymorphic, that is, they can transform from one type into another with the seasons. Classification based on stratification is grouped into a well-mixed, salt wedge, weakly and strongly stratified estuary. A well-mixed estuary is formed by a tidal forcing and a feeble discharge by the river. A weakly stratified estuary is the result of intermediate tidal forcing and moderate river discharge. A salt wedge estuary is formed by huge discharges from the river and feeble tidal forcing. It is strongly stratified during flood tide and it usually loses its stratification during the dry season. A strongly stratified estuary is formed from a moderate to large river discharge and weak to moderate tidal forcing. Its stratification is quite similar to a salt wedge with the stratification holding throughout the period.

The classification of hydrodynamics is credited to Hansen & Rattray (1972) who subdivided this classification into circulation and stratification parameters (Devlin & Pan, 2020). The ratio of sectionally averaged flow (Uf) to near-surface flow (Us), which is frequently connected to river discharge, is

23

the circulation parameter. In estuaries with active water exchange, outflow balances inflow resulting in a larger circulation parameter with the depth-averaged flow (Uf) being low. The stratification parameter is the top-to-bed salinity differential (dS), to the average salinity over the cross-section of the estuary. Smaller values indicate lower water column stratification and estuaries often have a stratification parameter of less than 1 (Devlin & Pan, 2020).

2.5 Sediment

Sediment refers to the conglomerate of materials, organic and inorganic, that can be carried away by water, wind or ice (Langland & Cronin, 2003). It refers to both mineral matter, decaying sediments as well as inorganic biogenic material matter (Wetzel, 2001). The majority of mineral sediment is a result of erosion and weathering, whereas organic sediment consists mainly of detritus and decomposed materials like algae (Spehar et al., 2007). These particles are typically small in size, with clay defined as particles less than 0.00195 mm in diameter and coarse sand reaching a diameter of only 1.5 mm (Osmond et al., 1995). However, during high-flow events like floods, even large rocks can be considered sediment as they get carried downstream (Perlman, 2014).

Sediment is a naturally occurring component found in many water bodies, but it can be influenced by human activities (Spehar et al., 2007). Geologic, geomorphic, and organic factors all contribute to the quantity, composition, and size of the transported sediment in any given stream (Fondriest Environmental, 2022).

24

2.5.1 Classification of sediments

Sediments are classified in several ways. Webb (2022b) categorizes the classification of sediment into sediment texture, composition and origin. For sediment texture, the grain size is the first factor looked out for. It ranges from a size of 0.004 mm (finest clays) to the largest of about > 256 mm sizes (big boulders) in diameter. The size of the sediment gives a representation of the conditions the sediment underwent before deposition onto the shore. Larger particles are deposited usually in high-energy areas with the finer particles being moved away. Smaller particles will settle out and form finer sediments under lower energy conditions (Webb, 2022b).

Sorting is another method of categorizing sediments. Sorting refers to the degree of grain size homogeneity. It is used to mainly describe sediments or sedimentary rock. The amount of transit the silt has undergone determines the degree of sorting (De Mahiques, 2016). It also refers to the uniformity of sediments in terms of size (Webb, 2022b). Similar-sized grains make up well-sorted sediments, which are the product of extensive sediment transport and earth processes that separated the sediment by depositing different size fractions in various locations. Because they are too heavy to be transported far, coarse sediments are typically located closest to the source location, while fine sediments like silt and clay travel the furthest (Webb, 2022b).

Again, another classification is maturity or how long the particles have been moved by water or other materials (Webb, 2022b). The amount of sorting, the rounding of the particles, and the makeup of the sediment can all be indicators of maturity. Sediment that has reached its textural maturity is well-rounded (because rounding improves with distance and time travelled)

25

and well-sorted (Nelson & Fringer, 2018). Due to particles' abrasion over time, the maturity is very rounder. Since the tiniest of particles will be moved away and particles of equal size will go the same distance with the same amount of energy, sorting to a high degree denotes maturity (De Mahiques, 2016).

The classification of sediments has been grouped into many different schemes according to multiple reports. According to Blott & Pye (2012), the Udden (1898) and Wentworth (1922) schemes provided a great and consistent framework for their usage. The classification of the sediments by Udden (1898) suggests that all size classes must have the same significance. All particles ranged between 250 µm – 2 mm per the Whitney scale. These were adopted in the early stages by most researchers. Years over, research by Udden separated these sizes below the 250 µm to > 125 µm. Thorough research performed by Wentworth into Udden's research helped shape the classification of sediments. Particles larger than 2.0 mm which were initially termed gravels were subdivided into granules, pebble, cobbler and boulder gravel. Wentworth paid much attention to the subdivisions of the sand particles as compared to the gravels and this gave other researchers like Doeglas, (1968) to propose more subdivisions for the other particles. Now, the most preferred classification of sediment is the Wentworth classification of particle grades (Blott & Pye, 2012) as shown in Table 1.

Table 1: *Wentworth classification of particle grades (Wenthworth, 1922; Dzakpasu, 2019)*

Grade Name	Particle Size Range (φ)	Particle Size Range (mm)
Boulder	< -8.0	> 256
Cobble	-8.0 to -6.0	256 → 64
Pebble	-6.0 to -2.0	64 → 4
Granule	-2.0 to -1.0	4 → 2
Very coarse sand	-1.0 to 0	2 →1
Coarse sand	0 to 1.0	1 → 0.5
Medium sand	1.0 to 2.0	0.5 → 0.25
Fine sand	2.0 to 3.0	0.25 → 0.125
Very fine sand	3.0 to 4.0	0.125 → 0.0625
Silt	4.0 to 8.0	0.0625 → 0.0039
Clay	> 8.0	< 0.0039

2.6 Sediment Transport

Sediment movement is vital for many occurrences along the coasts. It is primarily responsible for coastal erosion and deposition over local areas and much wider geographic areas (Reeve et al., 2014). This process happens between a fluid in motion and a boundary (land) provided there was an interface. The movement of organic and inorganic particles in a water medium is sediment transport (Fondriest Environmental, 2022). In sediment transport, once sediment sets in motion, the flow becomes quite complex with two or more materials being involved. According to Fondriest Environmental (2022), sediment transport is mostly likely to be affected by either waves or currents or both simultaneously. Sand particles are considered in sediment movement. In general, there is always an increase in sediment movement once there is an increase in the flow rate (Czuba et al., 2011).

There are two ways in which sediment is transported: as either bedload

27

or suspended load (Reid et al., 1998). The rolling or sliding of sediment closer to the sea bed or bottom is termed bedload transport and the suspension of sediment in a water body is termed suspended load (Reeve et al., 2004). Other forms of sediment transport include the wash load and it is made up of extremely small particles that are suspended but did not originate from the bed. Usually, tributaries of rivers are where these particles enter the system. The makeup of the bed material cannot be used to anticipate their concentration (Wu et al., 2011).

The bedload is extended by the concept of sheet flow and is made up of numerous particles in motion in contact because when the transportation increases the multiple-grain particles are set in motion. For low-velocity rates for big grain sizes, bedload transport predominates and for huge velocity rates for small grain sizes, suspended load transport predominates (Reeve et al., 2004). Sand-sized fractions are transported both by bedload and suspended load in the marine environment, with suspended transport happening up to several meters above the bed. Gravel-sized fractions are mainly transported as bedload. The suspended transport in this scenario frequently exceeds the bedload transfer in size (Allen & Pye, 1992).

The longshore current can carry sediments on and off the beach during a forward and backward process and this process is termed as longshore drifting. Longshore drift is the transportation of sediments parallel to the coast along the shoreline. Longshore currents that approach the beach cause longshore drift (NOAA, 2022a).

2.6.1 Metrics of sediment transport

For both current and waves, the main equation governing bedload transport as reported by Reeve et al. (2004) is given by equation 2.1:

$$\phi = \frac{q\text{b}}{(g(s-1)D^3)^{\wedge}0.5} \qquad 2.1$$

where qb represents the bedload transport rate per unit width.

A more developed one by Neilsen (1992) which opens up more conditions and is widely used is represented in equation 2.2:

$$\phi = 12\boldsymbol{\theta}\text{s}^{\wedge}0.5\ (\boldsymbol{\theta}\text{s} - \boldsymbol{\theta}\text{CR}) \qquad 2.2$$

where $\boldsymbol{\theta}$s and $\boldsymbol{\theta}$CR represent the entrainment function and its critical value respectively. The suspended load is given by:

$$q(Z) = \text{u}(Z)\ .C(Z) \qquad 2.3$$

$$\text{qs} = \int_{Z_a}^{h} \text{u}(Z)C(Z)dZ \qquad 2.4$$

where q(Z) = Sediment transport rate per unit width at any given height Z

For total load sediment, the Van Rijn (1984) equation is given by equations 2.5, 2.6 and 2.7:

$$\text{q}_\text{t} = \text{q}_\text{b} + \text{q}_\text{s} \qquad 2.5$$

$$\text{q}_\text{b} = 0.005\bar{\text{u}}\hbar\left(\frac{\bar{\text{u}}-\bar{\text{u}}\text{CR}}{(s-1)hD50)^{\frac{1}{2}}}\right)^{2.4}\left(\frac{D50}{\hbar}\right)^{1.2} \qquad 2.6$$

$$\text{qs} = 0.005\bar{\text{u}}\hbar\left(\frac{\bar{\text{u}}-\bar{\text{u}}\text{CR}}{(s-1)hD50)^{\frac{1}{2}}}\right)^{2.4}\left(\frac{D50}{\hbar}\right)^{1.2}(\text{D}^*)^{-0.6} \qquad 2.7$$

Where $\bar{\text{u}}$CR= 0.19 $(D50)^{0.1} \log(\frac{4\hbar}{D90})\ for\ 0.1 \leq D50 \leq\ 0.5mm$

$\bar{\text{u}}$CR= 8.5 $(D50)^{0.6} \log(\frac{4\hbar}{D90})\ for\ 0.1 \leq D50 \leq\ 0.5mm$

2.6.2 Research work done on sediment transport

Major research done in sediment transport along the coast of West Africa was by Giardino et al. (2018). In the research, the SWAN model was

29

used to generate the wave climates, longshore transport rates along selected countries in the region. The aim was to estimate those parameters in ports and estuarine areas. The results of the research showed the sediment budget for the notable areas along the coast including the Volta River estuary, the ports of Lomé, Abidjan and Cotonou and other prominent areas were estimated.

Research done by Boateng et al. (2012) show that the fluvial sediment of the Volta River was estimated before and after the Akosombo dam construction. The results indicate that the amount of fluvial sediment being trapped by the Akosombo Dam was huge with the discharge rate pre-dam construction at 71×10^6 m³/a and being drastically reduced to 7×10^6 m³/a presently. In his discussion, he mentioned that it was the main reason why the eastern coast of Ghana was undergoing erosion prompting the constructions of hard engineering structures in Keta, Ada, Atorkor and other areas.

The amount of suspended sediment discharged from the rivers in Ghana was researched by Akrasi (2011). In the research, measurements ranging from sediment grain size, bedload and suspended load sediment were taken from 21 rivers stations and a simple model was used to show whether there was a correlation between suspended sediment and the mean runoff and to quantify the sediment being discharged. The results showed a total of between $15,000 - 1.2 \times 10^6$ t of annual sediment discharges into the sea.

According to Hayes et al. (2007), the sediment transport rates on Ghana's coast exceed 1 million yards which result in about 764,554.9 m³ of longshore sediment transport annually, due to our open coasts.

30

2.7 Modelling

The use of models has simplified many complex situations in science. This has reduced time-consuming processes into simple calculations which is saving time and energy. The development of diverse models has significantly advanced the field of morphodynamics in recent years. These models have developed into useful instruments for researchers and coastal engineers for evaluating erosion issues and assisting with the design of coastal remedies (Lesser et al., 2004; Pender, 2013). By 1990, morphodynamics models had advanced from straightforward analytical models to depth-averaged two-dimensional (2D) models through 1D network and coastal models (Lesser et al., 2004). These complex quasi-3D extensions used to create these depth-averaged models allow them to consider the undertow profile (Lesser et al., 2004; Roelvink & Reniers, 2011). Many models have been created, tested, and used on different coastlines across the world. The most widely used modelling systems include ROMS, Delft3D, ECOMSED, TELEMAC, and MIKE 21 models.

The MIKE 21 model package, which has been extensively used and validated at numerous sites, is adopted in this investigation (Bolle et al., 2015; Badru et al., 2022). Again, this package was useful and extensively used to investigate hydrodynamics, waves and sediment transport along the coast of Ada before the construction of the sea defence project (Bolle et al., 2015).

2.7.1 Sediment transport numerical modelling using MIKE 21/3

The MIKE 21/3 Coupled Model FM is a numerical model used extensively in the river, coastal and estuarine systems (MIKE, 2017). The modules that make up this model include; Mud and Particle Tracking, Spectral

31

wave, Sand Transport, Shoreline morphology, Hydrodynamic, and ECO Lab / Oil Spill modules. In this model, the basic computational elements are the Hydrodynamic (HD) and the Spectral Wave (SW) modules. The two combined can be used to simulate how waves and currents interact with one another.

The HD module is fundamental for other modules as it effectively utilises the water levels and flows change in response to a wide range of forcing functions in water bodies and coastal areas. This is used to solve both 2D and 3D challenges. It is used to effectively stimulate 2D flows in one-layer fluids as shown in equations 2.8, 2.9 and 2.10 (MIKE, 2020a). The conservation of mass coupled with momentum, which is integrated over the vertical to describe flow and water level change, is the primary guiding concept of the HD module (MIKE, 2020a)

$$\frac{\partial \zeta}{\partial t} + \frac{\partial p}{\partial x} + \frac{\partial p}{\partial x} = \frac{\partial d}{\partial t} \tag{2.8}$$

$$\frac{\partial p}{\partial t} + \frac{\partial}{\partial x}\left(\frac{p^2}{h}\right) + \frac{\partial}{\partial x}\left(\frac{pq}{h}\right) + gh\frac{\partial \zeta}{\partial t}$$

$$+ \frac{gh\sqrt{p^2+q^2}}{C^2.h^2} - \frac{1}{\rho\omega}\left[\frac{\partial}{\partial x}(h\tau_{xx}) + \frac{\partial}{\partial y}(h\tau_{x\gamma})\right] - \Omega * q \tag{2.9}$$

$$- f\, VV_x + \frac{h}{\rho\omega}\frac{\partial}{\partial x}(\rho_a) = 0$$

$$\frac{\partial q}{\partial t} + \frac{\partial}{\partial y}\left(\frac{q^2}{h}\right) + \frac{\partial}{\partial x}\left(\frac{pq}{h}\right) + gh\frac{\partial \zeta}{\partial y}$$

$$+ \frac{gh\sqrt{p^2+q^2}}{C^2.h^2} - \frac{1}{\rho\omega}\left[\frac{\partial}{\partial x}(h\tau_{\gamma\gamma}) + \frac{\partial}{\partial y}(h\tau_{x\gamma})\right] - \Omega * q \tag{2.10}$$

$$- f\, VV_\gamma + \frac{h}{\rho\omega}\frac{\partial}{\partial y}(\rho_a) = 0$$

Where $h\,(x,y,t)$ =   water depth (= ζ, -d, m)

           $d\,(x,y,t)$ = time varying water depth (m)

           $\zeta(x,y,t)$ =   surface elevation (m)

$p, q \ (x, y, t)$ = flux densities in x- and y- directions (m/s/m) =

(*uh, vh*); (*u, v*) = depth averaged velocities in x- and y-directions

$C \ (x, y)$ = Chezy resistance (m$^{1/2}$s)

g = Acceleration due to gravity

$f(V)$ = Wind friction factor

V, V_x, V_Y = Wind Speed and components in x- and y-direction (m/s)

Ω (x, y) = Coriolis parameter, latitude dependent s^-1

ρ_a (x, y, t) = Atmospheric pressure (kg/m/s²)

$\rho\omega$ = Density of water (kg/m^3)

x, y = Space coordinates (m)

t = time (s)

$\tau_{xY} \ \tau_{xY} \ \tau_{YY}$ =   components of effective stress

The Courant-Friedrich-Lévy (CFL) number in the cartesian coordinate which is a major stability constant in the HD module is given:

$$\text{CFL} = (\sqrt{gh} + \text{u}) \frac{\Delta t}{\Delta x} + (\sqrt{gh} + \text{v}) \frac{\Delta t}{\Delta v} \qquad 2.11$$

where h = the total water depth, u and v are the velocity components in the x and y-direction, respectively, g is the gravitational acceleration, x and Δy are characteristic length scale in the x- and y-direction and Δt is the time step interval. This is vital for the stability of the simulation.

The Smagorinsky formulation (Smagorinsky, 1963) is used for calibration in the HD module and this parameter is used to express sub-grid scale transports by an effective eddy viscosity related to a characteristic length scale. The sub-grid scale eddy viscosity in the horizontal direction is given by:

$$\text{V}^h_t \ = \text{c}^2_s \ \text{I}^2 \ \sqrt{2} \ \text{S}_{ij} \ \text{S}_{ij} \qquad 2.12$$

33

where Cs is a constant, I= characteristic length and the deformation rate is given by:

$$S_{ij} = \frac{1}{2}\left(\frac{\delta ui}{\delta xj} + \frac{\delta ui}{\delta xi}\right) \text{(i, j = 1.2)} \qquad 2.13$$

Another significant parameter for the HD module is the bed resistance of the area. For the bed resistance, the Chezy formulation is shown in equation 2.14 as:

$$\frac{gp\sqrt{p^2+q^2}}{c^2h^2} \qquad 2.14$$

For bed resistance, the resistance type may be Nikuradse, manning or Chezy parameter. Other parameters are compensated by the above formulations such that major changes occur once they are increased or reduced in the simulation process.

The SW component of the model is based on the directional parametric formulation. This is made in the frequency domain y introducing the zeroth and first moment of the wave action spectrum as dependent variables as described by Holthuijsen et al. (1989). Additionally, the 0th and 1st moments of the wave action spectrum can also depend on each other in the frequency domain (Holthuijsen et al., 1989). A formulation in terms of wave direction and relative angular frequency was chosen for the current model. The density, $\mathcal{N}(\theta, \sigma)$, is directly proportional to the energy density E (σ, θ), by:

$$\mathcal{N} = \frac{E}{\sigma} \qquad 2.15$$

In the propagation of wave over depths and currents varying slowly, the relationship between the relative and the absolute angular frequency is given by the linear dispensation relation as:

$$\sigma = \sqrt{g}\, k \tan(k\,d) = \omega - \text{k. U} \qquad 2.16$$

where g = acceleration due to gravity, U = current velocity and d = the water depth.

The wave action equation formulated by Komen et al. (1994) serves as the main governing equation. Wind input is vital for wave formation and propagation. According to Janssen (1989), the growth of wind is dependent on the wind generated and also on the age of the wave. In the formation of waves, wind input plays a role and it depends solely on the aerodynamic drag on the sea (MIKE, 2020b). The wind input source (S_{in}) is given by:

$$S_{in} (f, \Theta) = \max (\alpha, \gamma * E (f, \Theta)) \qquad 2.17$$

With α being the linear growth and γ, the non-linear growth rate.

The bottom friction of an area is also considered in the model. The dissipation rate as a result of bottom friction is given by:

$$S_{bot} (f, \Theta) = - (C_f + fc (\bar{u} . k)/k) \frac{k}{\sinh 2kd} E (f, \Theta) \qquad 2.18$$

C_f = friction coefficient, k = wave number, d = water depth, fc = friction coefficient for current and u = current velocity. According to Komen et al. (1994), the range of values for fc is normally between 0.001 m/s – 0.01 m/s depending on the bed and flow conditions.

The wave breaking parameter used is also formulated by Battjes & Janssen (1978) based on the theory that wave breaks only as a result of the wave height no longer supporting the water depth in shallow waters. The wave diffraction was modelled as propounded by Holthuijsen et al. (2003) using the phase-decoupled refraction-diffraction approximation. It is based on refraction and diffraction equations for slopes without including the phase information. For white capping, the formulation made by Janssen et al. (1989) included the whole energy spectrum. This was added since Hasselmann (1974)'s earlier

35

formulations left out additional causes, namely the attenuation of short waves caused by the passage of big whitecaps and the amount of whitecap covering (dependent solely on the total steepness of the wave). The white capping formulation used in the model is given by:

$$S_{ds}(f,\theta) = -C_{ds}\, ds\, \left(\frac{\tilde{\alpha}}{\tilde{\alpha}_{pm}}\right)^m \left\{(1-\delta)\frac{k}{k} + \delta\left(\frac{k}{k}\right)^2\right\}\sigma E(f,\theta) \qquad 2.19$$

Where Cds, δ and m = constant.

The Sediment Transport (ST) module is a non-cohesive module that incorporates the HD and SW modules (in case of current and wave) to generate and calculate sand transport rates and sediment properties. The Sediment Transport Application Quasi-3D (STPQ3D) is used to calculate the tabulated sediment movement rates. STPQ3D is a thorough intra-wave sediment transport software that determines the overall sediment transport rates in two perpendicular directions, longshore and cross-shore, using a Q3D description of the hydrodynamics and sediment transport (MIKE, 2020c). When computing the rates, STPQ3D takes into account the impacts of combined waves and current, arbitrary wave-current angles, waves, level beds and all types of silt (MIKE, 2020c).

Sediment transport rates are calculated either by applying the pure current or the combination of waves and currents. The rates are made based on the average horizontal velocity component in a way that doesn't involve the effect of inertia. Sediment transport calculations for pure current are performed in the course of the simulations using available conditions.

In pure current and combined current and wave calculations, the input velocity is very vital for its calculation. This is because bedload sediment in motion occurs close to the bottom (Reeve et al., 2004). The calculations are

36

mainly performed with the average mean horizontal component with the assumption that the vertical profile is in a logarithmic form (MIKE, 2020a). For MIKE 21, the average horizontal component is directly proportional to the depth-averaged velocity from the flow module. This is given by equation 2.20:

$$V = \int_0^h (z)\,dz \qquad\qquad 2.20$$

Where V(z) is the velocity component at z distance acting above the bottom. The drag coefficient is in the pure current option is given by equation 2.21:

$$Cf = \frac{g}{C^2} = \frac{g}{(Mh^{\frac{1}{6}})^2} = \left(\frac{g}{(a.h^b)^2}\right) \qquad\qquad 2.21$$

Where g = acceleration due to gravity, C = Chezy number, M = manning number, a = resistance coefficient and b = resistance

The drag coefficient for the current and waves combination is given by equation 2.22:

$$Cf = \frac{1}{\left(\frac{1}{K}(\ln\frac{30h}{ks})-1\right)^2} \qquad\qquad 2.22$$

where the value of *ks* is gotten from the HD simulation.

For pure current, sediment transport occurs basically between the bathymetry and the hydrodynamics with the bed materials interacting as well. Both suspended load and bed load are generated in the pure current option but the suspended load is taken into consideration during modelling (MIKE, 2020c). The suspended load is based on a theory developed by Galapatti (1983).

For combined waves and current, the transport rates are calculated by linear interpolation in the ST table. The values are calculated by the toolbox utility programme in the model. It calculates both bed load and suspended

37

separately in the table but the sediment values are for the total load (MIKE, 2020c).

2.8 The coastal zone of Ghana

Ghana can be found in West Africa at latitude 8 °N and longitude 2 °W (Anim et al., 2013). Ghana's coastline is approximately 550 km and it is a high-energy type (Boateng, 2012). The coastal area is about 7 % of the total land mass of Ghana (Ayisi, 2022). In terms of geomorphology, the eastern, central and western coasts make up the entire subdivision of Ghana's coastal area. The eastern coast is about 149 km long and its coast is a high-energy one with over a meter wave height (Ly 1980). The beaches in this region are mostly sandy with many rivers, lagoons and spits (Boateng, 2012). The middle coast is about 296 km and it extends from Prampram to Cape three point. It is the most developed part of Ghana's coastline. The western end of Ghana's coast is about 95 km and is made up of numerous beaches and lagoons. The coast extends from the estuary of the Ankobra River to the border with La Cote D'Ivoire (Boateng, 2012).

Wellens-Mensah et al. (2002) report that two types of waves approach the shores of Ghana and they include; wind waves and swell waves. The tides are regular and semi-diurnal. The average tidal range at the east, central and west coasts are 1.00 m, 0.96 m and 0.90 m respectively (Boateng, 2012).

Ghana has had a 2.1 mm sea level rise over the past ten years, and this data has helped forecast that the sea level will likely rise potentially heightening erosion issues on our coast (Xorse, 2013). The seashore contains a variety of geologically diverse rock formations from various times. The geology of the various coastal locations determines how resistant they are to

38

erosion processes. Stronger geological formations on the western coast of Ghana are more robust than flexible geological structures like the unconsolidated materials in the southeast and the shale in the Accra region (Xorse, 2013).

2.8.1 The Volta Delta

The Volta Delta, as described by Appeaning Addo et al. (2018b), is an area lying below 5m contour around the Volta River basin. It is approximately 150 km in length and it extends from the west of Ningo-Prampram to Aflao at the border between Ghana and Togo. The delta is located in south-eastern Ghana between longitudes 0˚ 40' E and 1˚10' E and latitudes 5˚ 25' N and 6˚ 20' N (Figure 6) covering an area close to 4562 km² (Codjoe et al., 2020). The area is characterized by sandy beaches which are actively shaped by ocean wave action. It lies within the Keta basin (Akpati, 1978).
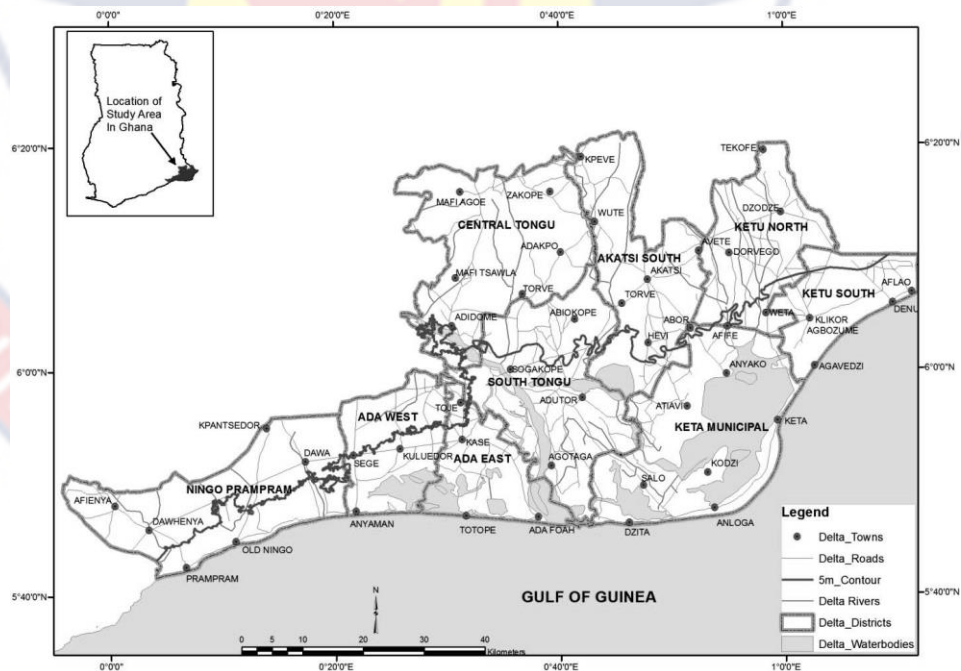
Figure 6: The Volta Delta and its administrative districts (Appeaning Addo et al., 2018b)

Additionally, the whole area is within the southern-eastern climatic zone. This makes the area affected by two air masses which are the northeast trade winds (dry) and southwest monsoon winds (moist) (Gampson et al., 2017). This results in two rainfall patterns; a minor one from August to November and a major one from March to July (Banoeng-Yakubo et al., 2006; Yidana & Chegbeleh, 2013; Appeaning Addo, 2015a). The average precipitation varies significantly and ranges from 146 mm - 750 mm annually which gradually increases north from the south (Appeaning Addo, 2015a). June is the wettest month and it has an average of 187.5 mm whilst January has an average of 10.6 mm with the annual evaporation being about 1785 mm (Yidana & Chegbeleh, 2013). The yearly average precipitation varies greatly between years, ranging from 146 mm to 750 mm (Awadzi et al., 2008).

The shorelines of the Volta Delta are actively shaped by ocean waves. Swell waves with periods of 11 s approach the beach from South to southwest (Angnuureng et al. 2016) and they have moderate to high energy plus a significant wave height of 1.4 m (Almar et al. 2015) whilst it reaches 2.5 m – 3 m with 6 s -16 s period in annual mean measurements (Nairn & Dibajnia, 2004). Due to the regular wave action and direction, the waves generate strong longshore currents that carry sediments to the east, resulting in about 1 - 1.5 x 10^6 m³/yr being moved annually (Anthony & Blivi, 1999; Nairn et al., 1999). Tides in the region are semi-diurnal tides with a tidal range of 1 m (Appeaning Addo et al., 2008). According to Angnuureng et al. (2013), the basic wind blows at an angle of about 45˚ to the coast in the same direction as the waves. The wind speed ranges between 1.7 m/s and 2.6 m/s on average monthly (Codjoe et al., 2020).

The delta coast is described as a resource-filled environment with a lot of dynamism changing constantly in space and time (Dada et al., 2016). Since the formation of the delta many years ago, it has been undergoing intense changes along the River Volta mouth since the Holocene (Nairn et al. 1999; Appeaning Addo et al., 2018). The Volta Delta, pre-construction of the hydropower dam at Akosombo, received fluvial sediment from the Volta River which sustained the shoreline of the site thereby having minimal erosion rates and huge accretion rates due to massive sediment transport and peak discharge. The construction of dams at Akosombo and Kpong in 1964 and 1982 respectively reduced fluvial sediment supply and flow discharge (Ly, 1980; Appeaning Addo, 2015a). The river's regulated flow is currently at 900 m³/s (Appeaning Addo, 2015a) and the sediment discharge has dropped from around 71 million m³/yr to around 7 million m³/yr (Boateng, 2009).

Massive swamps, grassland red mangrove areas (Kortatsi et al., 2005) and savannah woodland make up the vegetation of the Volta Delta (Manson et al. 2013). The expanding population has altered the land cover, topography, and land use in the delta region. Much vegetated land is increasingly being used for settlements and agricultural uses (Appeaning Addo, 2015a).

2.9 Historical trends of erosion and works done in the Volta Delta

There has been moderate erosion occurring along the frontal shoreline of the Volta Delta since the 1880s (Coode, 1929; Nairn et al., 1998). Since the erosions at that time were minimal no work was done to mitigate them. This changed as the erosion began to impact lives and properties. As a result of that works were scheduled to curb the new menace across the Keta region. According to Nairn et al. (1998), the first work on the region was first

41

recorded by Coode (1929). After this report, more research findings by Batley seemed to report counter information on the works of Coode. In his series of reports, Batley reported that the Keta area was not experiencing any erosions but rather diminishing due to the dynamics in the Volta River mouth (Nairn et al., 1998).

In other subsequent reports, Halcrow (1954) looked at the prospective effects of the hydropower dam at Akosombo. He concluded that the creation of the dam was going to result in the reduction of sediment deposits on the eastern coast. The first hard engineering structures were put up on the Keta coast upon the recommendation by the Department of Public Works of the country in 1960 (Nairn et al., 1998). The structure constructed was a 1,600 m long steel sea wall. Further reports by NEDECO (1964; 1974; 1980) and Delft Hydraulics (1993) suggested that there were multiple erosions and flooding that occurred after the sea wall construction. They agreed with the other reports that the erosion was shifting northwest. The idea to build groynes that will protect the shoreline between Keta and Horvie was developed in a series of reports in 1980.

Also, a report by Freedman (1955) before the construction of the hydroelectric power dam also indicated the pending effect of the Akosombo Dam on coastal erosion, especially at Keta (Nairn et al., 1998). After its construction, Ly (1980) confirmed the issues of erosion along the Volta Delta. In his report, he attributed the current occurrence of erosion and accretion situation to the trapping of fluvial sediment updrift causing the starvation of sediment downdrift. This, he says has been the major reason for the periodic erosion and flooding occurring along the area over these past few years.

42

Furthermore, Anthonio & Valentine (1995) also created a model that transformed nearshore waves to describe the dynamism in the longshore sediment moment solely on wave direction at Keta.

In recent years, studies done in the deltaic region to assess erosion and accretion have made use of Unmanned Aerial Vehicles (UAV), satellite images and video cameras. Works done by Appeaning Addo (2015a), Appeaning Addo et al. (2020), Angnuureng et al. (2019), Angnuureng et al. (2013), Jayson-Quashigah et al. (2013), Jayson-Quashigah (2019), Brempong et al. (2021) are but some few examples.

The application of medium to low-resolution satellite imageries, Appeaning Addo (2015a) used satellite images from 1986, 1991, 2001, 2004 and 2013 to assess changes in the Volta Delta shorelines. Jayson-Quashigah et al. (2021) also used historical satellite data from Digital Globe Foundation to asses shoreline changes and wave dynamics in the Volta Delta. Jayson-Quashigah et al. (2013) used medium satellite imageries from Landsat and Aster to monitor shoreline changes along the eastern coast of Ghana. Satellite images from 1986, 1991, 2001, 2007 and 2011 were used for this study and in the end, the results showed high erosion rates over the period of study. In another research by Appeaning Addo et al. (2018a), the use of low satellite images coupled with orthophoto maps were used to assess the changes in shorelines of the coastal areas closer to the Volta River. In the end, the results showed that across 125 years, there was massive erosion east of the estuary, patches of erosion and accretion at the west of the estuary and a massive erosion at the marine region of the estuary.

43

Appeaning Addo et al. (2011) assessed shoreline changes using medium-resolution satellite imageries along the coast of Keta to estimate the historic changes. Four Landsat and ASTER satellite images from 1986 - 2011 were obtained, processed and various shorelines were extracted and digitized. The digitized shorelines were merged and prepared for Digital Shoreline Analysis System (DSAS) using the statistics rate of change. The End Point Rate (EPR) and Weighted Linear Regression shoreline changes were calculated with their errors well accounted for. The results showed that between 1986 – 2001 (before the sea defence construction) erosion dominated with rates reaching -18 m/yr whilst accretion was about 19 m/yr high. The period after the sea defence between 2001 – 2011 showed that about 80 % of the coast accreted. Throughout the study period, there were patches of accretion and erosion with each hitting very high rates at certain points.

Angnuureng et al. (2013) assessed the influence of the sea defence project at Keta on the downdrift coast. In their methodology, six different dated shorelines from Landsat (satellite images), orthophotos and aerial photographs spanning from 1974 – 2011 were obtained and used for the analysis. At the end of the research, shoreline analysis between the respective years was obtained with the result indicating erosion rates of -3.2 m/yr before the construction of the project and -17 m/yr after its construction. This showed that the Sea defence project was having a knock-on effect on the downdrift side of its side.

In terms of Unmanned Aerial Vehicles (UAVs), Appeaning Addo (2011), Brempong et al. (2021), Jayson-Quashigah (2019), Appeaning Addo et al. (2018a) and a couple of others used this technology in the assessment of

44

erosion and accretion on shorelines in the Volta Delta.

Jayson-Quashigah (2019) in his research used a drone in Old Ningo, Fuveme and Keta to assess shoreline changes. The time of drone flights spanned between 2017 – 2018. He used the images to assess short-term variations in sediment volumes across all three sites. In the end, the results showed the erosion rates for Fuveme to be very high on the Western side (closer to the Volta estuary) and minimal on the Eastern side, very high at old Ningo and quite minimal at Keta.

Brempong et al. (2021) also used UAV technology to determine the short-term variations in Dzita. Drone flights were taken between May 2018 and December 2019. At the end of the study, the erosion rate for Dzita, over the entire period was -4.85 m/yr with the accretion rate at 0.00 m/yr indicating high erosion at Dzita.

Angnuureng et al. (2019) in their research, combined the usage of UAV and video camera. These two were used to assess both short-term variations and estimate longshore sediment drift at Dzita. At the end of the research, the hydrodynamic conditions including significant wave height, wave direction and period of waves around Dzita were rightly predicted and their impacts were established. The wave energy, total sediment, longshore and cross-shore fluxes over a 20 km coastline were accounted for. It was estimated that about 45 % of the sediment being transported was from the eastern side of the study site.

2.10 Coastal management in Ghana

Coastal erosion and flooding have detrimental effects on human well-being, economic activities, existing infrastructure, and the ecosystem services

provided by delicate environments (Appeaning Addo, 2015c). Coastal erosion leads to the retreat of coastlines, beach degradation, and poses threats to properties. Particularly, it heavily impacts the agriculture, tourism, and fisheries sectors and increases the risk of flooding. Floods commonly result in water pollution, outbreaks of water-borne diseases, invasion of mosquitoes, destruction of infrastructure, and disruption of activities (National Geographic Society, 2022). While not all floods cause direct harm to humans, property destruction creates long-term vulnerability and affects livelihoods (Appeaning Addo, 2015c).

Effective coastal management is essential for safeguarding and developing human, economic, and natural assets in coastal areas (Study Smarter, 2022). These measures should be collaboratively determined and implemented by the relevant stakeholders, aligning with the objectives of existing territorial public policies. Incorporating local knowledge from communities, interdisciplinary scientific studies, and technical expertise promotes the acceptability, efficiency, and sustainability of the envisioned management solutions (Alves et al., 2020).

According to scientific research, coastal erosion and/or flooding impact all West African nations, spanning from Mauritania to Nigeria, with varying degrees of severity (Alves et al., 2020). Certain regions may undergo a faster coastal retreat or experience more frequent and intense flooding compared to others (Tappan et al., 2016). Nonetheless, when considering the entire West African coastline, it becomes apparent that the risk extends throughout the region due to the significant presence of communities and properties in coastal areas along the stretch (Alves et al., 2020).

According to Croitoru et al. (2019), the population growth rate of major coastal West African cities is over 4 % and it constitutes about 1/3 of the area's human populace. With climate change, West African coastal areas will be more exposed to erosion and flooding in the coming decades, while experts' projection confirm the concentration of the region's demographic and economic growth on the coastal strip, near the ocean, increasing coastal risks.

According to Angnuureng et al. (2018), the West African coasts have been undergoing coastal erosions due to port, dam and harbour construction and these have made increased coastal management over the last few decades. Over the years, central governments have spent millions of dollars to protect their coast against climate change-related issues. From the coast of Mauritania to Sao Tome and Principe there has been an array of coastal defence structures ranging from jetties, groynes, revetments, and breakwaters (Alves et al., 2020).

In West Africa, the current management measures for coastal protection largely rely on "heavy engineering" or grey infrastructure, which involves constructing artificial structures to stabilize the coastline. One of the most commonly used coastal defence structures in the region is groynes (Alves et al., 2020), which are piles of rocks positioned perpendicular to the coast to retain sediment upstream of the wall (Study smart, 2022). In specific high-risk areas, such as Benin, Côte d'Ivoire, and Togo, where coastal erosion poses a significant threat, major breakwater construction projects have been implemented to safeguard critical locations. An example is the Abidjan port (Alves et al., 2020).

However, it has been shown that poorly maintained revetments can fail within a relatively short period. An example of this was observed in Jamestown, Ghana, where a revetment collapsed after just 15 years of use. To address this issue, a more technologically advanced and resource-efficient alternative was adopted, involving gabion-based revetments made of steel cages filled with rocks, which proved to be successful (Appeaning Addo, 2010).

These management measures are primarily focused on restoring natural coastal structures, allowing the dissipation of wave energy, and creating natural barriers against flooding. They also involve practices such as beach nourishment, dune replenishment, and the restoration of wetlands like mangroves and salt marshes. However, except for mangrove reforestation sites, which are relatively abundant in West Africa, these solutions are still underdeveloped in the region (Alves et al., 2020).

In Ghana, there has been an Integrated Coastal management plan in place which was commenced in 1995 (Hewawasam, 1998). According to Hewawasam (1998), the main objective of the plan was 'to determine whether coastal zone initiatives and projects were appropriate from an economic, social, and environmental standpoint', considering about 30 % of the population resides in these areas (Ashong & Gbeckor-Kove, 2022). The programme used a very interactive approach to identify the problems and interventions with a series of regional workshops held under the direction of the Environmental Protection Agency, which solicited input from stakeholders at the national, regional, local and community levels (Hewawasam, 1998). According to Appeaning Addo (2015c), Ghana uses reactive, site-specific, and

48

typically harsh engineering measures to manage coastal erosion. The government's existing methods are environmentally harmful and unsustainable (Appeaning Addo, 2015c).

Ghana's coastal zone is home to a wide range of ecosystems including sandy and rock beaches, estuaries, lagoons and mangrove stands (Anim et al., 2013). These areas provide vital benefits and services to folks living in and around them. Most people living in the coastal areas depend on these ecosystems mainly for food and productivity. For instance, it is estimated that about 10 % of the rural populace is employed in the fisheries and aquaculture value chain alone which has contributed to about 1% of the Gross Domestic Product (GDP) of Ghana's economy. The transportation, petroleum, tourism and energy sectors also contribute significantly to the economy just as the fisheries and aquaculture sector (Ashong & Gbeckor-Dove, 2022) and thus the need for coastal management to effectively protect and govern these areas.

In Ghana, two main approaches are taken to combat coastal erosion namely; the hard engineering approach and the soft engineering approach. The former is the most used as it holds and protects the area it is employed in (Alves et al., 2020). Hard engineering structures including groynes, jetties, and revetments have been used along the entire coast of Ghana to mitigate erosion.

Groynes have been built perpendicularly into the sea to reduce erosion. These structures trap sediment preventing it from straying too far inland. Concrete and less often wooden revetments are built acting as barriers against wave impact (Appeaning Addo, 2015c). They accelerate erosion elsewhere while stabilizing the beach in the protected area. On locations deemed to be extremely vulnerable, the government has also carried out significant maritime

49

defence projects. These include sea defence structures at Keta, Cape Coast, Atorkor, Elmina and other areas. Revetment and groynes were used in tandem for these constructions (Alves et al., 2020). However, in most instances, the site-specific actions are having a domino effect. For instance, due to sea defence structures at Keta, the down-drift coast near the Ghana-Togo border has seen a 50 % increase in coastal erosion (Angnuureng et al., 2013).

Seawalls have also been used as sea defence structures along some coastal areas in Ghana. An example is a seawall that was used to protect parts of the coast of Keta in 1956 but was destroyed after it failed (Nairn et al., 1999). Jetties have been built at Elmina Benya Beach to reduce the erosion of the tidal inlet of the lagoon (Angnuureng et al., 2022).

2.11 Chapter Summary

A lot of literature was reviewed in this chapter. The coastal areas including beaches and estuaries and the various processes that affect them have been reviewed. Sediment and sediment transport, the use of UAV in morphodynamic monitoring and the MIKE 21 model were also duly reviewed. In this chapter, it has been established that sediment transport-related works are scarce and research must be done into them using UAV and numerical models.

50

CHAPTER THREE

MATERIALS AND METHODS

3.1 Introduction

This chapter covers the study area description, various data collection procedures and methods used, research instruments, and the different approaches used in data analysis.

3.2 Description of Study Area

The newly created 'bridged estuary' (5° 46' 22.80" N 0° 41' 52.7994" E) is located at Fuveme, a suburb of Anloga in the Volta Region. It is about 1 km downdrift of the Volta Estuary (Figure 7) which is within the Volta Delta. The newly created estuary on the coast of Fuveme forms part of the eastern stretch of Ghana's coast. Typical of Volta Delta shorelines, the coast of Fuveme is wave dominated by moderate to high energy with long wave periods (Appeaning Addo et al., 2018a). A wave period of about 11 s and a significant wave height of about 1.4 m approach the coast of Fuveme (Angnuureng et al., 2013). Swell waves approach the study area uninterrupted from the south-southwest direction (Angnuureng et al., 2016). Semi-diurnal tides, with a meter range, are experienced off the coast of Fuveme (Appeaning Addo et al., 2008). Normally around September - October some migratory birds visit the small lagoon on the eastern side of the area closer to the river. The detailed oceanographic conditions, climatic conditions and vegetation of the area are covered in detail in Section 2.8.1.
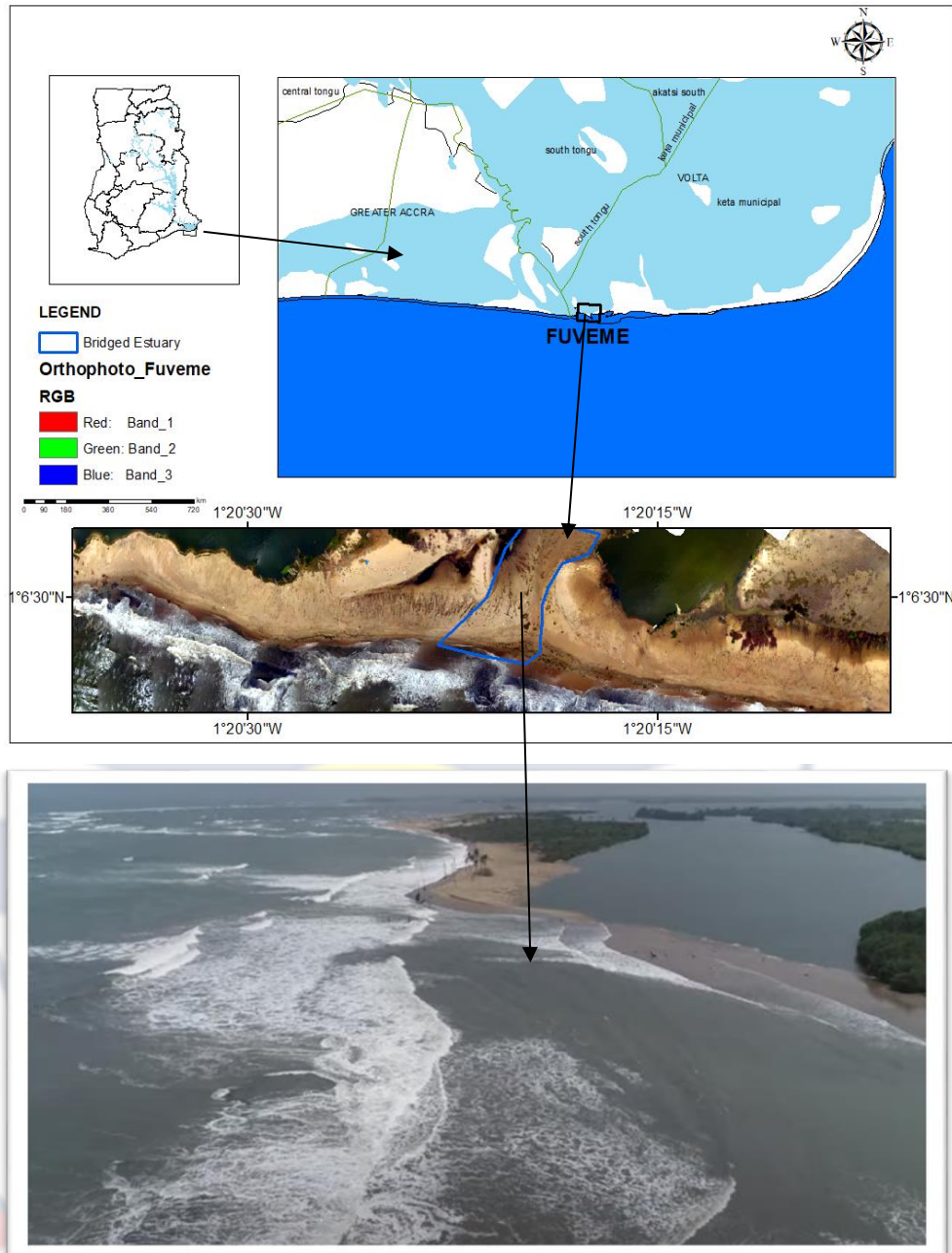
Figure 7: An image of the study area

3.3 Data Collection

3.3.1 Unmanned Aerial Vehicle (UAV) data

The data required for objectives 1 and 2 were largely dependent on Unmanned Aerial Vehicle (UAV) surveys. This survey helped to take aerial images needed for shoreline changes, sediment volume changes, beach profiles and the building of georeferenced shorelines and Digital Elevation

52

Models (DEMs) for MIKE 21 model. With a 4k camera (12 megapixels), a DJI Phantom IV was used to take aerial images of the beach.

Ground Control Points (GCPs) were built with well-labelled concrete pillars, buried into the ground (Figure 8a) before drone flights of the area were taken as done by Brempong (2019). This was vital for accurate georeferencing of aerial images taken.
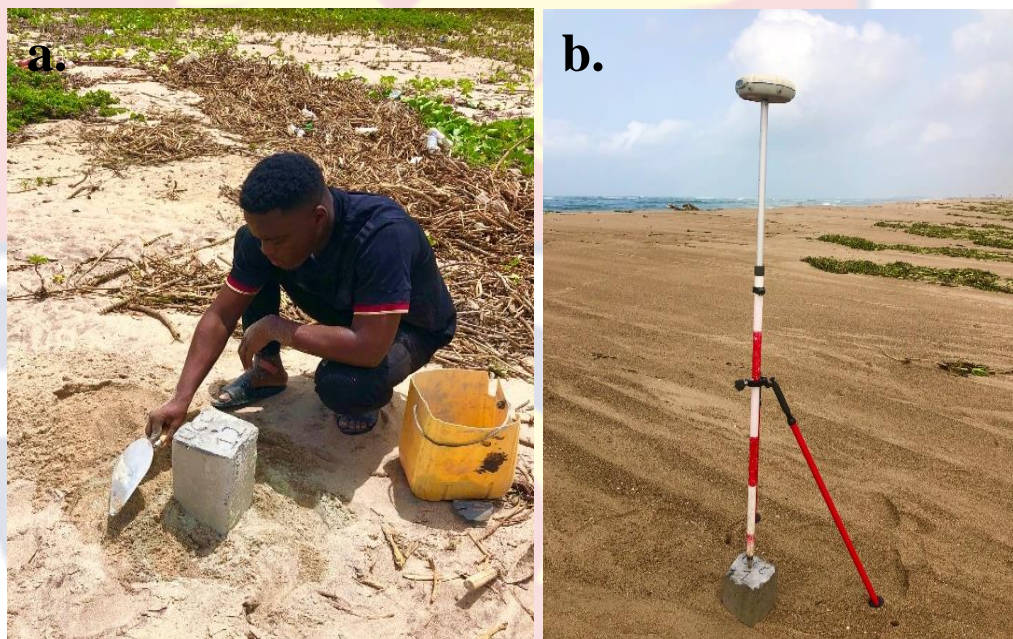
Figure 8: a) Establishment and b) coordination of Ground Control Points (GCPs) at Fuveme Beach

Once all the GCPs were firm into the ground, coordinates (x, y and z) were obtained using a static Differential Global Positioning System (DGPS) as shown in Figure 8b. This was performed by connecting the DGPs to a base station to obtain referenced x, y and z coordinate to the national grid. On average, the DGPS was kept on each GCP for a period of 45 mins to minimise errors. The data gathered was then processed using Topcon software to get the coordinates to the nearest millimetre. A total of 12 georeferenced points, which were enough for photogrammetric analysis, were mounted and used for this study (Wolf et al., 2000).

A flight plan for the drone was drawn using the Flight Deploy application. This was done to issue instructions to the drone on how to take the images and places of interest to capture for the study. The drone took images from 70 m above the ground to capture the full extent of the beach, covering 2.6 km length of the area and a width of 30 m with a ground resolution of 0.03 m/px. Additionally, front and side overlaps of 80 % and 70 % respectively were pre-defined in the flight plan setting to improve stereoscopy and 3D reconstruction (Jayson-Quashigah, 2019). The flight normally lasted for 30 – 60 minutes depending on wind conditions. The drone was normally flown during low tides so that the watermarks were easily identified during image processing. Printed GCPs platforms were placed on the GCP pillars before each flight so that during pre-processing analysis, they would be easily identified. The GCPs were built and planted across the whole study area so that for every 150 m – 200 m one GCP was found as shown in Figure 9. The dates of flights throughout the period are shown in Table 2.

54
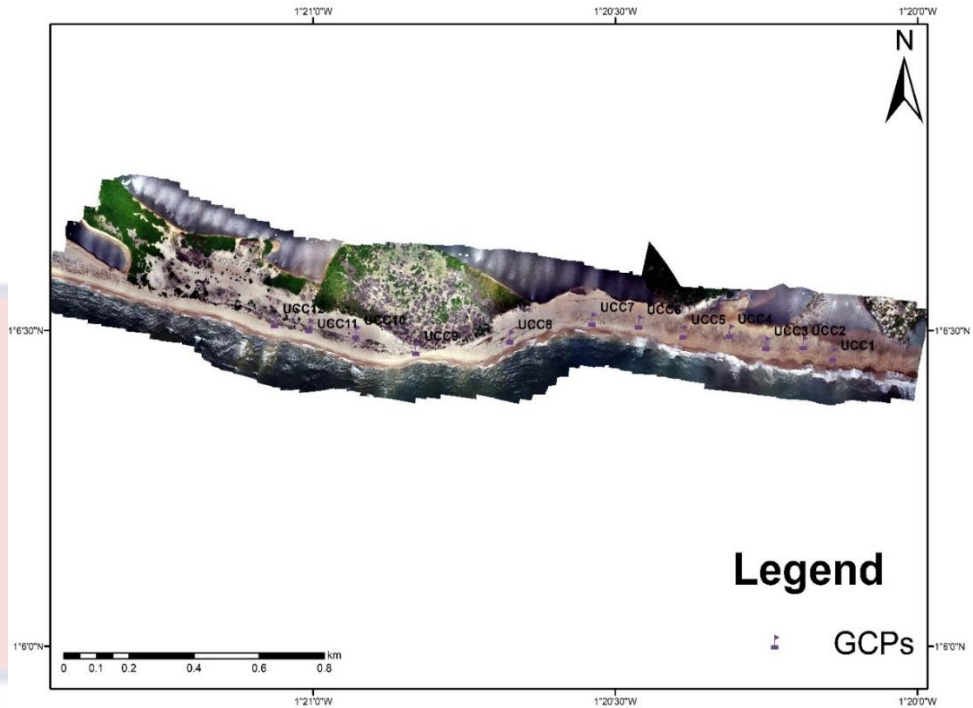
Figure 9: The distribution of GCPs across Fuveme Beach

Table 2: *Dates of UAV flights*

Site	Date of Flight
Fuveme (1km from the Volta Estuary)	22nd October 2021
	03rd March 2022*
	21st April 2022*
	17th May 2022
	13th June 2022
	07th July 2022
	07th September 2022*
	13th October 2022

*Images were not used for analyses due to technical errors.

3.3.2 Bathymetry Data

As one of the crucial parameters for the MIKE 21 model, the bathymetry of the sea closer to the coast of Fuveme was measured and recorded. This was done using a MIDAS Surveyor echo sounder. The echo

55

sounder, together with its transducer and GPS, was carefully mounted on a vessel to receive signals. Once the GPS and transducer were all logged to the echo sounder the data collection started. The echo sounder was programmed to start the data collection from inland the Volta River through the mouth of the estuary and to Fuveme then back to the mouth of the estuary. Once this was done the data, including the x and y coordinates, the depth and the date/time of data, from the echo sounder was downloaded and processed in ArcGIS 10.4.1 software.

3.3.3 Water Level Data

The surface elevation is another parameter needed for this study, especially for objectives two and three. The HOBO water data logger was deployed into the Volta River to generate water levels for days at specific times. The water logger measured the temperature and the atmospheric pressure simultaneously at 15 minutes intervals. These two parameters were then processed using MATLAB 2021B to get the water level data for the entire period.

3.3.4 Wave Data

In order to force the SW module, hindcast wave data were downloaded from Era-Interim Global Reanalysis (C23, 2017). This consisted of significant wave height, mean wave direction and peak wave period as shown in Figure 10. The wave data was taken as a polygon between the Volta estuary and the end of the Fuveme area. The wave data was downloaded from April 2022 to August 2022. In order to validate the wave data for the simulation, another wave data was obtained from Copernicus Marine and Environmental

56

Monitoring Services (CMEMS) which was made up of daily Significant Wave Heights from April 2022 – August 2022.
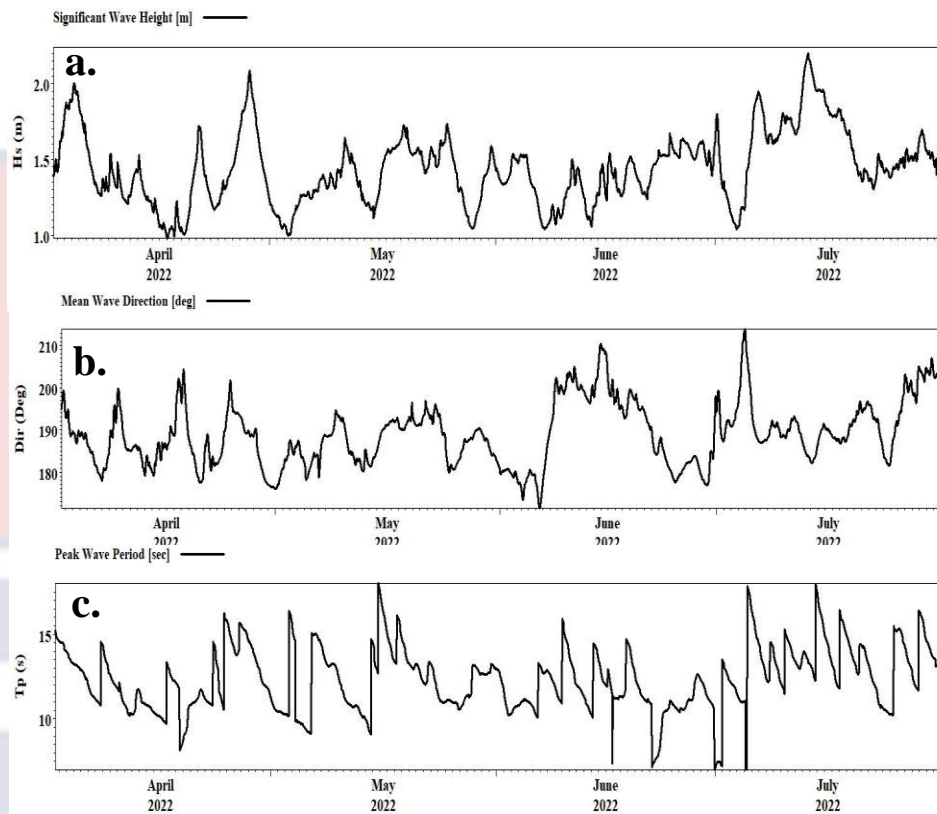
Figure 10: Hydrodynamic conditions at Fuveme Beach a) Significant Wave Height b) Mean Wave Direction c) Peak Wave Period (C23, 2017)

3.3.5 Sediment Characteristics

Sediment samples from Fuveme were taken along the beach from the Low Water Line (LWL), berm and backshore from five stations across the area. Sediment samples collected were kept in tight Ziplock bags and transported to the laboratory for further analysis (Dzakpasu, 2019). About 200 g of well-dried samples were poured into a 0.05 mm (50 µm) mesh sieve and washed thoroughly with 10 % NaOH solution to break the bonds between the particles. All the finer particles were washed away and then the remaining samples were pre-weighed in aluminium foil trays and dried at a temperature of 105 °C in an oven. This was done until a fair weight was obtained. The

57

samples which were dried in the oven were weighed to account for the weight loss. 100 g were then collected, weighed and sieved through a set of sieves of different mesh sizes (4 mm, 2 mm, 0.5 mm, 0.125 mm) and a collector (pan). Samples retained in each sieve were collected, weighed and recorded. Calculations were made for the weight of each sieve fraction in percentages using equation 3.1 below:

$$\text{composition of sieve content(\%)} = \frac{\text{weight of sieve content}}{\text{weight of dry samples}} \times 100 \qquad 3.1$$

Using the calculation method by Yankson (2000) and adopted by Dzakpasu (2019), the Mean Particle Size (MPS) was calculated using equation 3.2 as:

$$MPS = \frac{\sum(x.Y)}{100} \qquad 3.2$$

Where x = mean size (mm) and Y = corresponding percentage composition. The Mean Particle Size calculated was then compared to the Wentworth classification as shown in Table 1.

3.4 Data Processing and Analysis

3.4.1 UAV Data

About 300 images were captured for each flight. These images were uploaded such that those blurred were removed using Agisoft Metashape PhotoScan (AMP) software. Uploaded images were used to rebuild 3D scenes in AMP (Agisoft, 2022). According to Sona et al. (2014), AMP's algorithms gave better results as compared to other software (Jayson-Quashigah, 2019). The structure from motion analyses (sfm) includes image alignment which involves the detection, matching of image features, providing the basic image structure, pixel-based dense stereo reconstruction using the aligned data, ground control points and the building of DEM and orthophotos. The DEM

58

was categorized to only capture as much bare ground as possible, reducing the exaggeration of topographic heights. Images captured after each flight were uploaded into AMP and aligned by detecting points in the images captured. This led to the formation of point clouds together with the orientation and positions of the images. After this, all marker positions were identified on the printed GCP platforms in the images and labelled as distributed. This helped to optimize camera positions and orientations to obtain better model reconstruction results. The positions of the twelve surveyed markers were then imported into AMP to georeference the images. The importation of the twelve coordinated markers recalculated the positions of the images giving them georeferenced positions, orientations and coordinates. After this, the depth information was generated for each camera and used to generate a single dense cloud with a Red, Green and Blue (RGB) scale. Using the RGB dense cloud, a Digital Elevation Model (DEM) was created and an Orthophoto (Figure 11) was generated as well. These were then exported in Ghana Metre Grid coordinate system in the tiff file. The whole process normally lasted 16 hours for each flight processing.

59
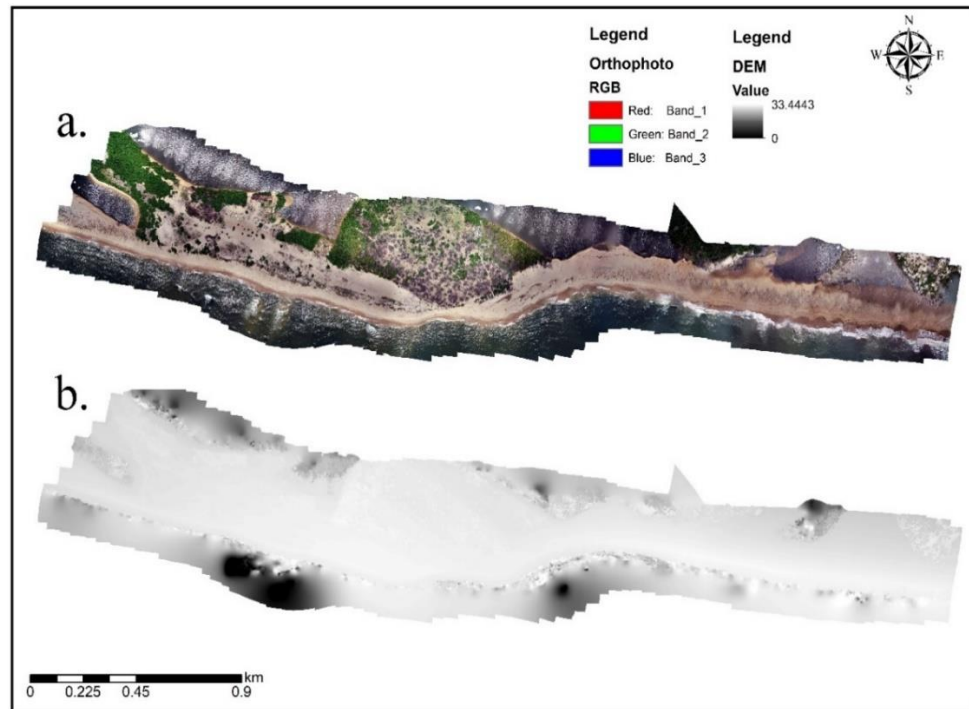
Figure 11: Images of a) Orthophoto and b) Digital Elevation Model (DEM) of Fuveme area

3.4.2 Shoreline extraction

For shoreline extraction, numerous proxies have been adopted including vegetation lines, high and low water lines (Appeaning Addo, 2009). According to Brempong (2019), the High Water Line (HWL) has been utilized mostly in previous studies and it was used for this one as well. The HWL can be detected as a change in tone left by the maximum run-up from a preceding high tide and was used because it was easily identified in the processed drone images for this research (Jayson-Quashigah, 2019). The HWL was easily identified on orthophotos and was digitized in ArcGIS 10.4.1 software.

3.4.3 Analysis of shoreline changes

The Shoreline change analysis was performed using ArcGIS 10.4.1 software and Digital Shoreline Analysis System (DSAS) version 5.1, an extension of the ArcGIS tool developed by the United States Geological

60

Survey (USGS). DSAS was used for shoreline analysis because it calculates rate-of-change statistics from a time series of vector shoreline positions (Himmelstoss et al., 2018). DSAS was used to generate orthogonal transects starting from a reference baseline and intersecting the shoreline positions at 20 m intervals. A baseline was constructed by manually digitizing the shoreline about 60 m offshore away from the closest shoreline. Transects were then constructed with a total of about 130 transects being cast. The transects were cast at simple right angles from the baseline offshore for the coastline. The distance measurements between the transect intersections and the baseline were then used to calculate the rate-of-change statistics (Romine et al., 2011).

All the extracted shorelines were merged into one shoreline and given appropriate attributes. For rate of change estimation, End Point Rate (EPR) and Net Shoreline Movement (NSM) were calculated. The NSM calculates the distance between an old and the youngest shoreline in meters. The EPR calculate the distance between the oldest and the youngest shoreline over time elapsed (Himmelstoss et al., 2018).

3.4.4 Estimation of errors for shoreline changes

According to Jayson-Quashigah et al. (2021), there are four errors associated with shoreline positional accuracy and they include; the ground sampling distance (E_p), geo-referencing error (E_g), which is obtained from the average RMSE from geo-referencing, the digitizing error (E_d) which is also estimated to be 1.5 of a pixel and tidal error (E_t). For this study, three errors were associated with the shoreline including E_p, E_g and E_d. The overall positional error (Er) for each shoreline was then estimated using the expression in equation 3.3:

61

$$\text{Er} = \sqrt{\text{Ep}^2 + \text{Eg}^2 + \text{Ed}^2} \qquad\qquad 3.3$$

where Ep was 0.03m, Eg was 0.2m and Ed was 0.15m

In order to get the rate annually, equation 3.4 was used given by:

$$Ex = \frac{\sqrt{\text{Ea}^2 + \text{Eb}^2 + \text{Ec}^2 + \cdots \text{Ez}^2}}{\text{T}} \qquad\qquad 3.4$$

where E_a, E_b, E_c, E_d and E_e are individual shoreline positional errors and T is the time period (Jayson-Quashigah, 2019). For this study, the time elapsed (T) was 1 year.

3.4.5 Geomorphic Change Detection

The standard DEM of Difference (DoD) method, a geomorphological estimation method by Brasington et al. (2000) was used for sediment estimation. This was done by subtracting an earlier DEM (Z_1) from a newer DEM (Z_2) as shown in equation 3.5:

$$\Delta DEM = Z_2 - Z_1 \qquad\qquad 3.5$$

where 'ΔDEM' = DoD, Z_2 = newer DEM and Z_1 = earlier DEM

The individual total RSME from the image processing was used as the uncertainty for each DEM. The total RMSEs for the DEMs were propagated as shown in equation 3.6:

$$\delta u = \sqrt{(\delta z_1 + \delta z_2)} \qquad\qquad 3.6$$

where δu is the propagated error, δz_1 and δz_2 are errors from the individual Digital Elevation Models. This propagated error was used as a minimum level of detection threshold (minLoD) to distinguish actual surface changes from the inherent noise (Brasington et al., 2003; Wheaton et al., 2010).

3.5 Sediment evolution using MIKE 21 model

MIKE 21/3 Coupled was used to simulate sediment evolution along the study site. It is a 2D modelling system for regional and coastal water bodies

62

using realistic or idealized multiscale approaches. Its application areas include Water Resources, Coast and Sea, Groundwater & Porous Media (MIKE, 2017). The MIKE 21 package was used extensively for this objective and it includes the MIKE Zero, Flow Model (FM) and Spectral Wave (SW).

MIKE Zero contains time series (.dt0 and .dfs0) used purposefully for wave, tide and water level data generation for the Hydrodynamic Flow Model (HD FM) and Sand Transport (ST FM) and it also contains a mesh generator (.mdf) used to generate the mesh of an area given a referenced bathymetry (.xyz). Additionally, MIKE Zero contains a toolbox (.mzt) which is also used to generate a sediment transport table (.ion) as input data for the Sand Transport Flow Model (ST FM).

3.5.1 Model configuration

3.5.1.1 Bathymetry and topography

Mesh generation is very vital for any simulation in MIKE 21. This serves as a computational domain on which the whole simulation occurs. It is an ASCII file that contains information on the geographical positions, the bathymetry of each node point and the node connectivity as well (MIKE, 2020a). For this research, the bathymetry information was obtained from an echo sounder and complimented by GEBCO (General Bathymetric Chart of the Oceans) data. All three were uploaded to ArcGIS 10.4.1 processed, digitized and converted to x, y and z points for the model. For land topography, the shorelines from Planet images and Orthomosaic images from drone flights were used.

All points from ArcGIS were uploaded to MIKE 21 (Figure 12) with the geographic reference as WGS 1984 UTM Zone 31N. The Mesh generator

in MIKE 21 Toolbox was used to prepare the mesh of the area (MIKE, 2017). The mesh was generated using nodes, arcs and polygons. The nodes were 1234 and the elements were also 2131. The generated mesh was refined by 1 bisector and interpolated using the natural neighbour to aid in the bathymetry generation. To determine the natural neighbour areas, a triangulated irregular network was constructed using the scatter data points in the dataset uploaded. Two areas were defined in the mesh generation; the land boundary and the offshore boundary. The land boundary was given a code of 1 for arc property whilst the offshore boundary was given a code value of 2. After this the bathymetry of the domain was generated (Figure 13). Points on the offshore boundary were selected and used to generate water level boundaries from the DHI global tide model.
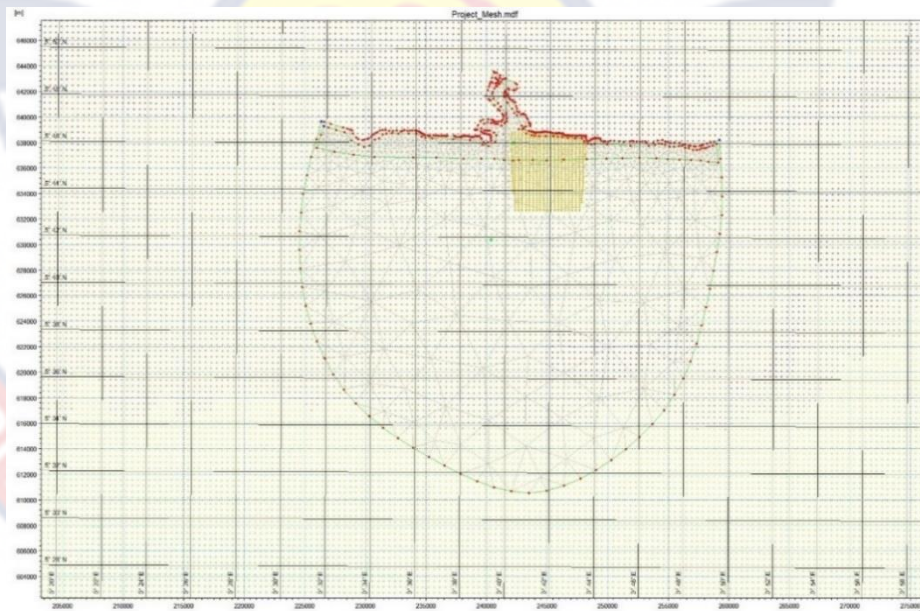
Figure 12: A scatter data of the domain in MIKE 21
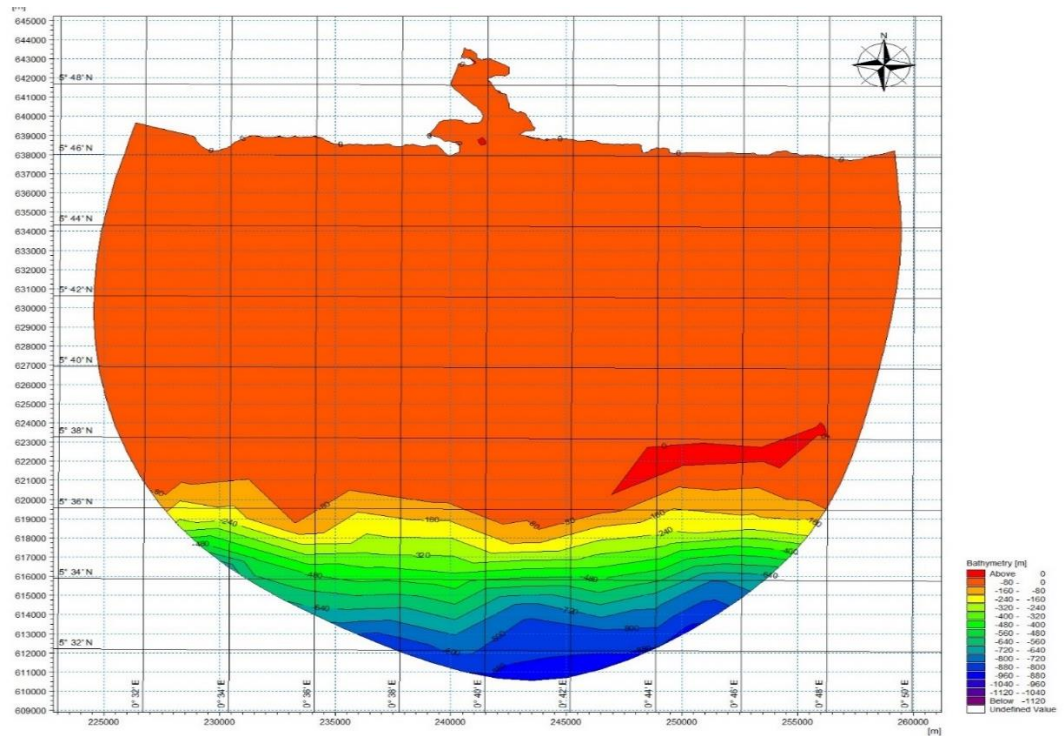
Figure 13: The bathymetry (m) of the study domain

3.5.1.2 Tides prediction data

The tides prediction data was used as a forcing in the Hydrodynamic module. This set of data was generated in MIKE 21 toolbox (MIKE, 2017). The tidal prediction of heights was used to generate this data with 15 coordinates selected within the area. The start date and time together with the time interval were inputted as well. After about two minutes, the Global tide prediction of height was generated for the area. The water level data from the HOBO water logger, which was left in the river for some days anytime I went to the field, was also generated using MATLAB and used to validate the Global tides data.

3.5.1.3 Wave parameters

Daily hindcast wave data from 1st April – 1st August 2022 was used as input for the wave data generation in the model. The input included SWH, PWP and MWD and the Dimensionless Factor. An Ascii file was generated

65

using the MIKE Zero Time series plot (MIKE, 2017). The axis type for the asci file included Equidistant Calendar Axis, a start time of 01st April 2022, 12:00 am and a time step interval of 1800 s. The time step was 3672 and this corresponded to the end date of 1st August 2022, 12:00 am. The wave data was saved as Wave_Data_Apr_Aug_22 and then generated as a .dfs0.

3.5.1.4 Grain size of sediment samples

The MPS (Table 3) analysis showed that coarse sand dominated the low water line and the backshore areas whilst the berm area was dominated by medium sand. The d_{50} was also calculated for the berms using GRADISTAT v8 and the results were 0.54 mm, 0.18 mm, 0.15 mm, 0.17 mm, and 0.17 mm for stations 1, 2, 3, 4 and 5 respectively. The average (0.250 mm) was used as an input for the sediment grain size for the ST module.

Table 3: *Sediment grain sizes for the various stations*

Stations	Low Water Line (LWL)	Berm	Backshore
S1	0.52	0.51	0.65
	Coarse Sand	Coarse Sand	Coarse Sand
S2	0.44	0.22	0.28
	Medium Sand	Fine Sand	Fine Sand
S3	0.97	0.44	0.60
	Coarse Sand	Medium Sand	Coarse Sand
S4	0.81	0.47	0.68
	Coarse Sand	Medium Sand	Medium Sand
S5	0.53	0.45	0.62
	Coarse Sand	Medium Sand	Coarse Sand

3.5.2 Model setup

The HD and SW modules were used as the basis to run the ST module. The mesh and bathymetry generated were uploaded into the mesh and bathymetry domain. The material and infrastructure sections were unchecked because there were no structural inputs. The time section, specifying the simulation period was 5184 with a time step interval of 1800 s. The stimulation start date was 15th April 2022 and the stimulation end date was 1st August 2022.

3.5.2.1 Hydrodynamic module

For the hydrodynamic module section, the first sub-section was the solution technique and this consisted of the shallow water and the transport equations; time integration and space discretization. The two subsections were checked to a higher order to attain accurate results. To get the stability of the simulation, the minimum time step, maximum time step and the critical CFL number for shallow water were checked at 0.01 s, 1800 s and 0.45 respectively. The depth and the depth correction type were unchecked as there were no specified bed level change data. The flood and dry sections were included at constant values as suggested by MIKE (2020a) as 0.005, 0.05 and 0.1 for drying depth, flooding depth and wetting depth. This was done to ensure the stability of the flow velocity and the simulation as a whole. The density type was checked at barotropic to keep the density and temperature fairly constant within ranges as suggested by MIKE (2020a).

The Smagorinsky formulation parameter in the HD module which is to express sub-grid scale transports by an effective eddy viscosity related to a characteristic length scale was expressed as done in equations 2.12 and 2.13.

The Smagorinsky formulation was used for the Horizontal Eddy viscosity and the format was kept constant with a value of 0.45. The Eddy parameters were inputted as 0.0000018 m²/s and 100000000 m²/s for minimum and maximum eddy parameters respectively. The Coriolis type, the precipitation-evaporation, ice coverage and the infiltration section were all unchecked. The tidal potential was also unchecked as a precaution by MIKE (2020a) since it is very weak and can be negligible. For wind forcing, the wind speed and direction were kept constant at 2.5 m/s and 227 °.

For bed resistance, the resistance type was the manning number and was kept at a constant value of 37 $m^{1/3}$/s. This was used to ensure the stability of the simulation as shown in equation 2.14.

The structures section was unchecked since there are no weirs, culverts, dikes and others at the study site. The decoupling section was left unchecked as the flux, area and volume were not expected as outputs for this particular objective. The initial conditions containing the surface elevation, initial velocity (u-velocity) and final velocity (v-velocity) were uploaded in a .dfsu file containing a pre-run simulation from 15th April – 30th April 2022 to help kickstart the simulation. The boundary conditions were kept as generated in the mesh process as the land boundary and offshore boundary.

The final process for this module was the creation of an output (.dfsu) which shows how the file outcome should look like. The output specifications included data and time step subsections. The data subsection includes the field type, data type output format, flood and dry. The field type was checked as 2D (horizontal), the data type was checked as discrete values, the Output area was checked as Area series and the flood and dry was checked for the whole area.

The time step was checked to use simulation start and end times. The output file was saved as *'Final_Project_HD. Dfsu'*.

3.5.2.2 Spectral Wave module

The Spectral Wave is based on the directional parametric formulation. This is made in the frequency domain y introducing the zeroth and first moment of the wave action spectrum as dependent variables as described by Holthuijsen et al. (1989) in equations 2.15 and 2.16. The Directional Decoupled parametric formulation and Quasi Stationary formulation were checked for Spectral and time formulation respectively. The time parameter start time was checked to 0. The spectral discretization which consists of frequency and directional discretization was checked at logarithmic and 360 degrees rose respectively. The number of directions was left at 16. The solution technique made up of the Quasi-Stationary formulation was checked for several sections. The Geographical Space Discretization was checked at higher order for accurate results. The method used was the Newton-Raphson iteration as suggested by the model manual to ensure stability. The maximum iterations and relaxation factor were checked at 500 and 0.1 respectively. The Tolerance for RMS-norm of residual and Maximum-norm of change in Significant Wave Height was pegged at 0.0001 and 100000 m respectively. The water level and current variation were from the Hydrodynamic module. The wind forcing was also pegged at 2.5 m/s and 227° similar to the Hydrodynamic module. The ice coverage was left unchecked.

The diffraction approximation is based on the mild slope for refraction and diffraction. The diffraction was checked and the smoothing factor was pegged at 1. The number of smoothing steps was 5. The wave-breaking type

69

used for this study is the Specified Gamma, with a constant value of 0.28. The Alpha and Gamma were 3 and 1 respectively to ensure stability. The 'include effect on mean frequency' was left unchecked as a precaution to stabilize the simulation.

Bottom friction is one of the calibrating parameters of this module. The sand grain size, d50 was checked for bottom friction due to the nature of the area. The sand grain size was checked at 0.00025 m. The current friction was set to zero. Include effect on mean wave frequency was checked. Since there were no structures points or line structures in the area there were left unchecked.

The initial condition was a spectral file of a pre-run simulation containing the Significant Wave Height, Peak Wave period, Mean Wave Direction and Dimensional Factor from 15th April – 30th April 2022. The boundary conditions were left as the generation of the mesh. The offshore boundary was checked as Wave parameter (version 1) with a wave file generated serving as input.

Once all these parameters were defined, the output file was generated with output specification, integral wave items, model items and input items all well-defined. For the output specification, data, time step and area series were all defined with filed type-checked as parameters, data type-checked as discrete values, output format checked as area series, the flood and dry checked as the whole area with the output file saved as *'Final_Project_SW.dfsu'*. The time step defines the simulation start and end with the frequency checked at 1.

3.5.2.3 Sand Transport module

The foremost thing done in the sand transport module was the generation of Quasi-3D (Q3D) sediment table. In the Q3D table generation, the tolerance in calculation of calculation was 0.00001, maximum number of wave periods, 1000, steps per wave period was 140, relative density of sediment was 2.65, critical value of shields parameter was 0.05 and the water temperature was pegged at man temperature of 28 °C (Codjoe et al., 2020). The ripples and streaming effects were included but the bed slope, density currents and centrifugal acceleration were all excluded in the sediment table generation as a precaution (MIKE, 2020c). The bed concentration was checked at deterministic. The Stokes theory was the wave theory assigned since the simulation was based on the current-wave type. The breaking wave parameters for Gamma 1 and 2 were set to 1 respectively and the order of solution was set to 5. The Sediment table Axis parameters were inputted as shown in Table 4. The last three parameters were kept content as per the model calibrations.

Table 4: *Sediment table axis parameters for the various parameters in ST table generation*

Sediment Table Axis parameters	First Value	Spacing	Number of Points
Current Speed	0.05	0.1	5
Wave Height	1.2	0.2	8
Wave Period	10	1	3
Wave Height/Water Depth	0.01	0.1	8
Angle Current/Waves	0	30	12
Grain Size	0.25	2.000	3
Sediment grading	1.1	0.15	3
Bed slope, current direction	-0.01	0.01	3
Slope, normal to current	-0.02	0.02	3
Centrifugal acceleration	10	0.001	1

71

The main sand transport type used was current and waves. The current and waves was used due to the influence of both waves and currents in sediment transport on the shores of Fuveme. The sediment porosity which is the volume of sand was kept constant at 0.4. The median grain of 0.25 mm and the grading coefficient was 1.1. The spectral wave simulation was used as a forcing for the wave field. For the morphology, the max bed level change was left at 1 m/day with a speed factor of 1. The feedback on hydrodynamic, waves and sand transport were included. No bank erosion was included. The offshore boundary format was zero sediment flux gradient for outflow. The output specifications were similar to the spectral wave and hydrodynamic module. The output items included bed level change, bed level, total load - magnitude and total load - direction.

3.5.3 Model calibration

The model was calibrated using some parameters within the individual models to get accurate results. These parameters were run multiple times to tune the model to the conditions before proceeding to the final simulation. For the hydrodynamic module, the horizontal Eddy viscosity (eddy type) was mainly tweaked to get the right eddy parameter. The Smagorinsky formulation constant which is normally between 0 and 1 was changed several times before it was left at a constant of 0.45. The bed resistance, Manning number, was also changed from the constant value of 32 $m^{1/3}$s to 37 $m^{1/3}$s. To attain stability in the HD module the CFL number was also changed from 1 to 0.58 for the module to run.

For the Spectral wave, the diffraction was left at 1 for smoothing factor and 5 for smoothing steps. The white capping which primarily controls the

72

steepness of the waves was left at 4.5 and the delta, dis was also left at 0.5. For sand transport, most of the simulations were often from the influence of the HD and SW simulations so no calibrations were done.

3.5.4 Keeping parameters unchecked to alternate results

After multiple runs, the model was calibrated with results having good Root Mean Square Errors (RMSE) which were good for the simulation. In order to fully achieve the third objective, some parameters were kept constant after the model was well calibrated. In order to know the hydrodynamic conditions that affected the coast of Fuveme the most, the wave, water level (surface elevation) and current were unchecked during some times of the simulation. Using the bathymetry and the mesh generated as a base for all parameters together with other secondary parameters such as the CFL number, bed resistance, bed friction and the Smagorinsky formulations. In order to check the effect of waves, no wave parameters were activated in the simulation. In order to check for current, the currents from the HD and SW modules were not checked. In order to check the effects of surface elevation, no water level was included in the simulation.

3.5.5 Model limitation

The first and foremost issue has to do with the bathymetry data used for the area. There was a bathymetric survey but it was not enough to capture the whole area and so the bathymetry was coarse and did not perfectly represent the area even with additional bathymetric data from GEBCO. The wave parameters used for the study were also from secondary sources making the validation quite difficult. The results could have been better with on field data of these parameters or proper data from the right agencies in the country.

Despite these drawbacks, the model was deemed to be a good representation of the local conditions after sufficient calibrations were made as shown in section 4.3.

3.6 Chapter Summary

This chapter provided information on the materials and methodology used for the study. The study area, "newly created estuary" at Fuveme, was described with the various oceanographic, geologic conditions described. Data collection for drone, bathymetry, water level, waves, sediment and tides were described including dates and times all the data sets were taken. The pre-processing and post processing of these data sets were also described in this chapter. Appropriate statistical analyses were performed on pre-processed data sets to obtain great results. The process used to simulate sediment movement involving MIKE 21 model was described in details. The model calibration and limitations were also described to ensure best results were generated for the second and third objectives as well.

CHAPTER FOUR

RESULTS

4.1 Introduction

This Chapter covers results including shoreline changes, sediment volume dynamics and profiles extracted from DEMs and Orthophotos. The validation results between the modelled values and observed values and results from the simulations.

4.2 Results from Unmanned Aerial Vehicle images

4.2.1 Shoreline dynamics

Overall, shoreline changes showed varying patterns of accretion and erosion. To assess the pattern of shoreline changes for the entire period, shoreline changes were analyzed between October 2021 and May 2022, May 2022 and June 2022, June 2022 and July 2022, July 2022 and October 2022 and finally October 2021 and October 2022. The coast of Fuveme was dynamic over the twelve months study period, dominated strongly by erosion on the western side with the central and eastern sides experiencing accretion (Figure 14). The results for the average NSM are shown in Table 5. Between October 2021 and May 2022, the average land lost was -39.76 m and average land gained was 24.81 m as shown in Figure 15. Between May 2022 and June 2022, average land lost and gained were -7.17 m and 7.57 m, respectively as shown in Figure 16. Between June 2022 and July 2022, average land lost gained were -8.47 m and 5.41 m, respectively indicating a very strong erosion as shown in Figure 17. Between July 2022 – October 2022, average land lost was -12.28 m and that of land gained was 24.24 m indicating a major deposition as shown in Figure 18. During the entire period, the NSM recorded

75

for both average land lost and gained were -46.44 ± 0.25 m/yr and 58.41 ±

0.25 m/yr as shown in Figure 19.

The End Point Rate (EPR) for the entire period was -48.43 ± 0.25 m/yr

for erosion and 60.91 ± 0.25 m/yr for accretion as shown in Table 6. A graph

of the EPR is shown in Figure 19 and the mean NSM and EPR were -18.07 ±

0.25 m/yr and -18.96 ± 0.25 m/yr respectively, which means for the entire

period erosion was dominant.
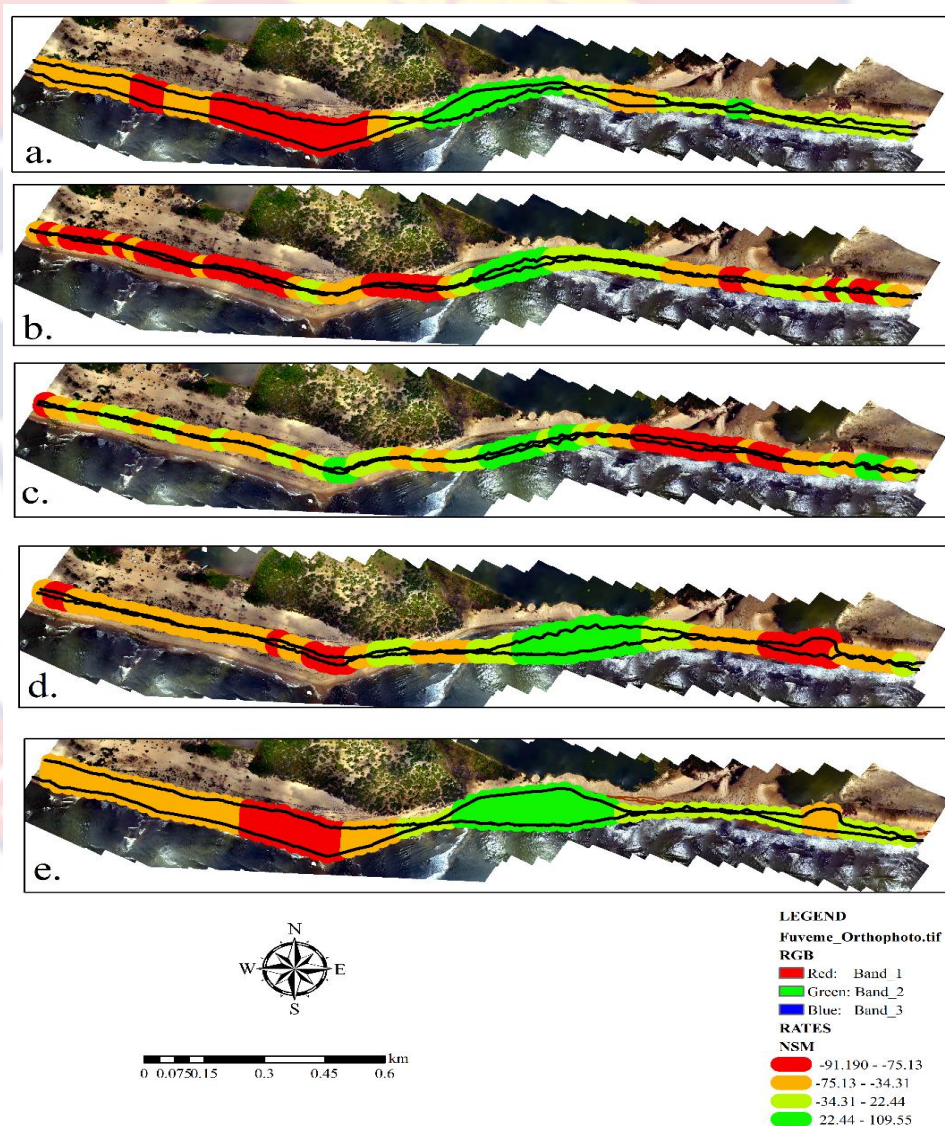
Figure 14: Spatial variation of Net Shoreline Movement on Fuveme Beach between a) October 2021 – May 2022 b) May 2022 – June 2022 c) June 2022 – July 2022 d) July 2022 – October 2022 e) October 2021 – October 2022 (the entire study period).

Table 5: *Average Net Shoreline Movement from October 2021 to October 2022*

| | Net Shoreline Movement (NSM) | |
Period	Average Erosion (± 0.25 m)	Average Accretion (± 0.25 m)
October 2021 – May 2022	-39.76	24.81
May 2022 – June 2022	-7.17	7.57
June 2022 – July 2022	-8.47	5.41
July 2022 – October 2022	-12.28	24.24
October 2021 – October 2022	-46.44	58.41

Table 6: *Average End Point Rate from October 2021 to October 2022*

| | End Point Rate of Change (EPR) | |
Entire Period	Average Erosion (± 0.25 m/yr)	Average Accretion (± 0.25 m/yr)
October 2021 – October 2022	-48.43	60.91
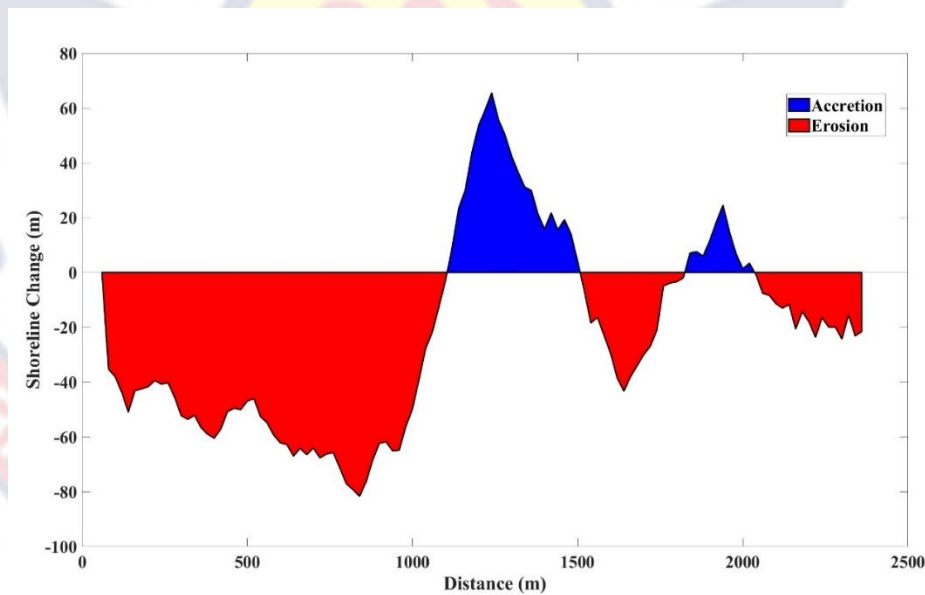
Figure 15: Net Shoreline Movement between October 2021 and May 2022

77
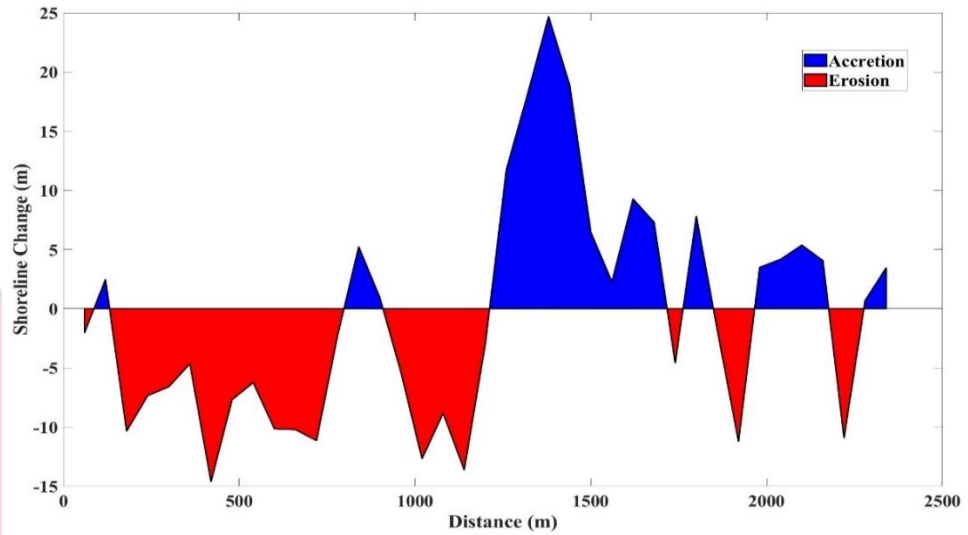
Figure 16: Net Shoreline Movement between May 2022 and June 2022
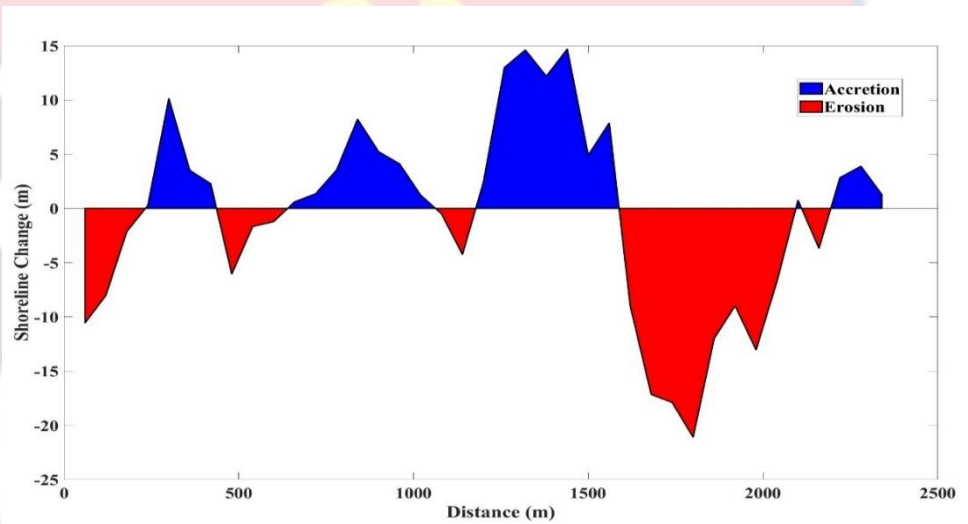
Figure 17: Net Shoreline Movement between June 2022 and July 2022
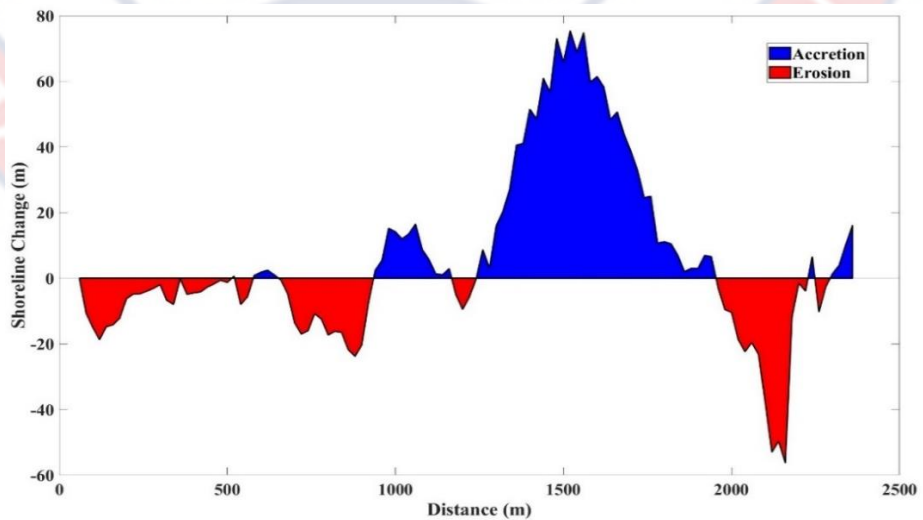
Figure 18: Net Shoreline Movement between July 2022 and October 2022

78
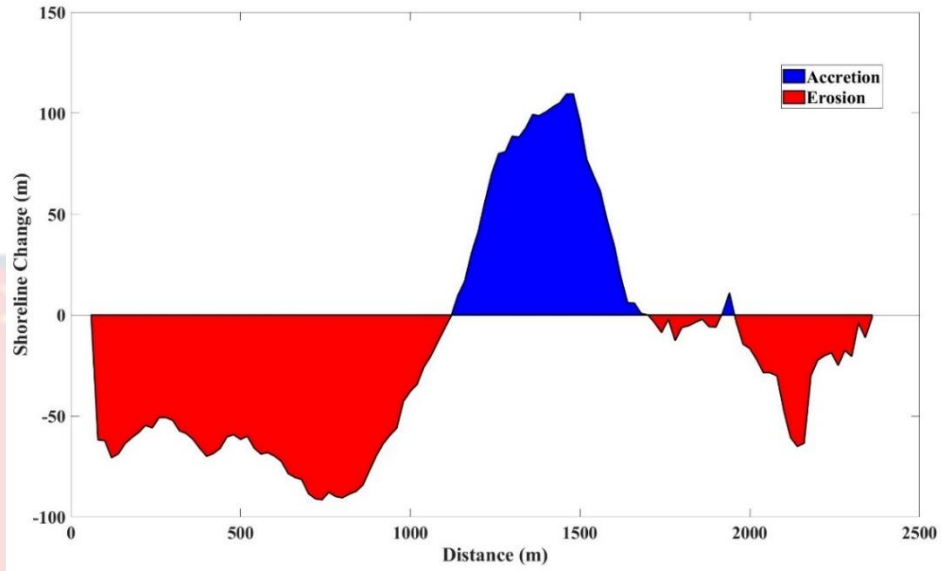
Figure 19: Net Shoreline Movement for the entire period of study (October 2021 to October 2022)
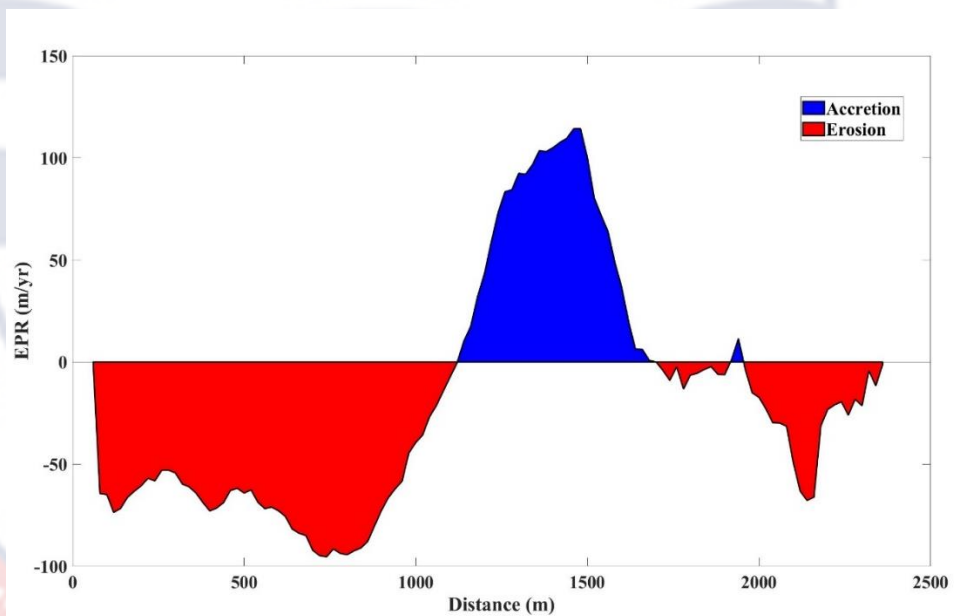
Figure 20: End Point Rate of change for the entire period of study (October 2021 to October 2022)

4.2.2 Sediment volume changes at Fuveme Beach

The results for sediment volume changes between the successive months throughout the study period are shown in Table 7. A spatial variation is also shown in Figure 21 as well as elevation changes in Figure 22.

79

Table 7: *Sediment Volume Changes from October 2021 to October 2022*

Measured Parameter	Period				
	Oct 21 to May 22	May 22 to Jun 22	Jun 22 to Jul 22	Jul 22 to Oct 22	Oct 21 to Oct 22
Erosion (Volume/m³)	62,064 (± 5,220)	90,245 (± 22,111)	16,476 (± 5,116)	52,436 (± 8,589)	35,359 (± 3,385)
Average Depth of Erosion (Height/m)	2.38 (± 0.20)	0.82 (± 0.20)	0.64 (± 0.20)	1.22 (± 0.20)	2.09 (±0.20)
Deposition (Volume/m³)	57,798 (± 4,344)	15,682 (± 5,659)	15,569 (± 5,777)	221,608 (± 20,039)	126,979 (± 9,065)
Average Depth of Deposition (Height/m)	2.66 (± 0.20)	0.55 (± 0.20)	0.54 (± 0.20)	2.21 (± 0.20)	4.47 (± 0.20)
Net Volume Change (m³)	-4,266 (± 6,791)	-74,564 (± 22,824)	-907 (± 7,717)	169,172 (± 1,319)	91,622 (± 6,612)
Sediment Imbalance (%)	-2	-35	-2	31	23

80
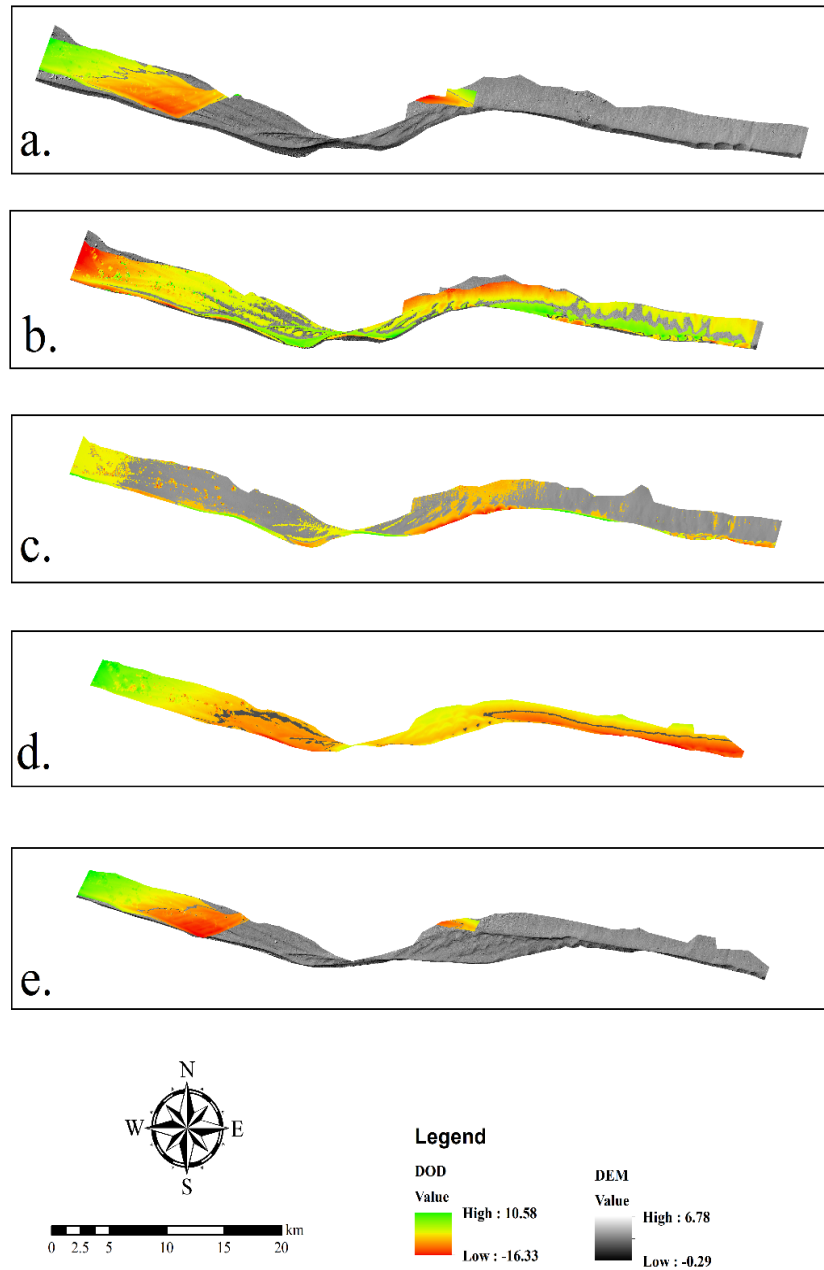
Figure 21: Spatial distribution of Sediment volume changes on Fuveme Beach from (a) October 2021 – May 2022 (b) May 2022 – June 2022 (c) June 2022 – July 2022 (d) July 2022 – October 2022 (e) October 2021 - October 2022

81
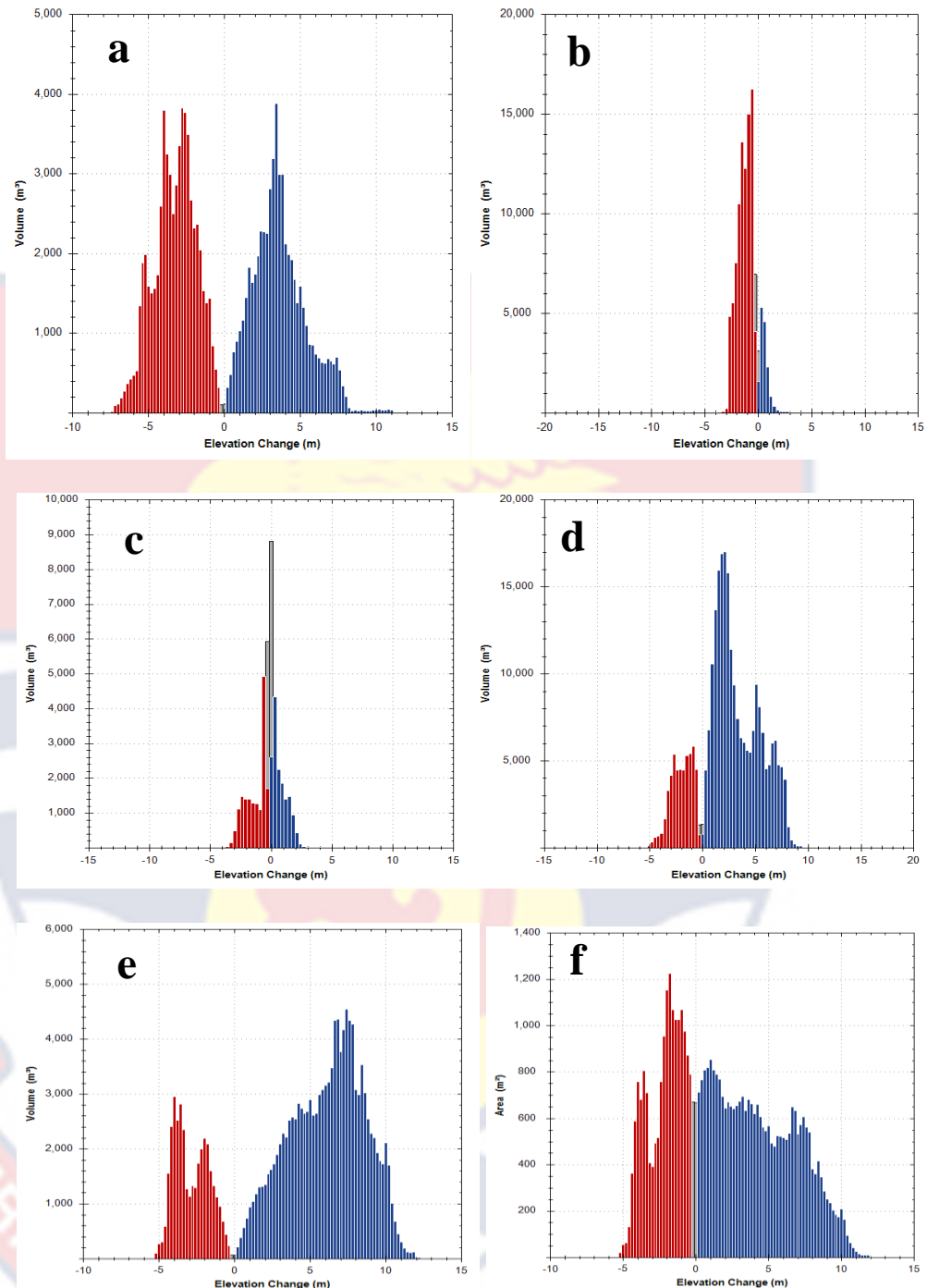
Figure 22: Sediment dynamics for Fuveme: a) October 2021 – May 2022 b) May 2022– June 2022, c) June 2022 – July 2022 d) July 2022 – October 2022 e) October 2021 - October 2022 (Entire period) and f) Areal change for the entire period (October 2021 to October 2022)

4.2.3 Beach profiles extracted from DEMs

Profiles were cast in three transects across the beach. The transects were cast in the western part (Profile 1), the central part (Profile 2) and the

82

eastern part (Profile 3) of the area. The beach profiles extracted from the DEMs were plotted for each profile as shown in Figure 23.
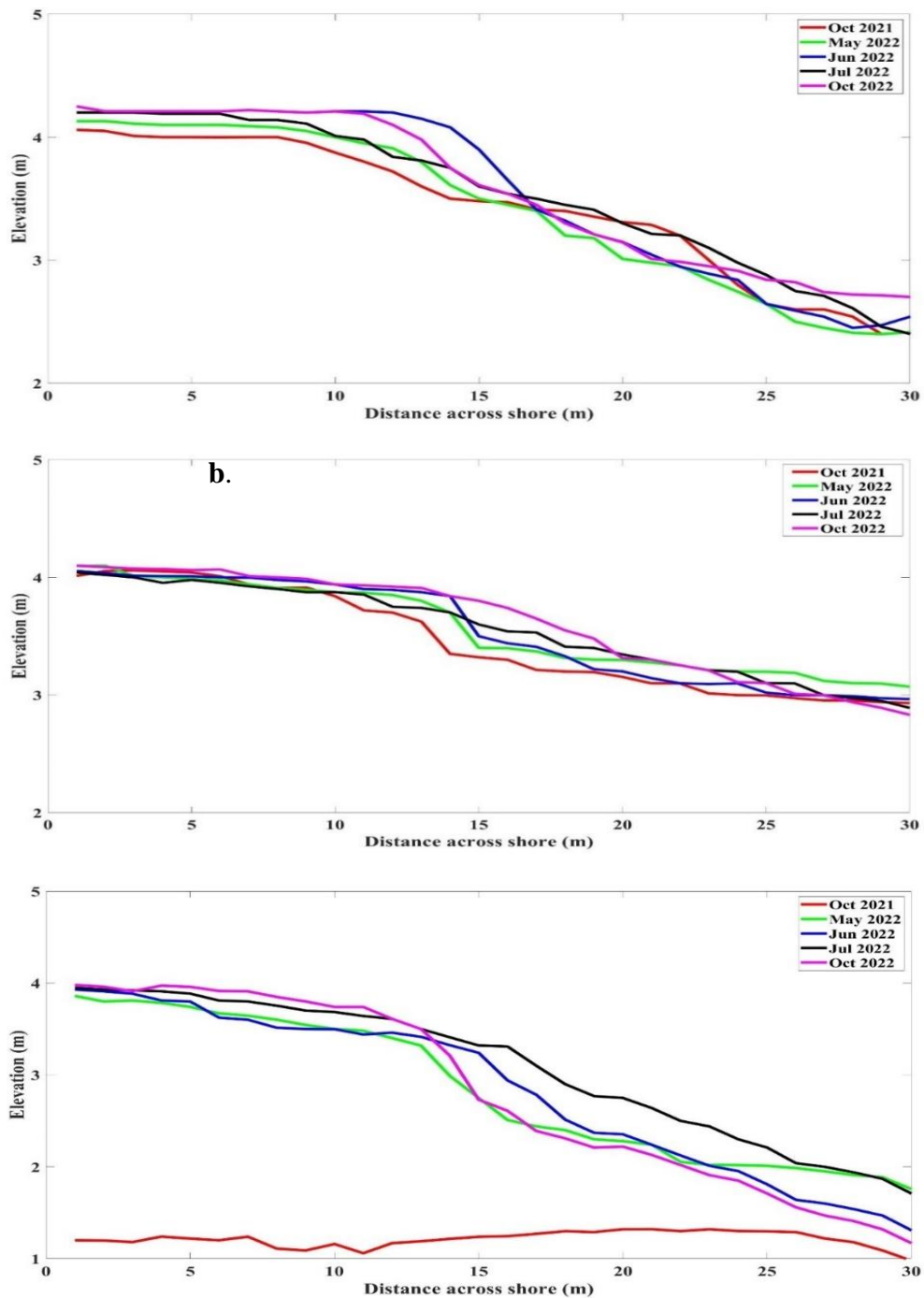
Figure 23: Beach Profiles along the a) western section b) central section c) 'newly created estuary' (eastern end) of Fuveme Beach

83

4.3 Model Validation

The simulation ran from 1ˢᵗ May 2022 to 1ˢᵗ August 2022 with results showing the surface elevation (water level), current, Significant Wave Height (SWH), Peak Wave Period (PWP), Mean Wave Direction (MWD) and Total load transport (magnitude, direction and bed level changes). The hydrodynamic and spectral wave results were validated with on field water level data and significant wave height data from CMEMS, respectively.

4.3.1 Validation for the Hydrodynamic module

In order to ensure results obtained from the HD module were accurate, the Mean Square Errors (MSE) and Root Mean Square Errors (RMSE) of the surface elevation results were calculated between the modelled results and on field measured water levels. For the HD validation, three points (t1, t2 and t3) were selected across the study area and compared. Point 1 (t1) was on the western end of the area and the correlation between the modelled and the measured surface elevation values was strong as shown in Figure 24. Point 2 (t2) was in taken in the newly created estuary and the correlation between the modelled values and the measured values was also strong as shown in Figure 25. Point 3 (t3) was in taken in the far east and the correlation between the modelled and measured surface elevation values was also strong as shown Figure 26. All three points had MSE of 0.010 and RMSE of 0.10.
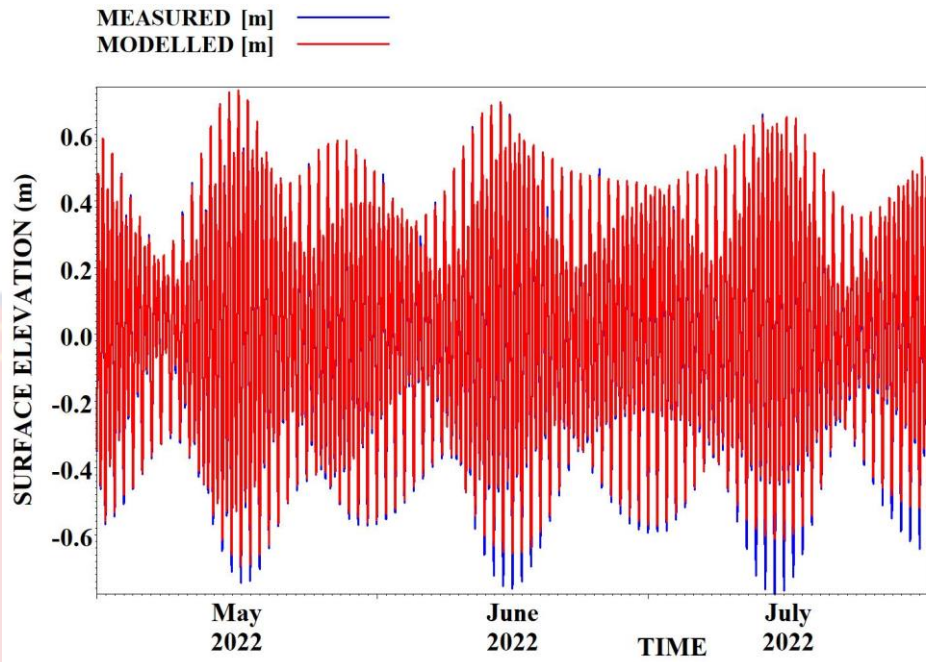
Figure 24: The modelled and measured surface elevations for t1
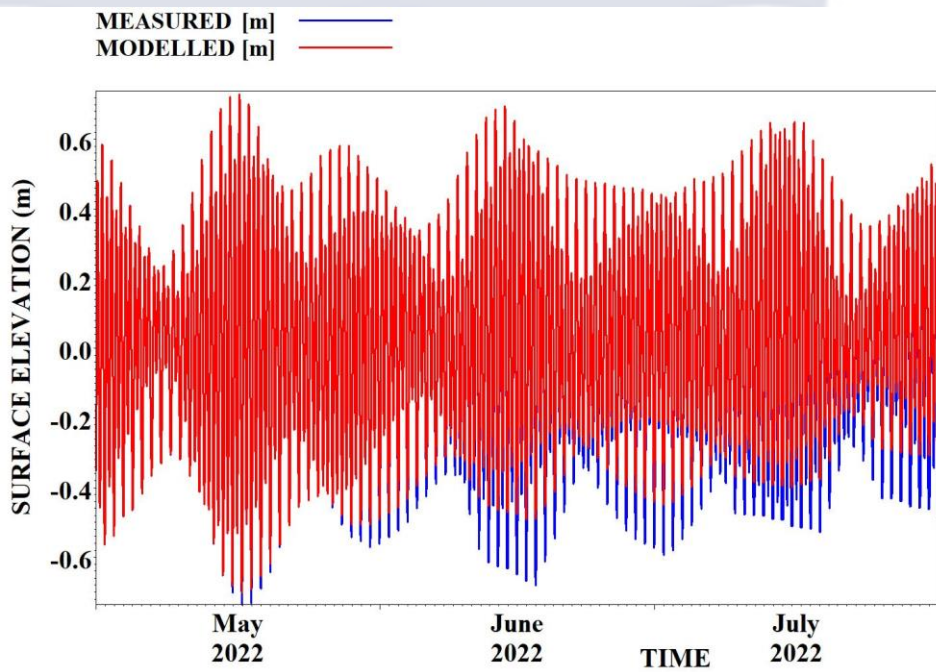
Figure 25: The modelled and measured surface elevations for t2

85
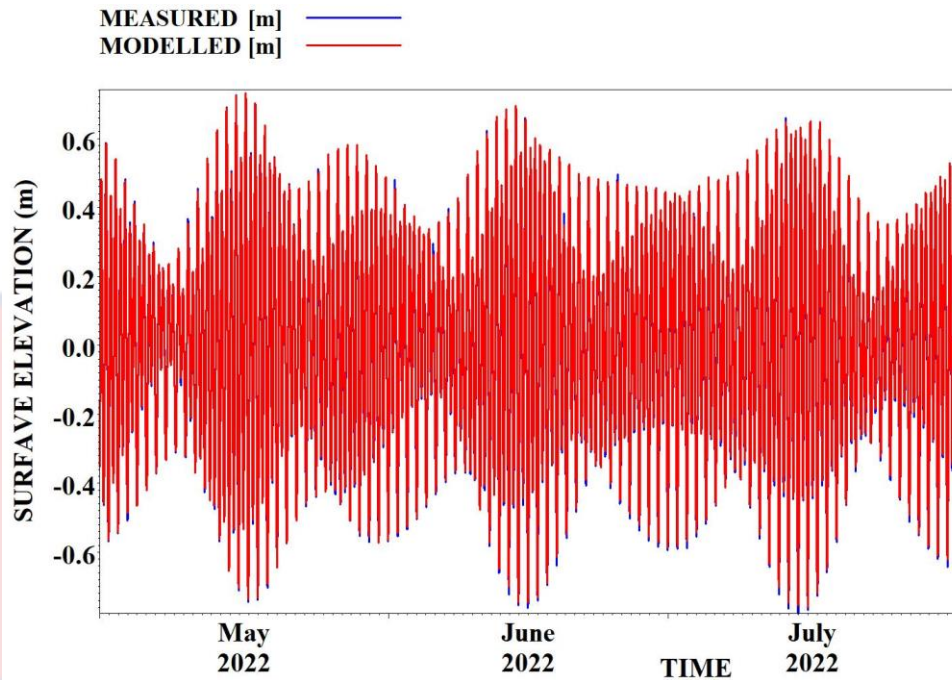
Figure 26: The modelled and measured surface elevations for t3

4.3.2 Validation for the Spectral Wave module

The validation for the Spectral Wave module showed a MSE of 0.505

and RMSE of 0.22 which shows a strong correlation between the modelled

SWH and the modelled SWH from CMEMS as shown in Figure 27.
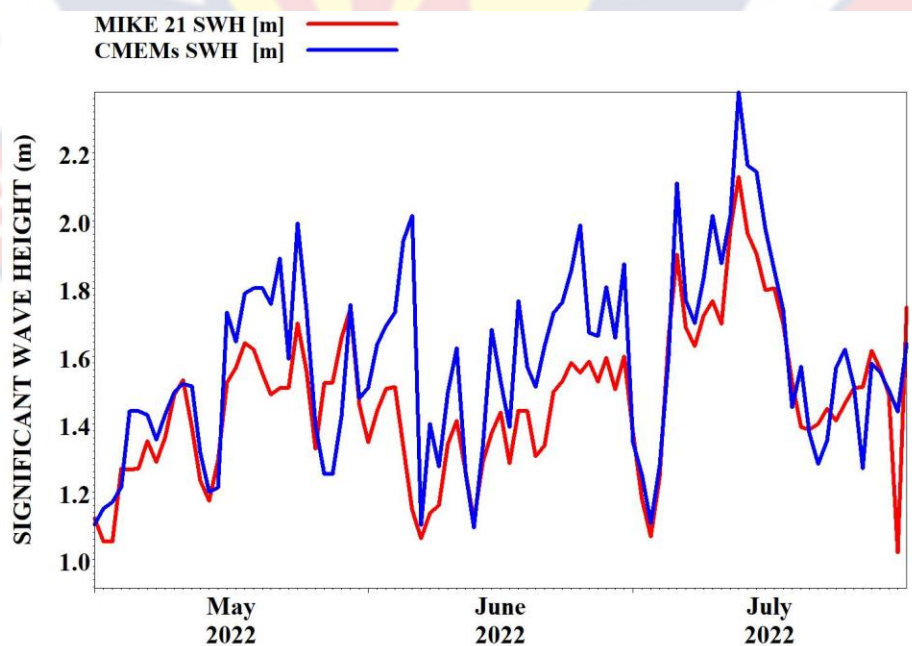
Figure 27: Modelled SWH and modelled SWH from CMEMS

4.4 Results from MIKE 21 Hydrodynamic (HD) module

4.4.1 Results for Surface Elevation

The results for surface elevation was obtained from the HD model. The statistical result for surface elevation (water levels) for selected points is shown in Table 8 and a spatial variation of the surface elevation is shown in Figure 28.

Table 8: *Statistical results for surface elevation at selected points*

Location Code	Easting	Northing	Surface Elevation Mean (m)	STD
t1	244047	638735	0.003	0.332
t2	245000	638800	0.004	0.330
t3	246000	638720	0.003	0.322
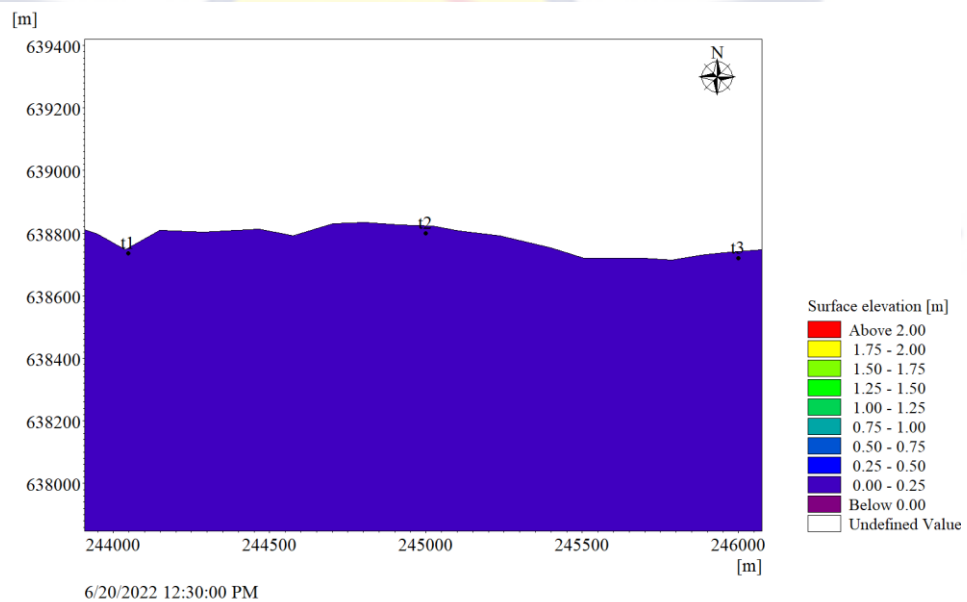
Figure 28: Spatial variation of the surface elevation at time step 3193

4.4.2 Results for Current Speed

Another parameter obtained from the HD model was the current speed.

The statistical results for current speed is shown in Table 9 and the spatial

variation is shown in Figure 29.

Table 9: *Statistical results for current speed at selected points*

Location Code	Easting	Northing	Current speed Mean (m/s)	STD
t1	244047	638735	0.013	0.009
t2	245000	638800	0.022	0.012
t3	246000	638720	0.014	0.011
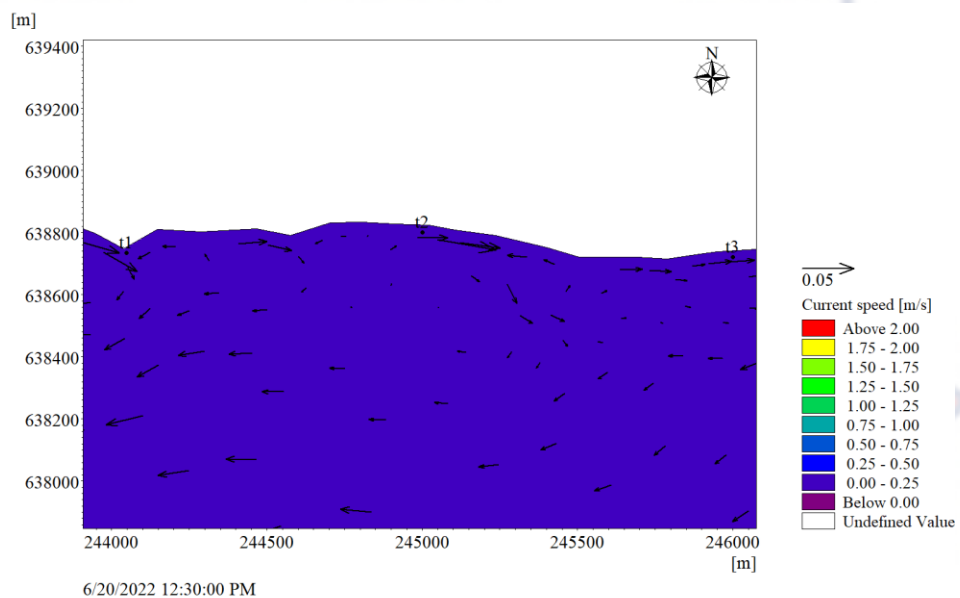
Figure 29: Spatial variation of the current speed and direction at time step
3193

4.5 Results from MIKE 21 Spectral Wave (SW) module

4.5.1 Results for Significant Wave Height (SWH)

One of the results obtained from the SW simulation is the Significant

Wave Height. The statistical result is shown in Table 10 and the spatial

variation is shown in Figure 30.

88

Table 10: *Statistical results for the significant wave height at selected points*

Location Code	Easting	Northing	SWH MEAN (m)	STD
t1	244047	638735	0.431	0.061
t2	245000	638800	0.228	0.076
t3	246000	638720	0.299	0.063
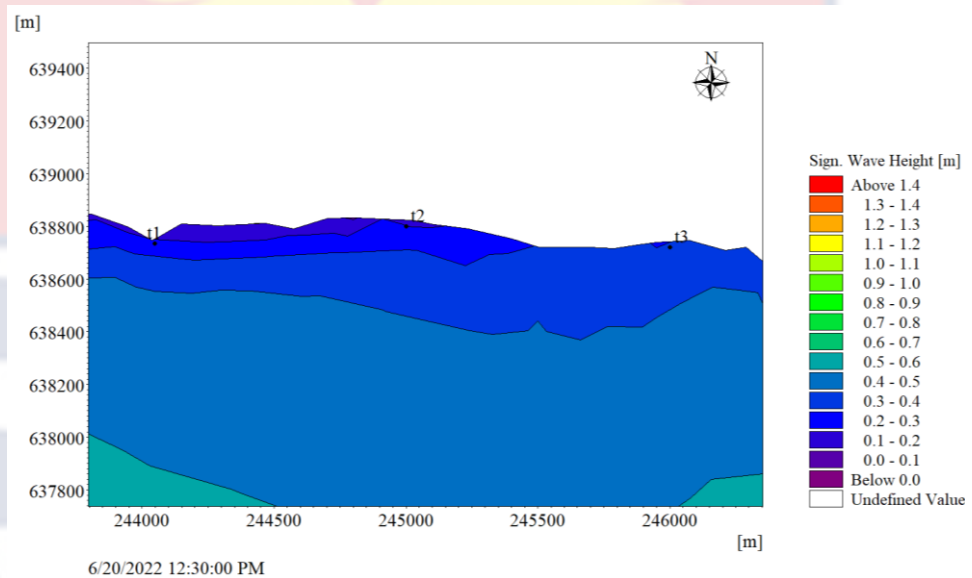
Figure 30: Spatial variation of significant wave height at time step 3193

4.5.2 Result for Peak Wave Period (PWP)

The Peak Wave Period (PWP) across the domain was also obtained courtesy the SW model. The statistical result for PWP is shown in Table 11 and the spatial variation of PWP is shown in Figure 31.

89

Table 11: *Statistical results for peak wave period at selected points*

Location Code	Easting	Northing	PWP Mean (s)	STD
t1	244047	638735	12.33	1.98
t2	245000	638800	12.31	1.98
t3	246000	638720	12.34	1.99
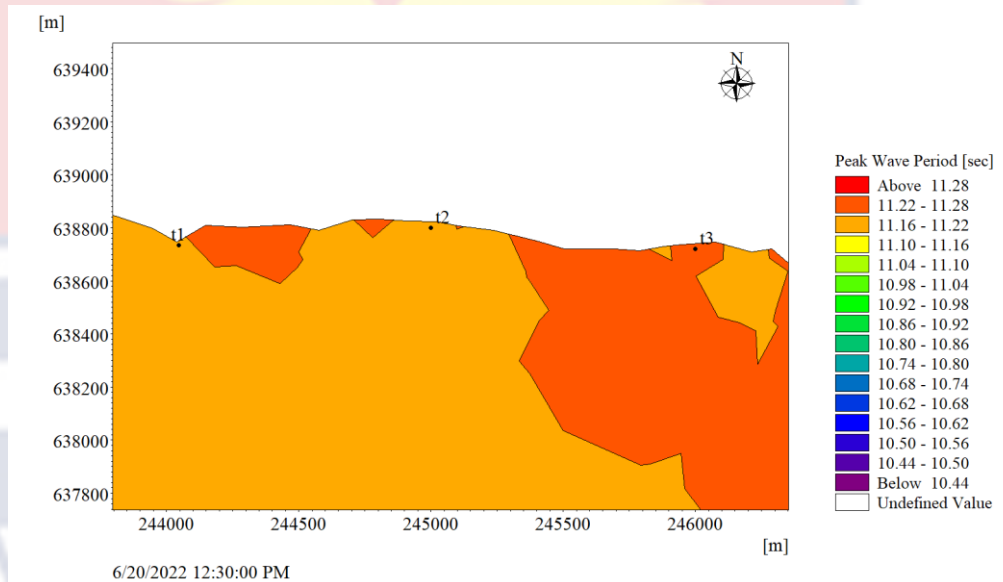
Figure 31: Spatial variation of peak wave period at time step 3193

4.5.3 Result for Mean Wave Direction (MWD)

The result for the Mean Wave Direction (MWD) across the study area was obtained from the SW model. The statistical result for MWD is shown in Table 12. A spatial representation of MWD is also shown in Figure 31.

90

Table 12: *Statistical results for mean wave direction at selected points*

Location Code	Easting	Northing	MWD MEAN (°)	STD
t1	244047	638735	192.23	1.81
t2	245000	638800	185.61	1.81
t3	246000	638720	180.26	2.33
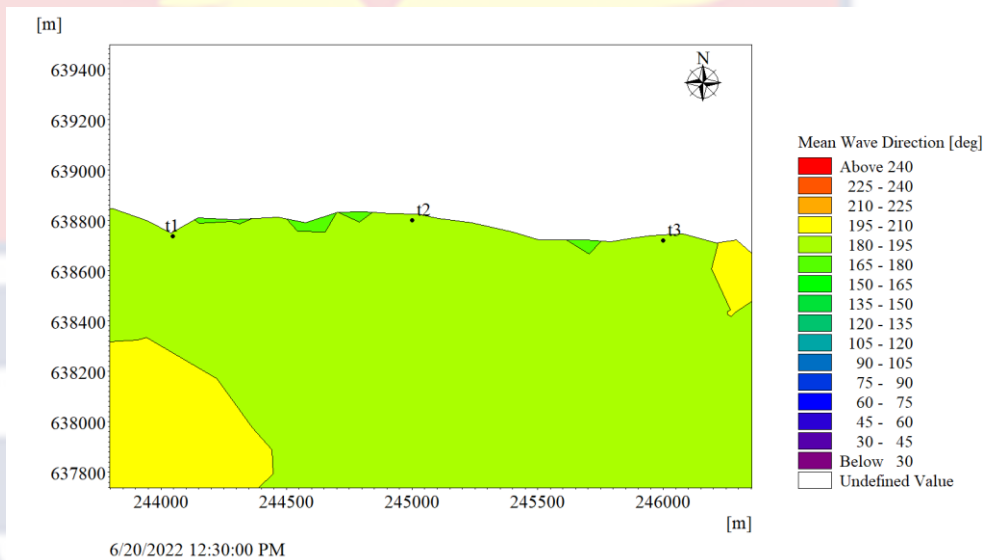
Figure 32: Spatial variation of mean wave direction at time step 3193

4.6 Results from MIKE 21 Sediment Transport (ST) module

4.6.1 Results for sediment transport (total load) magnitude

The result for total load magnitude was generated by the Sediment Transport module and its statistical result is shown in Table 13 and the spatial variation is shown in Figure 33. A graph for sediment transport (total load) magnitude, sediment direction and the bed level change for Point 3 (estuary area) was shown in Figure 36.

91

Table 13: *Statistical results for total load magnitude at selected points*

Location Code	Easting	Northing	Total load Mean (10^{-5} m³/s/m)	STD (10^{-5})
t1	244047	638735	0.801	0.207
t2	245000	638800	1.59	2.39
t3	246000	638720	0.834	0.431
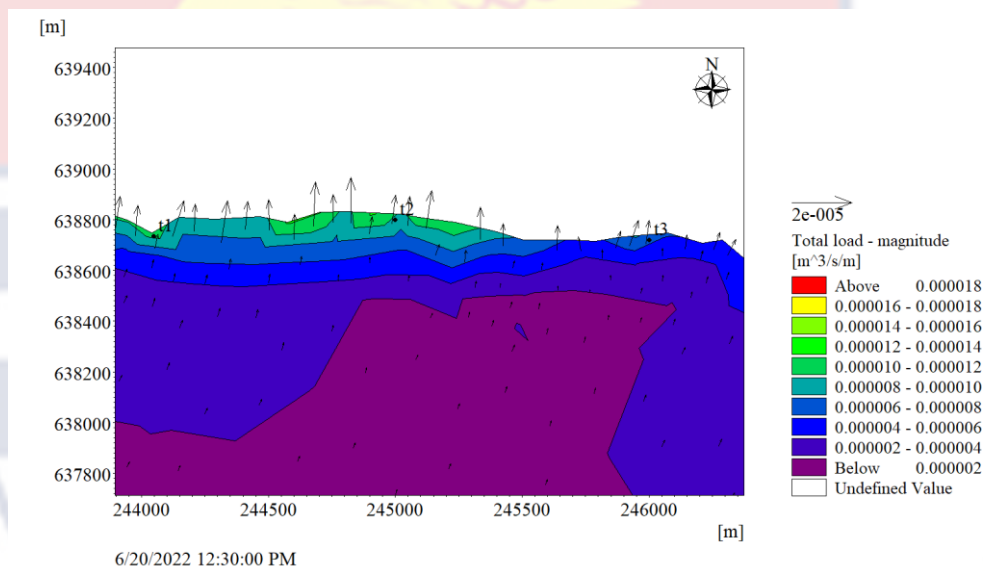
Figure 33: Spatial variation of sediment transport (total load) at time step 3193

4.6.2 Results for Sediment transport direction

The statistical load direction results at selected points in shown in Table 14 and the spatial variation is shown in Figure 34.

Table 14: *Statistical results for sediment direction at selected points*

Location Code	Easting	Northing	Sediment Direction Mean (°)	STD
t1	244047	638735	13.72	23.49
t2	245000	638800	29.25	86.56
t3	246000	638720	21.17	48.40
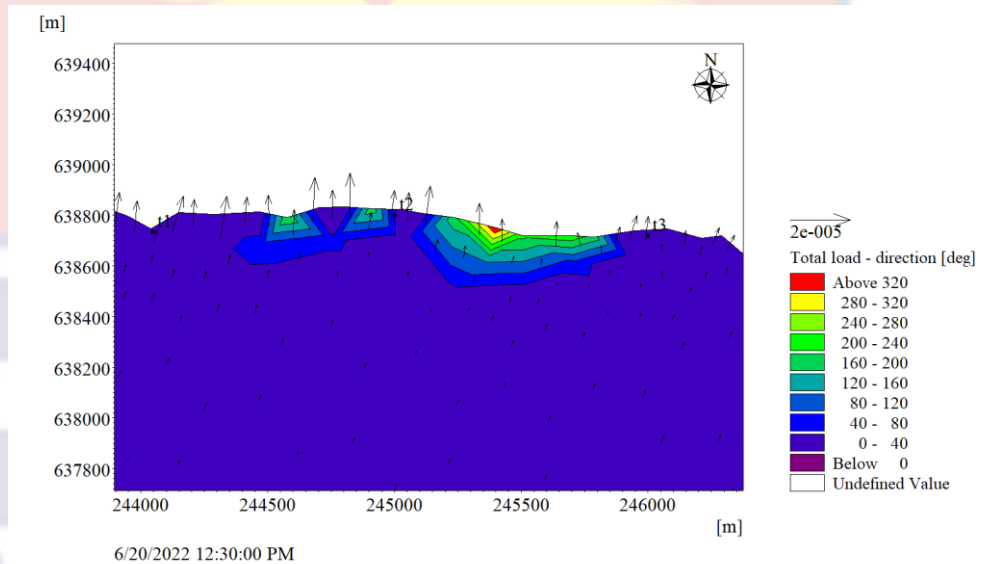
Figure 34: Spatial variation of sediment transport direction at time step 3193

4.6.3 Results for bed level change

The statistical bed level change results at selected points in shown in

Table 15 and the spatial variation is shown in Figure 35.

93

Table 15: *Statistical results for bed level change at selected points*

Location Code	Easting	Northing	Bed level change Mean (m)	STD
t1	244047	638735	0.509	0.009
t2	245000	638800	0.470	0.270
t3	246000	638720	0.588	0.282
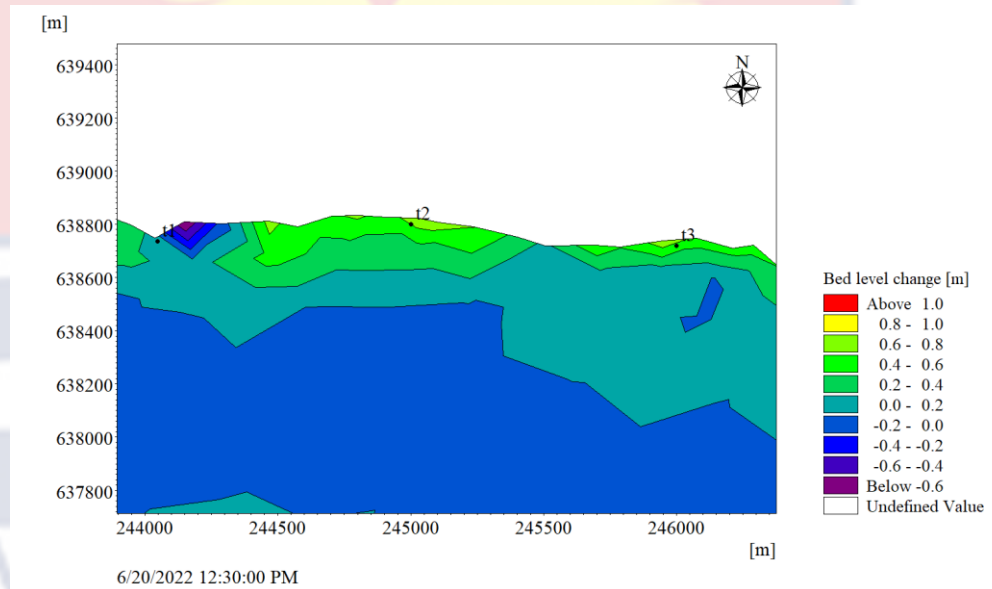
Figure 35: Spatial distribution of bed level change at time step 3193
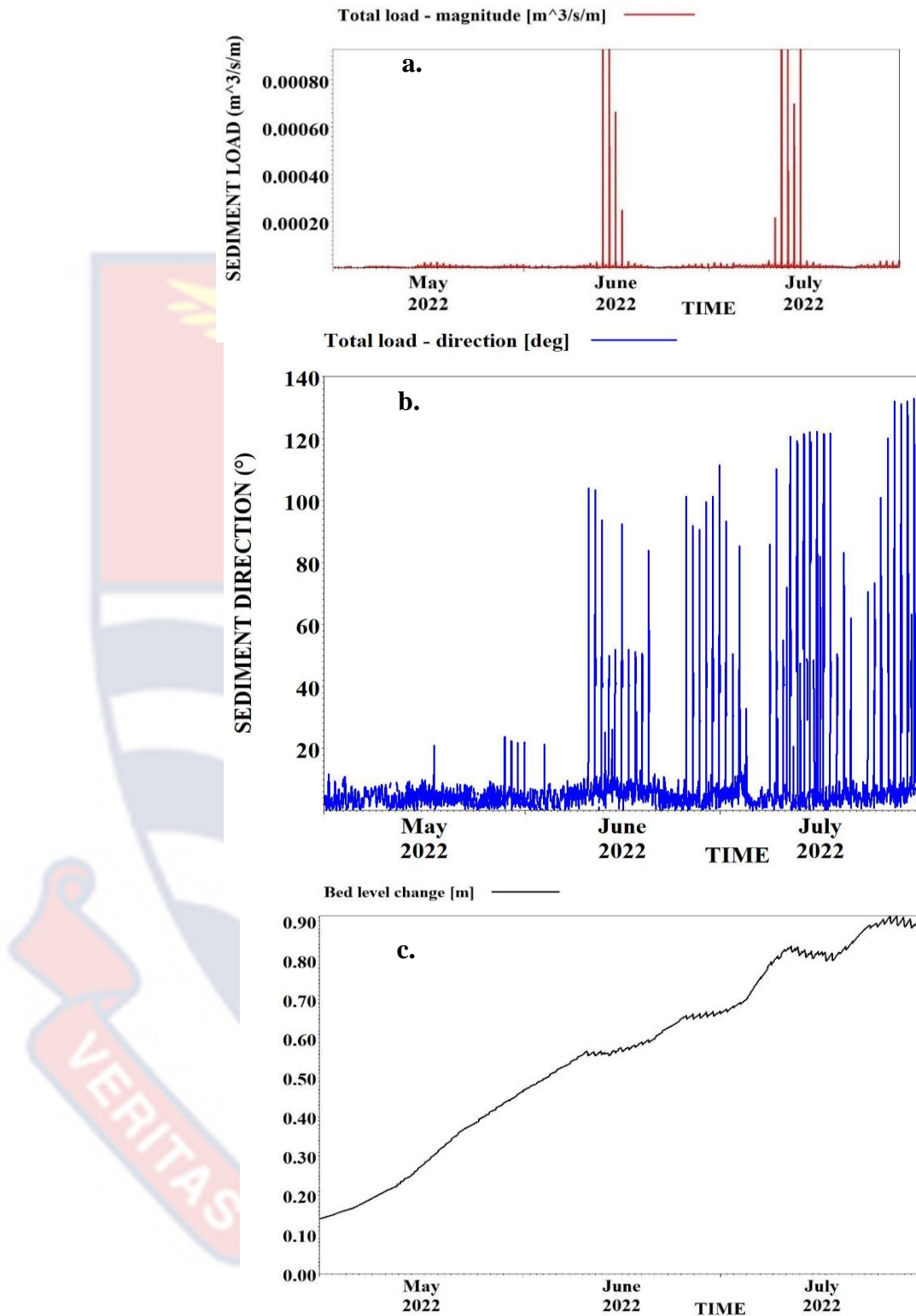
Figure 36: a) Sediment (total load) magnitude b) load direction and c) bed level changes for point 2 (the estuary location)

95

4.7 Results for unchecked parameters

In order to ascertain the hydrodynamic condition that affects the beach the most, some vital parameters were unchecked. The water level data, waves and current were unchecked as the simulation was ran with the same initial conditions. The results are presented in the subsections below.

4.7.1 Unchecked current data

The values for the sediment transport magnitude were quite similar to the values attained when all parameter were checked. This goes to show that the current was so small to effect changes in the sediment movement in Fuveme. The results for selected points are shown in Table 16. A spatial variation is also shown in Figure 37.

Table 16: *Statistical results for total load magnitude without current at selected points*

Location Code	Easting	Northing	Total load Mean (10^{-5} m³/s/m)	STD (10^{-5})
t1	244047	638735	0.468	0.207
t2	245000	638800	1.370	1.240
t3	246000	638720	0.648	0.304

96

6/20/2022 12:30:00 PM
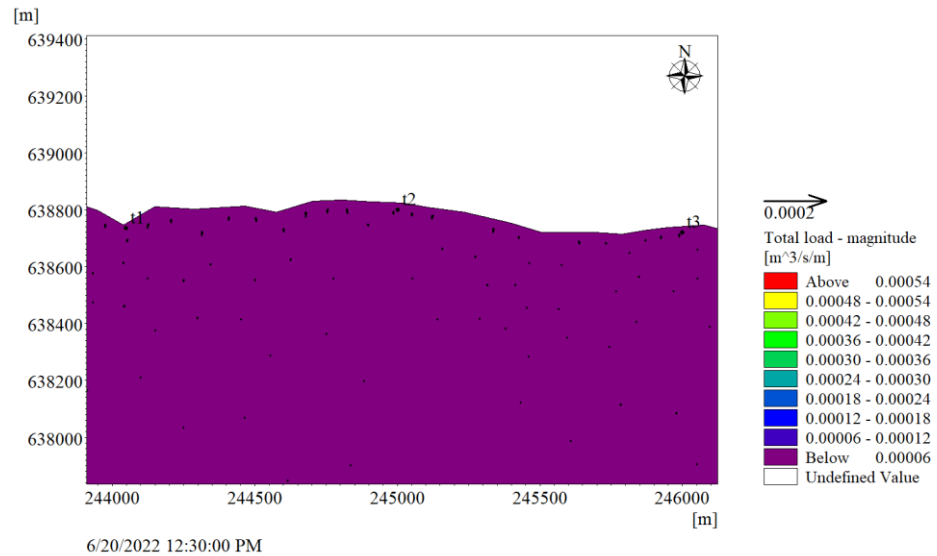
Figure 37: Spatial variation of sediment transport (total load) without current at time step 3193

4.7.2 Unchecked water level data

The values for the sediment transport magnitude were very small as compared to the values attained when all parameter were checked. This goes to show that the water level (surface elevation) affects sediment movement in the area but not as much as waves does. The results for such coordinate points are shown in Table 17. A spatial variation is also shown in Figure 38.

Table 17: *Statistical results for total load magnitude without water level at selected points*

Location Code	Easting	Northing	Total load Mean (10^{-5} m³/s/m)	STD (10^{-5})
t1	244047	638735	0.0221	0.010
t2	245000	638800	0.0842	0.034
t3	246000	638720	0.0642	0.028

97
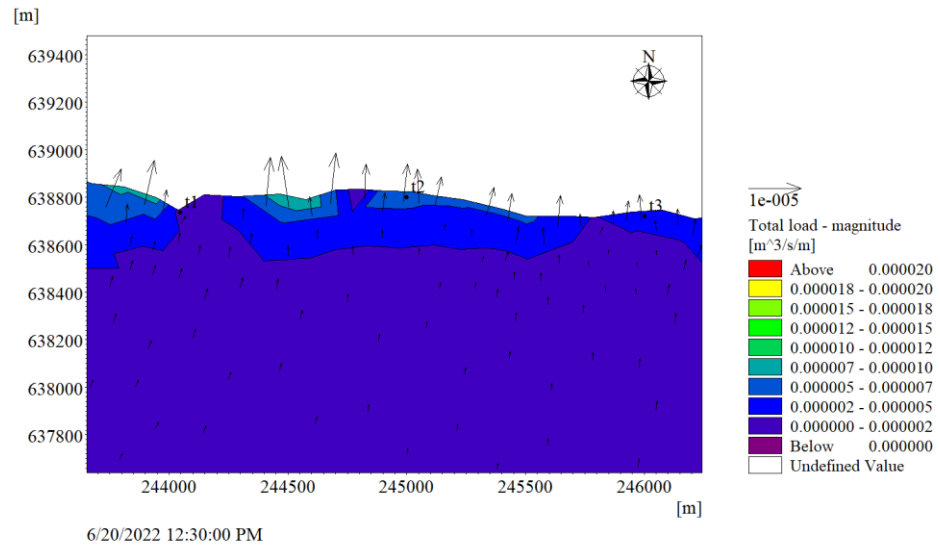
Figure 38: Spatial variation of sediment transport (total load) without water levels at time step 3193

4.7.3 Unchecked waves parameters

There were no values for the sediment transport magnitude recorded when the waves parameters were unchecked. This undoubtedly shows that waves are very significant in sediment transport along the coast of Fuveme. The results for selected points are shown in Table 18. A spatial variation is shown in Figure 39.

Table 18: *Statistical results for total load magnitude without waves at selected points*

Location Code	Easting	Northing	Total load Mean (m³/s/m)	STD
t1	244047	638735	0.00	0.00
t2	245000	638800	0.00	0.00
t3	246000	638720	0.00	0.00

98

6/20/2022 12:30:00 PM
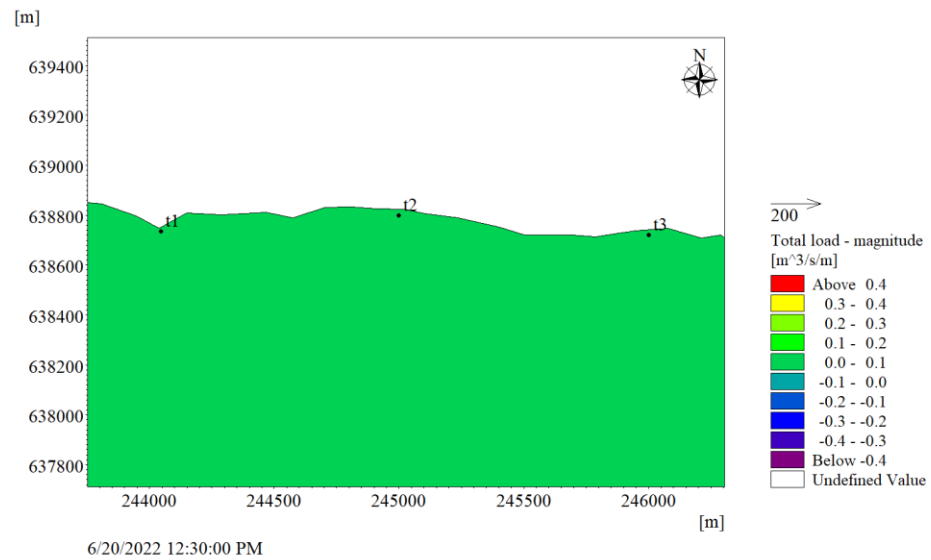
Figure 39: Spatial variation of sediment transport (total load) without waves at time step 3193

4.8 Chapter summary

The results for this study were duly captured in this chapter. The results included the shoreline variation for the area between October 2021 and October 2022. The NSM and EPR for the entire study were -46.44 m/yr and -48.43 m/yr for erosion respectively and 58.41 m/yr and 60.91 m/yr for accretion respectively as well. The sediment volume dynamics was also recorded with over 35,359 m³ being lost and 126,979 m³ gained over the period. The elevations of the beach were also noted for three transects representing all sides of the beach. The HD and SW were validated using data from onshore and CMEMS. The surface elevation and SWH showed values of 0.10 and 0.22 correlation between modelled and measured values respectively. The results for the SWH, PWP and MWD were recorded as well. At the end of all simulations, the waves parameter was the most vital as it was responsible for sediment transport in the area.

CHAPTER FIVE

DISCUSSION

5.1 Introduction

This chapter explains the results including shoreline changes, sediment volume dynamics and profiles extracted from DEMs. It further discusses the validation results between the modelled values and observed values, results from the MIKE 21 simulations as well. The outcome of this study is also compared to other works.

5.2 Sediment morphodynamics from Unmanned Aerial Vehicle images

5.2.1 Shoreline analysis along Fuveme Beach

Over the study period, the Fuveme Beach showed dynamism highlighting high erosion and accretion at various sections as shown in Figure 14. According to Boateng (2012), the bridge in sediment discharge from the Volta River affected sediment distribution along the downdrift side of the Volta Estuary particularly the immediate coast close to the Volta Estuary. Also, according to Brempong (2019), the construction of hard engineering structures to curb erosion on the eastern coast has been a major factor in the constant increase in erosion rates both on a short and long-term basis. The sea defence structures at Ada, which consists of groynes restricts sediments from moving down-drift thereby trapping sediments as observed and reported by Angnuureng et al (2013). This is because coarse sediments that would have drifted along the shoreline from west to east have been restricted and thus reduced to only the transport of fine sediment which are easily moved or carried away by aeolian processes.

5.2.2 Sediment volume dynamics across Fuveme Beach

Fuveme Beach experienced a high sediment deposition across the study period as shown in Table 7 and Figure 22. The sediment lost between October 2021 and May 2022 was 62,064 m³ and the sediment gained was 57,798 m³. From Figure 21a, sediment accretion was predominant in the foreshore areas in the central and eastern stretch of the area. The sediment deposited along the coast accounted for the closing up of the estuary and thus building the beach up on that stretch. The erosion intensified across the entire beach between May 2022 and June 2022. In this period, sediment changes were 15,682 m³ and 90,245 m³ for sediment deposition and loss respectively. This was more paramount on the western end of the area as is clearly depicted in Figure 21b. Between June 2022 and July 2022, the sediment gained and lost over the area were 16,476 m³ and 15,569 m³ respectively. There was a massive accretion of sediment between July 2022 and October 2022. The changes were paramount in the mid-western stretch of the area and the extreme end of the eastern part of the area as shown in Figure 21d. The volume of sediment deposited was 221,608 m³ and the amount of sediment lost was 52,436 m³. Overall, the sediment gained and lost across the study period was 126,979 m³ and 35,359 m³ respectively and a positive sediment imbalance of about 23% was recorded. This showed that overall (Figure 21e), the sediment gained was higher compared to the sediment lost over the year study period. This could be attributed to eastward longshore drift and about enough sediment from offshore bed eroding gradually and being deposited in the area as rightly reported by Jayson-Quashigah (2019).

101

Comparing the sediment volume changes to that of Jayson-Quashigah (2019), the overall sediment changes were 69,188 m³ and 74,330 m³ for erosion and accretion respectively and a percentage imbalance of 2 %. In the time frame from June 2016 – April 2018, sediment deposition was more similar to the findings in this study.

5.2.3 Beach profiles from Digital Elevation Models (DEMs)

The beach front of profile 1 built up significantly within the period as shown in Figure 23a. The elevation rose by a few meters in the first period of the study. By the middle period, the beach had built up very well due to the deposition of sediment. The berm also accreted and elevated from October 2021 to June 2022 and started experiencing erosion towards the end of the study. The backshore experienced erosion in the first few months and accreted towards the end of the study.

The mid-section profile (Figure 23b) was very stable across the study period. The foreshore was stable across the entire period of study. The berm built up from October 2021 – May 2022. There was a slight erosion in the berm by July but the berm recovered from this erosion in the last period of the study. The backshore also remained fairly stable over the period.

The profile in the eastern part of the beach from October 2021 to July 2022 showed different elevations at each period in time. The profile for October showed a flat beach indicating the time the 'bridged estuary' was in existence. This changed drastically from March 2022 to May 2022. There was massive deposition of coarse sediment between March 2022 – October 2022 as the elevation remained stable until the end of the study (Figure 23c). There were few patches of accretions and erosions in the berm and the backshore but

102

generally the berm built up in the last period.

From a similar study done by Jayson-Quashigah (2019), the beach profiles were irregular with extreme erosion across the study period (June 2016 – April 2018), the berm eroded extensively during the period with less erosion at the fore shore of the area. Comparatively, the beach profiles for Fuveme were quite stable between October 2021 and October 2022 as compared to June 2016 and April 2018.

5.3 Sediment morphodynamics from MIKE 21 model

5.3.1 Surface elevation and current results from Hydrodynamic Module

The results from the hydrodynamic module show the surface elevation, current speed and its direction as well. The relationship between the modelled surface elevation data and on-field water levels showed a Root Mean Square Error of 0.01 for all the three points signifying a strong correlation. The surface elevation for the domain was between 0.001 m and 0.70 m. The current speed was between 0.0001 m/s – 0.3 m/s. for the entire simulation period. On average the current at Fuveme area was about 0.028 m/s. The direction of the current closer to the shore was from South to north but once very close to the shoreline it moved from west to the east as shown in Figure 29 but the direction is mostly in the clockwise direction offshore depending on wind speed and direction as well. The current speed in the domain was predominantly low in the region.

A similar trend was seen in the research done by Badru et al. (2022) downdrift the Bight of Benin. In their research, current speed values recorded were between 0.25 m/s and 1.47 m/s. This was higher as compared to current speed values in Fuveme area as a result of the area location, orientation, bed

103

level, wind speed and wind angle. No current data was available for the validation of the current result.

5.3.2 Wave results from Spectral Wave module

The results from the Spectral Wave show the Significant Wave Height (SWH), Peak Wave Period (PWP) and Mean Wave Direction (MWD). The validation of the spectral waves was done for only SWH since it was the only available data for the time period. The ERA 5 wave data made up of all the aforementioned wave parameters were used to force the model and the wave data from Copernicus Marine and Environment Monitoring Services (CMEMS) was used to validate it. The RMSE value was 0.22 and it showed a good correlation between the modelled results and modelled CMEMS data. The SWH was between 0.20 m and 0.80 m. The SWH around the Fuveme nearshore area was about 0.418 m between May 2022 and July 2022. All wave parameters were very high offshore and reduced significantly approaching the shore. The wave period recorded in the region were also between 7 s – 16 s. The mean wave direction was also smaller in the western end and increased moving eastward the area. The orientation of the study shoreline was also a huge factor in the wave direction and hence its angle. The MWD also ranged between 160 ° and 240 ° with a mean wave angle of 191.15 ° over the study period. The direction of the wave was from mainly from the south-south west direction similar to findings by Almar et al. (2015). According to Almar et al. (2015), waves approach the whole Bight of Benin area (Fuveme inclusive) from the south-southwest direction.

5.3.3 Sediment transport magnitude and direction from Mike 21 model

The sediment transport magnitude and direction for the domain alternated across the domain during the simulation. This is as a result of the different conditions at each time during the simulation period. The sediment transport magnitude, direction and the corresponding bed level changes for Points 1, 2 and 3 were noted. For this research, the total load was hugely from offshore and deposited onshore. The mean directions of the sediment were within the north-east direction with the directions. According to Nairn et al. (1999), sediments are transported eastward in the region and so it confirms the direction of the sediment load.

The mean total load magnitude was 0.00000601 m³/s/m, 0.0000207 m³/s/m and 0.0000159 m³/s/m for t1, t2, and t3, respectively. The sediment load was highest at t2 which had a bed level change of 0.470 m, that for t3 also recorded a bed level change of 0.588 m whilst that of t1 had a bed level change of 0.509 m. The load changed across the area due to alternating bed changes. The volume of sediment accrued between May 2022 – July 2022 from the Geomorphic Change Detection (GCD) software was estimated to be over 106,892 m³ of sediment eroding during that period and over 31,251 m³ of sediment accreting. The ST model generated over 34,338.93 m³ total sediment for the whole area and that of the GCD was 31,251 m³ of sediment between May 2022 and July 2022. The model generated more total sediment for the entire area as compared to the GCD software.

The respective sediment transport direction also showed mean values of 13.72 °, 29.25 ° and 21.17 ° for t1, t2, and t3, respectively. The mean sediment direction during the entire simulation was 41.01°. As confirmed

earlier, all longshore sediment transport were due to the east from the true north. This could indicate the sediment deposition in the eastern part of the area within the simulation period. There was extensive beach build-up between May and July on the eastern side of Fuveme, possibly because of the angle at which sediment was deposited in that section. Additionally, an estimated alongshore sediment transport profiles A, B and C corresponding to perpendicular lines drawn through t1, t2 and t3 were 36,664.5 m³/y, 56,449.44 m³/y and 43,519.68 m³/y. The quantity of alongshore sediment also proves the sediment deposition is higher on the eastern stretch of the area. This is in line with findings from Badru et al. (2022). According to Badru et al. (2022), sediment transport is predominant in the eastward direction from the Volta estuary to the Niger Delta. Again, the sediment transport rates and directions recorded in Fuveme are similar to that of the Apakin, Araromi, Aiyetoro and Awoye in the Niger Delta, a few kilometres from Fuveme, as reported by Badru et al. (2022). The sediment load magnitude was 0.0000104 m³/s/m, 0.0000123 m³/s/m, 0.0000118 m³/s/m, 0.0000107 m³/s/m and the sediment load direction were 263.53°, 266.64°, 278.25° 262.31° for Apakin, Araromi, Aiyetoro and Awoye respectively.

In the course of the simulation periods between June - August, there were massive spikes in sediment transport rate to about 0.00150 m³/s/m coupled with a significant wave height of 0.954 m and both were attributed to the reasons why the waves and sediments overtopped the sand bar and moved into river on the other side of the area. This occurred frequently in the subsequent month until another estuary was created in October 2022.

In the absence of sediment transport data along the Fuveme Beach, the sediment transport results from the simulation were not validated.

5.4 Hydrodynamic parameters that affected Fuveme Beach

The hydrodynamic condition which affected the sediment movement on the Fuveme Beach in the course of the study was established. The wave parameter (significant wave height, peak wave period and mean wave direction) was the main hydrodynamic condition that affected Fuveme Beach, such that once all were unchecked there was no sediment transport recorded in the entire domain. This was followed by the water levels which was responsible for the flow of the water masses. The sediment transport rate decreased as compared to the main sediment transport generated when the water level was included in the simulation. The current was the least parameter that affected sediment transport as there were few changes from the sediment rates. From the hydrodynamic module it was evident as the values of the currents were too low to cause any changes. According to Jayson-Quashigah et al. (2021), waves in the Volta Delta are the most prevalent oceanographic condition that affects sediment transport (shoreline morphology) in the area and thus confirms the results.

5.5 Issues affecting sediment dynamics along Fuveme Beach

Sediment movement in Fuveme is affected mainly by east littoral drift as has been observed in the Volta Delta (Anthony et al., 2016). This is as a result of the high wave impact occurring in the region and as predicted by the simulation. According to Ly (1981), the major sediment deposition into the region comes from two sources; the Volta River and the weathering of quaternary deposits exposed on the coasts. The issue of the Volta River is due

107

to the trapping of coarse sediment by the Akosombo Dam thus allowing for the deposition of finer sediment as opposed to coarse sediment onto the coast of Fuveme. According to Jayson-Quashigah (2019), this could be the reason why the coast of Fuveme is undergoing these intense changes within the shortest possible time.

Additionally, the issue of sea defence structures having a knock-on effect on downdrift areas could also be a reason as reported by Angnuureng et al. (2013). The construction of groynes just 2 km west of Fuveme could be trapping sediments updrift the area thereby starving the coast of Fuveme. More so, the sediment grain sizes of the Ada region of 0.920 mm (Jayson-Quashigah, 2019) as to 0.250 mm for Fuveme shows clearly that coarse sediments are being trapped updrift allowing for finer sediments to be transported to the area. Fine sediments are susceptible to erosion since they are well-rounded and sorted, they could be moved easily by wind and waves.

From the simulation, the bed level changes were sharp closer to the coast of Fuveme and were particularly higher towards the eastern end and lower towards the western end. This contributed to the sediment movement hugely as well. According to Jayson-Quashigah (2019), there is an underwater bar situated in the estuary mouth and it may be responsible for the bed level changes causing waves to break offshore with sediment being moved around thus feeding sediment to the area.

108

CHAPTER SIX

SUMMARY, CONCLUSIONS AND RECOMMENDATIONS

6.1 Summary

Fuveme Beach is a dynamic beach that experienced a lot of changes over the years. The overall objective of this study was to determine the geomorphic variabilities surrounding the 'bridged estuary' at Fuveme Beach and also to establish how sediment was transported along this coastal area. There have been a couple of research done in the area, but none employed the use of a numerical model for the simulation of sediment transport in the area thus this study is the first of its kind.

The study was divided into three specific objectives and the first objective was to assess sediment dynamics on Fuveme Beach. The results indicate that the coast of Fuveme eroded in the western part, accreted in the mid-section and eroded in the extreme eastern part leading to the formation of yet another bridged estuary. There was a positive sediment rate for the entire period. The profile of the area during the study period was also seen to be changing over the period. Sediment grain size was evident to show reasons for the changes seen along the coast, The sediments were well rounded with medium grain sizes at the berm and the low water level.

The second objective was to simulate the sediment evolution along the coast of Fuveme using MIKE 21 model. Results from the model were surface elevation (water level), current speed and direction, significant wave height, peak wave period, mean wave direction, sediment transport magnitude, sediment direction and bed level changes for the nearshore area of Fuveme. The surface elevation of the area was between 0.001 m – 0.7 m showing

109

relatively small water levels for the entire period. The current speed was between 0.0001 m/s – 0.3 m/s. for the entire period in the domain.

The current direction was dynamic across the study period. For every timestep, there were different directions of the current in relation to its speed. The significant wave height was predominantly high offshore, reaching as high as over 0.80 m and reaching as low as 0.20 m at the beach side. Similar to the significant wave height, the wave period of the area changed depending on the time steps. A wave period of 16 s was recorded at certain points in the simulation and a wave period as low as 7 s was also recorded. The Wave direction recorded were between 160 ° and 240 °. The simulation showed that the waves arrived at the coast predominantly from the South direction and occasionally from the South-southwest direction as confirmed by many reports. The sediment transport direction was mostly in the eastward direction. The bed level change was between 0.01 m and 2.0 m. The magnitude of the sediment transport for the area at specific points were between -0.0000010 m³/s/m and 0.00090 m³/s/m.

For the third objective, the hydrodynamic condition which affected the sediment movement was made known from the simulation. The wave parameter was the main hydrodynamic parameter that affected Fuveme Beach the most. This was followed by the tidal data which was responsible for the flow of the water masses. The current was the least parameter that affected the area. From the hydrodynamic module it was evident as the values of the currents were low to cause any changes.

110

6.2 Conclusions

The study about the beach dynamics of Fuveme has provided some results worthy of notice. The results have helped in the following conclusions;

Fuveme Beach is very dynamic and changes occur frequently in a matter of days or weeks. Erosion and accretion occur all year round at areas specifically close to the Volta Estuary and the area closer to Atiteti. Even though erosion was predominant on the extreme western and eastern end of the area with over 35,359 m³ of sediment being lost over the entire study period, deposition was also very colossal with over 126,979 m³ of sediment also gained over the period.

Additionally, sediment (total load) movement is in the same direction as waves, mainly from the south direction but longshore transport moves eastwards and parallel to the shoreline as well. Also, waves move from the south direction onto the shores of Fuveme, current moves in the eastward direction on shore and moves clockwise, offshore. Current in the region is low closer to the shore and higher offshore.

Finally, wave action is the biggest contributor to sediment movement in the area as shown by the simulation. Tides and current generated in the region contribute to sediment movement but its impacts are low as compared to waves. Waves coupled with high tides cause the overtopping of the sand bar resulting in the periodic erosion and flooding of the area.

6.3 Recommendations

It is recommended that a detailed bathymetric survey is done for the entire nearshore region as it forms the basis for further analysis of the ocean area. In as much as there are secondary data for most of the parameters, there

111

should be on field data collection for the various parameters including wave, tides and current so as to validate results obtained from numerical models.

There should be further monitoring of the Fuveme Beach using UAV, Video camera, satellite images and numerical models to give a better understanding of the dynamics of the area.

Finally, a thorough research needs to be done for the entire stretch from the Fuveme Beach to the Dzita Beach to fully understand the dynamics of the region. This helps so that in the event that a coastal management plan be established, then the whole stretch will be considered.
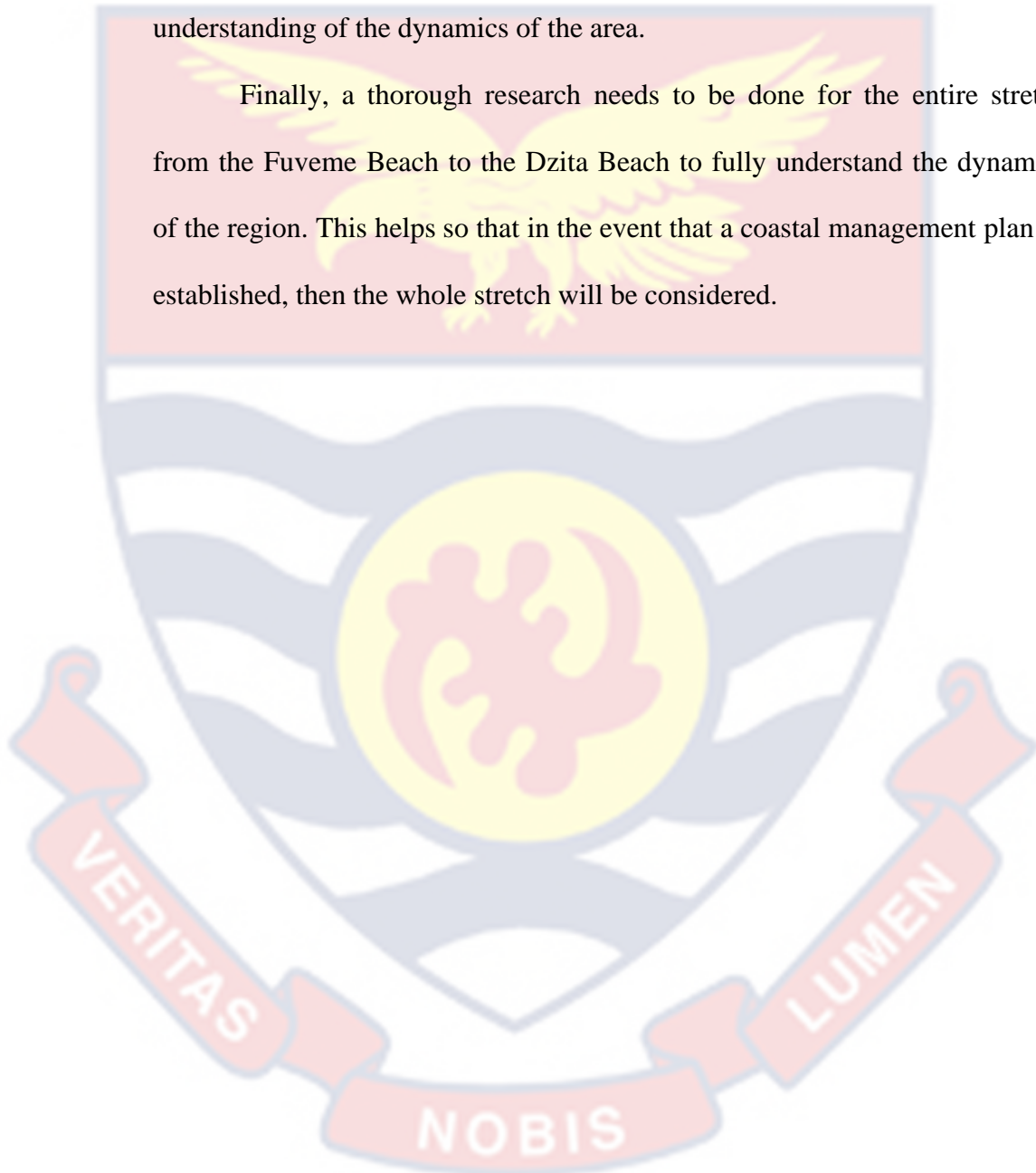
REFERENCES

Aagaard, T. (2002). Modulation of surf zone processes on a barred beach due to changing water levels; Skallingen, Denmark. *Journal of Coastal Research*, 25-38.

Agisoft (2022). Agisoft PhotoScan. Retrieved from http://www.agisoft.com

Akpati, B.N. (1978). Geologic structure and evolution of the Keta Basin, Ghana West Africa. *Geological Society of America Bulletin*, 89(1), 124–132.

Akrasi, S. A. (2011). Sediment Discharges from Ghanaian Rivers into the Sea. *West African Journal of Applied Ecology*.

Allaby & Allaby (Ed.). (2018). *Coastal Process*. Encyclopaedia.org Retrieved from: https://www.encyclopedia.com/earth-and-environment/ecology-and-environmentalism/environmental-studies/coastal-processes

Allen, J. R. L., & Pye, K. (1992). Coastal saltmarshes: their nature and importance. *Saltmarshes: Morphodynamics, conservation and engineering significance*, 1-18.

Almar, R., Kestenare, E., Reyns, J., Jouanno, J., Anthony, E. J., Laibi, R., ... & Ranasinghe, R. (2015). Response of the Bight of Benin (Gulf of Guinea, West Africa) coastline to anthropogenic and natural forcing, Part1: Wave climate variability and impacts on the longshore sediment transport. *Continental Shelf Research*, 110, 48-59.

Alves, R. B., Angnuureng, B. D., Almar, R., Louarn, A., Rossi, P. L., Corsini, L., & Morand, P. (2022). Compendium: Coastal management practices in West Africa: existing and potential solutions to control coastal

113

erosion, prevent flooding and mitigate damage to society. The World Bank.

Anim, D. O., Nkrumah, P. N., & David, N. M. (2013). A rapid overview of coastal erosion in Ghana. *International Journal of Scientific & Engineering Research*, 4(2), 1-7.

Angnuureng, D. B., Amankona, G., Brempong, E. K., & Attipoe, E. (2022). Short-term effect of sea defence on shoreline and wave variability in Elmina Bay, Ghana. *Journal of Coastal Conservation*, 26(6), 1-14.

Angnuureng, D. B., Jayson-Quashigah, P. -N., Appeaning Addo, K., Aheto, D. W., Almar, R., Bonou, F., & Brempong, E. (2019). Quantification of the shoreline evolution of an open beach between coastal defences. *In Coastal Sediments 2019: Proceedings of the 9th International Conference* (pp. 1562 - 1576).

Angnuureng, D. B., Appeaning Addo, K., Almar, R., & Dieng, H. (2018). Influence of sea level variability on a micro-tidal beach. *Natural Hazards*, *93*(3), 1611-1628.

Angnuureng, D. B., Almar, R., Appeaning Addo, K., Castelle, B., Senechal, N., Laryea, S. W., & Wiafe, G. (2016). Video Observation of waves and shoreline change on the microtidal James town beach in Ghana. *Journal of Coastal Research*, (75 (10075)), 1022-1026.

Angnuureng, D. B., Appeaning Addo, K., & Wiafe, G. (2013). Impact of sea defence structures on downdrift coasts: The case of Keta in Ghana. *Academia Journal of Environmental Sciences*, *1*(6), 104–121.

114

Anthonio, S. L. & Valentine, E. M. (1995). Influence of Wave Climate on Coastal Erosion in Keta, South Eastern Ghana. *Int. Conf. on Coastal and Port Engineering in Developing Countries*, pp. 253 - 262.

Anthony, E., Almar, R., & Aagaard, T. (2016). Recent shoreline changes in the Volta River Delta, West Africa: the roles of natural processes and human impacts. *African Journal of Aquatic Science*, 41(1), 81 – 87.

Anthony, E. J., and Blivi, A. B. (1999). Morphosedimentary evolution of a delta sourced, drift-aligned sand barrier-lagoon complex, western Bight of Benin. *Marine Geology*, 158, 161-176.

Appeaning Addo, K., Brempong, E. K., & Jayson-Quashigah, P. -N. (2020). Assessment of the dynamics of the Volta River Estuary shorelines in Ghana. *Geoenvironmental Disasters*, 7(1), 1-11.

Appeaning Addo, K., Jayson-Quashigah, P. -N., Codjoe, S. N. A. & Martey, F. (2018a). Drone as a tool for coastal flood monitoring in the Volta Delta, Ghana. *Geoenvironmental Disasters*, *5*(1), 17.

Appeaning Addo, K., Nicholls, R. J., Codjoe, S. N. A., & Abu, M. (2018b). A Biophysical and Socioeconomic Review of the Volta Delta, Ghana. *Journal of Coastal Research*, *345*(5), 1216–1226.

Appeaning Addo, K. (2015a). Assessment of the Volta Delta shoreline change. *Journal of Coastal Zone Management*, *18*(3), 1–6.

Appeaning Addo, K. (2015b). Monitoring sea level rise-induced hazards along the coast of Accra in Ghana. *Natural Hazards*, *78*(2), 1293-1307.

115

Appeaning Addo, K. (Ed.). (2015c). Why Ghana needs a new approach to stop the erosion of its coastline. *The Conversation Africa Inc*. Retrieved from: https://theconversation.com/why-ghana-needs-a-new-approach-to-stop-the-erosion-of-its-coastline-44018

Appeaning Addo, K., Jayson-Quashigah, P. -N., & Kufogbe, K. S. (2011). Quantitative analysis of shoreline change using medium resolution satellite imagery in Keta, Ghana. *Marine Science*, 1(1), 1–9.

Appeaning Addo, K. (2009). Detection of coastal erosion hotspots in Accra, Ghana. *Journal of Sustainable Development in Africa*, 11(4), 253-265.

Appeaning Addo, K., Walkden, M., & Mills, J. T. (2008). Detection, measurement and prediction of shoreline recession in Accra, Ghana. *ISPRS Journal of Photogrammetry and Remote Sensing*, 63(5), 543-558.

Ashong, S., N., A. & Gbeckor-Kove, P., D. (2020). Evidence-based regulation for sustainable development - coastal protection in Ghana. *Focus Africa.*

Awadzi, T. W., Ahiabor, E., & Breuning-Madsen, H. (2008). The soil-land use system in a sand spit area in the semi-arid coastal savanna region of Ghana: Development, sustainability and threats. *West African Journal of Ecology,* 13, 132–143.

Ayisi, E., (Ed.). (2022). As rising seas destroy Ghana's coastal communities, researchers warn against a seawall-only solution. *Mongabay.org USA*.

Badru, G. S., Odunuga, S. S., Omojola, A. S., & Oladipo, E. O. (2022). Numerical modelling of sediment transport in southwest coast of

116

Nigeria: Implications for sustainable management of coastal erosion in the Bight of Benin. *Journal of African Earth Sciences*, 104466.

Balasubramanian A., (2014). The Ocean Currents. *December, 2014 Conference: Country-wide Classroom Educational TV programme-Gyan Darshan*. University of Mysore.

Banoeng-Yakubo, B. K., Akabzaa, M., Hotor, V. & Danso, S.K. (2006). Application of Electrical Resistivity Techniques in Delineation of Saltwater-Freshwater in Keta Basin, Ghana. *Groundwater Pollution in Africa.* London: Taylor & Francis, pp. 193–202.

Battjes, J.A. & Janssen, P., (1978). Energy loss and set-up due to breaking of random waves. *International Conference on Coastal Engineering*, ASCE, New York, 569-587.

Belliard, J. P., Toffolon, M. Carniello, L. & D'Alpaos A. (2015). An ecogeomorphic model of tidal channel initiation and elaboration in progressive marsh accretional contexts. *Journal of Geophysical Research: Earth Surface*, 1040–1064, doi:10.1002/2015JF003445.

Bhattacharya, J. (2003). Deltas and Estuaries. In: G. V. Middleton, M. J. Church, M. Coniglio, L. A. Hardie, & F. J. Longstaffe (Eds.), *Encyclopaedia of Sediments and Sedimentary Rocks* (pp. 310–322). Springer Netherlands.

Blanchette, C. A., O'Donnell, M. J., & Stewart, H. L. (2008). Waves as an Ecological Process. *Encyclopaedia of Ecology*. 3764–3770.

Blott, S. J., & Pye, K. (2012). Particle size scales and classification of sediment types based on particle size distributions: Review and recommended procedures. *Sedimentology*, 59(7), 2071-2096.

Boateng, I. (2012). An application of GIS and coastal geomorphology for large   scale assessment of coastal erosion and management: a case study of Ghana. *Journal of Coastal Conservation*, 16, 383-397.

Boateng, I., Bray, M., & Hooke, J. (2012). Estimating the fluvial sediment input to the coastal sediment budget: A case study of Ghana. *Geomorphology*, 138(1), 100-110.

Boateng, I. (2009). Development of Integrated Shoreline Management Planning: A Case Study of Keta, Ghana. In: *Federation of International surveyors Working Week 2009, Surveyors Key Role in Accelerated Development* (pp. 1–19). Eilat: International Federation of Surveyors.

Bolle, A., das Neves, L., & Rooseleer, J. (2015). Coastal protection for Ada, Ghana: A case study. *Proceedings of the Institution of Civil Engineers: Maritime Engineering*, 168(3), 1–9.

Brasington, J., Rumsby, B. T., & Mcvey, R. A. (2000). Monitoring And Modelling Morphological Change in a Braided Gravel-Bed River Using High Resolution GPS-Based Survey. *Earth surface processes and landforms: The Journal of the British Geomorphological Research Group*, 25(9), 973–990.

Brempong, E. K., Angnuureng, D. B., Appeaning Addo, K., & Jayson-Quashigah, P. -N. (2021). Short-term seasonal changes of the Dzita Beach of Ghana using geographic information system and photogrammetry. *Interpretation*, 9(4), SH87-SH97.

118

Brempong, E. K. (2019). *Assessing Short-Term Beach Morphological Dynamics of a Microtidal Beach: A Case Study of The Dzita Beach Ghana*. Unpublished master's thesis. University of Ghana. Legon-Accra, Ghana.

Buschmann, J., Berg, M., Stengel, C., Winkel, L., Sampson, M. L., Trang, P. T. K., & Viet, P. H. (2008). Contamination of drinking water resources in the Mekong delta floodplains: Arsenic and other trace metals pose serious health risks to population. *Environment International*, *34*(6), 756-764.

C3S (2017). ERA5: Fifth generation of ECMWF atmospheric reanalyses of the global climate. *Copernicus Climate Change Service (C3S) Data Store*. Retrieved (28 October, 2022) from https://cds.climate.coperni cus.eu/cdsapp#!/dataset/reanalysis-era5-single-levels-monthly-means?tab=overview

Cameron, W. M., & Pritchard, D. W. (1963). Estuaries. Pp. 306ō324 in Hill, MN (Ed.): *The sea*, vol. 2.

Coastal Processes (2022). Coastal Processes. *Geography Revision*. Retrieved from:https://geography-revision.co.uk/gcse/coastal-landscapes/coastal-processes/

Cochran, J. K. (2014). Estuaries *Elsevier Inc*. Netherlands

Codjoe, S. N. A., Appeaning Addo, K., Addoquaye Tagoe, C., Nyarko, B. K., Martey, F., Nelson, W. A., Jayson-Quashigah, P, N., Atiglo, D. Y.Adjei, P. O., Anderson, K., Mensah, A., Ofori-Danson, P.K., Amisigo, B. A., Ayamga, J., Asmah, E. E., Asenso, J.K., Owusu, G., Quaye, R. M., … & Abu, M. (2020). The Volta Delta, Ghana:

119

Challenges in an African Setting. *In Deltas in the Anthropocene (pp. 79-102)*. Palgrave Macmillan, Cham.

Cohn, N., Brodie, K. L., Johnson, B., & Palmsten, M. L. (2021). Hotspot dune erosion on an intermediate beach. *Coastal Engineering*, *170*, 103998.

Coode, A. T. (1929). Keta coast erosion - Rept. Messrs Coode, Wilson, *Mitchell & Vaughan-Lee*, Accra, 1929-30: 13 pp.

Croitoru, L., Montero M., Jose, J., & Maria, S. (2019). *The Cost of Coastal Zone Degradation in West Africa : Benin, Cote d'Ivoire, Senegal, and Togo (English)*. Washington, D.C. The World Bank Group.

Czuba, J. A., Magirl, C. S., Czuba, C. R., Grossman, E. E., Curran, C. A., Gendaszek, A. S., & Dinicola, R. S. (2011). Comparability of Suspended-Sediment Concentration and Total Suspended Solids Data Sediment Load from Major Rivers into Puget Sound and its Adjacent Waters. *USGS Fact Sheet 2011–3083*. Tacoma, WA: US Geological Survey

Dada, O. A., Li, G., Qiao, L., Ding, D., Ma, Y., & Xu, J. (2016). Seasonal shoreline behaviours along the arcuate Niger Delta coast: Complex interaction between fluvial and marine processes. *Continental Shelf Research*, *122*, 51-67.

Dawson, A. G. (2003). *Tsunami: The underrated hazard*. Cambridge University Press, Cambridge, 2001 (320 pp).

De Mahiques, M. M. (2016). Sediment Sorting. In: Kennish, M.J. (eds) Encyclopaedia of Estuaries. *Encyclopaedia of Earth Sciences Series*. Springer, Dordrecht.

120

Dean, R. G. & Dalrymple, R. A. (2004). *Coastal processes with engineering applications*. Cambridge University Press.

Defeo, O., McLachlan, A., Schoeman, D. S., Schlacher, T. A., Dugan, J., Jones, A., ... & Scapini, F. (2009). Threats to sandy beach ecosystems: a review. *Estuarine, Coastal and Shelf Science*, 81(1), 1-12.

Delft Hydraulics Laboratory (1993). *Keta-Kedzi Road Rehabilitation Project*. Coastal Hydraulic Aspects. Prepared for Wayss & Freytag AG.

Del Río, L., Plomaritis, T. A., Benavente, J., Valladares, M., & Ribera, P. (2012). Establishing Storm Thresholds for the Spanish Gulf of Cádiz coast. *Geomorphology*, 143, 13-23.

Devlin, A. & Pan, J. (2020). Estuaries and Coastal zones: Dynamics and response to environmental changes. *Intech Open*, London

Drishtiias (2022). *Ocean Currents* Retrieved from: https://www.drishtiias.com/to-the-points/paper1/ocean-currents1#:~:text=What%20are%20Ocean%20Currents%3F%201%20Ocean%20currents%20are,the%20biosphere%20due%20to%20their%20influence%20on%20climate.

Dzakpasu, M. F. A (2019). *Ecological Assessment of some Coastal Lagoons and Estuaries in Ghana: Abiotic and Biotic Approaches*. (PhD Thesis, University of Cape Coast). Retrieved from https://ir.ucc.edu.gh/xmlui/bitstream/handle/123456789/7132/DZAKPASU%2c%202019.pdf?sequence=1

Earth network (2018). *Rip current definition and Safety Tips (A definitive Guide).* Retrieved from: https://www.earthnetworks.com/blog/rip-current-definition-and-safety-tips-a-definitive-guide/

121

Ecoshape (2022). *Sandy Beaches.* The Netherlands. Retrieved from: https://www.ecoshape.org/en/landscapes/sandycoasts/

Edmonds, D. A., & Slingerland R. L. (2010). Significant effect of sediment cohesion on delta morphology. *Nature Geoscience*, 3(2), 105–109.

FAO (2011). *AQUASTAT Transboundary River Basins – Ganges-Brahmaputra Meghna River Basin.* Food and Agriculture Organization of the United Nations (FAO). Rome, Italy.

Finkl, C. W. (2004). Coastal classification: systematic approaches to consider in the development of a comprehensive scheme. *Journal of Coastal Research*, *20*(1), 166-213.

Fondriest Environmental (2022). *Sediment Transport and Deposition.* Fondriest Environmental Inc. Retrieved from: https://www.fondriest. com/environmentalmeasurements/parameters/hydrology/sediment-transport-deposition/

Freedman (1955). Referenced in AESC, 1976 Technical Rept. CE/2.

Galapatti, R. (1983). *A depth integrated model for suspended transport.* Department of civil engineering, Delft University of Technology.

Gampson, E. K., Nartey, V. K. Golow, A. A., Akiti, T. T., Sarfo, M. A., Salifu, M., Aidoo, F., & Fuseini, A. R. (2015). Physical and isotopic characteristics in peri-urban landscapes: A case study at the lower Volta River Basin, Ghana. *Applied Water Science*, 7(2), 729–744.

Garrison, T. (2013). *Oceanography: An invitation to Marine Science.* California: Wadsworth Inc.

Giardino, A., Schrijvershof, R., Nederhoff, C. M., De Vroeg, H., Brière, C.,
Tonnon, P. K., Caires, S., Walstra, D.J., Sosa, J., Van Verseveld, W.,
Schellekens & Sloff, C. J. (2018). A quantitative assessment of human
interventions and climate change on the West African sediment budget.
Ocean and Coastal Management, *156*, 249–265.

GK Today (2016). *Ocean Currents: Meaning and Types*. Retrieved from:
https://www.gktoday.in/topic/ocean-currents-meaning-and-types/

Gregory, F. (2011). *Review of Coastal Processes and Evaluation of the Impact
of the Constructed Groynes along Lady Robinsons Beach, Botany Bay,
New South Wales, Australia.* University of Wollongong, pp. 1 – 109.

Hansen, D. V. & Rattray Jr, M. (1972). Estuarine Circulation Induced by
Diffusion. *Journal of Marine Resources*, 30, pp. 281-294

Hapke, C., Reid, D., Richmond, B. M., Ruggiero, P., & List, J. (2006).
National assessment of shoreline changes Part 3: Historical shoreline
change and associated coastal land loss along sandy shorelines of the
California Coast. *US Geological Survey Open File Report,* 2006-1219.

Hardisty, J. (1990). *Beaches: Form and Processes*. London: Unwin Hyman,
324 p.

Hasselmann, K. (1974). On the spectral dissipation of ocean waves due to
white capping. *Boundary-Layer Meteorology*, 6(1), 107-127.

Hayes, M. O., Michel, J., and Holmes, J. M. (2007). *A Coast for All Seasons:
A Naturalist's Guide to the Coast of South Carolina.* Pandion Books.

Heaslip, E. (Ed.). (2022). *Understanding Surface Ocean Current vs Deep Sea Current* Sofar Ocean. Retrieved from: https://www.sofarocean.com/posts/understanding-surface-currents-vs-deep-ocean-currents

Hewawasam, I. (1998) *Coastal management Strategy for Ghana. Africa Region Findings & Good Practice.* The World Bank. Retrieved from https://openknowledge.worldbank.org/handle/10986/9894

Himmelstoss, E. A., Henderson, R. E., Kratzmann, M. G., & Farris, A. S. (2018). *Digital Shoreline Analysis System (DSAS) version 5.0 user guide (No. 2018-1179).* US Geological Survey.

Holt, B. (2022). *Longshore Currents.* NASAgov. Retrieved from: https://www.earthdata.nasa.gov/topics/ocean/coastal-processes/longshore-currents

Holthuijsen, L. H., Herman, A., & Booij, N. (2003). Phase-decoupled refraction–diffraction for spectral wave models. *Coastal Engineering*, *49*(4), 291-305.

Holthuijsen, L. H., Booij, N., & Herbers, T. H. C. (1989). A prediction model for stationary, short-crested waves in shallow water with ambient currents. *Coastal Engineering*, *13*(1), 23-54.

Janssen, P. A., (1989). Wave induced stress and the drag of airflow over sea waves. *Journal of Physical Oceanography*, 19, 745-754.

Jayson-Quashigah, P. -N., Appeaning Addo, K., Wiafe, G., Amisigo, B. A., Brempong, E. K., Kay, S., & Angnuureng, D. B. (2021). Wave dynamics and shoreline evolution in deltas: A case study of sandy coasts in the Volta delta of Ghana. *Interpretation*, *9*(4), SH99-SH113.

124

Jayson-Quashigah, P. -N. (2019). *Measuring and Simulating Shoreline Morphodynamics in the Volta Delta.* (PhD Thesis, University of Ghana). Retrieved from: https://ugspace.ug.edu.gh/bitstream/handle /123456789/33501/measuring%20and%20simulating%20shoreline%2 0morphodynamics%20in%20the%20volta%20delta,%20%20ghana.pdf

Jayson-Quashigah, P. -N., Appeaning Addo, K. & Kufogbe, S. K., (2013). Shoreline monitoring using medium resolution satellite imagery, a case study of the eastern coast of Ghana. *Journal of Coastal Research*, 65: 511-516.

Komen, G.J., Cavaleri, L., Doneland, M., Hasselmann, K., Hasselmann S. & Janssen, P.A. (1994). *Dynamics and modelling of ocean waves*. Cambridge University Press, UK, 560pp.

Kortatsi, B.K., Young, E., & Mensah-Bonsu, A., (2005). Potential impact of large-scale abstraction on the quality of shallow groundwater for irrigation in the Keta Strip, Ghana. *West African Journal of Applied Ecology*, 8(1), 1–12.

Langland, M & Cronin, T. M. (2003). *A summary report of sediment in Chesapeake Bay and watershed.* US Geological Survey Water Resources Investigations Report 03-4123, 109p

Lesser, G. R., Roelvink, J. V., Van Kester, J. T. M., & Stelling, G. S. (2004). Development and validation of a three-dimensional morphological model. *Coastal engineering*, 51(8-9), 883-915.

Living Deltas, (2022). *Creating Sustainable Deltas.* United Kingdom. Retrieved from: https://livingdeltas.org/

Luan, H. L., Ding, P. X., Wang, Z. B., & Ge, J. Z. (2017). Process-based morphodynamic modelling of the Yangtze Estuary at a decadal timescale: Controls on estuarine evolution and future trends. *Geomorphology*, *290*, 347-364.

Luijendijk, A., Hagenaars, G., Ranasinghe, R., Baart, F., Donchyts, G., & Aarninkhof, S. (2018). The State of the World's Beaches. *Scientific reports*, *8*(1), 1-11.

Ly, C. K. (1980). The role of the Akosombo Dam on the Volta River in causing coastal erosion in central and eastern Ghana (West Africa). *Marine Geology*, *37*(3-4), 323-332.

Mancini, F., Dubbini, M., Gattelli, M., Stecchi, F., Fabbri, S., & Gabbianelli, G. (2013). Using Unmanned Aerial Vehicles (UAV) for High-Resolution Reconstruction of Topography: The Structure from Motion Approach on Coastal Environments. *Remote Sensing*, *5*(12), 6880-6898.

Manson, A. A., Appeaning Addo, K., & Mensah, A., (2013). Impacts of shoreline morphological change and sea level rise on mangroves: The Case of the Keta Coastal Zone. *Journal of Environmental Research and Management*, 4(10), 0334–0343.

Mariotti, G., & Canestrelli, A. (2017). Long-term morphodynamics of muddy back barrier basins: Fill in or empty out? *Water Resources Research,* 53(8), 7029-7054.

126

Masselink, G., Hughes, M., & Knight, J. (2014). *Introduction to coastal processes and geomorphology*. Routledge.

McGlashan, D. J., Duck, R. W., & Reid, C. T. (2005). Defining the foreshore: coastal geomorphology and British laws. *Estuarine, coastal and shelf science*, *62*(1-2), 183-192.

Mentaschi, L., Vousdoukas, M., Pekel, J., Voukouvalas, E., Feyen, L., (2018). Global long-term observations of coastal erosion and accretion. *Scientific Report*, 8, 12876.

MIKE (2020a). *Hydrodynamic Model Flow FM, User Guide*. Horsholm: DHI Retrieved from: https://manuals.mikepoweredbydhi.help/2017/Coast _and_Sea/MIKE_321 _FM_Scientific_Doc.pdf

MIKE (2020b). *Spectral Wave FM, All Modules: Scientific Documentation*. Horsholm: DHI Retrieved from: https://manuals.mikepoweredbydh i.help/2017/Coast_and_Sea/M21SW_Scientific_Doc.pdf

MIKE (2020c). *Sediment Transport FM, All Modules: Scientific Documentation*. Horsholm: DHI Retrieved from: https://manuals.mike poweredbydhi.help/2017/Coast_and_Sea/MIKE_FM_ST_Scientific_D oc.pdf

MIKE (2017). *21/3 Coupled Model FM, User Guide*. Horsholm: DHI Retrieved from: https://manuals.mikepoweredbydhi.help/ 2017/Coast_ and_Sea/MIKE_213_Coupled_Model_FM.pdf

Morton, R. A., Miller, T., & Moore, L. (2005). Historical shoreline changes along the US Gulf of Mexico: a summary of recent shoreline comparisons and analyses. *Journal of Coastal Research*, *21*(4), 704-709.

Murray, A. B. (2003). Contrasting the goals, strategies, and predictions associated with simplified numerical models and detailed simulations. *Geophysical Monograph-American Geophysical Union*, 135, 151-168.

Nairn, R. B., & Dibajnia, M. (2004). Design and construction of a large headland system, Keta Sea Defence Project, West Africa. *Journal of Coastal Research*, 33, 294–314.

Nairn, R. B., MacIntosh, K. J., Hayes, M. O., Nai, G., Anthonio, S. L., & Valley, W. S. (1999). Coastal erosion at Keta lagoon, Ghana–large scale solution to a large-scale problem. *In Coastal Engineering 1998* (pp. 3192-3205).

National Geographic Society (2022). *The Many Effects of Flooding.* Retrieved from: https://education.nationalgeographic.org/resource/many-effects-flooding

Nelson, K. S., & Fringer, O. B. (2018). Sediment dynamics in wind wave-dominated shallow-water environments. *Journal of Geophysical Research: Oceans*, 123(10), 6996-7015.

NEDECO (1980). *Coastal Erosion and protective measures at Keta*. Project Report.

NEDECO (1974). *Ghana - Keta coast erosion - report of an identification mission*. Project Report.

NEDECO (1964). *Flood relief and resettlement plan for Keta Town*. Project Report.

Nienhuis, J. H., Ashton, A. D., Nardin, W. Fagherazzi, S & Giosan, L. (2016), Alongshore sediment bypassing as a control on river mouth morphodynamics. *Journal of Geophysical Research: Earth Surface*, 121 (4), 664–683.

NOAA (2022a). *Longshore Currents.* United States of America. Retrieved from: https://oceanservice.noaa.gov/education/tutorial_currents/03coastal2.html

NOAA (2022b). *What is an Estuary?* United States of America. Retrieved from: https://oceanservice.noaa.gov/facts/estuary.html

NOAA (2011). *Ocean Currents.* United States of America. Retrieved from: https://www.noaa.gov/education/resource-collections/ocean-coasts/ocean-currents

Osmond, D. L., Line, D. E., Gale, R. W., Knott, C. B., & Bartenhagen, K. A. (1995). *Water, Soil and Hydro-Environmental Decision Support System.* Scientific Research Publishing Inc.

Oyedotun, T. T. (2014) Shoreline Geometry: DSAS as a Tool for Historical Trend Analysis. *Geomorphological Techniques (Online Edition),* 2:1–12

Perlman, H. (2014). *Sediment and suspended sediment*. The USGS Water Science School.

Pender, D. (2013). *A statistical-process based approach for modelling profile variability*. University of Glasgow.

Pinet, P. R. (2009). Invitation to Oceanography. *In Jones and Bartlett Publishers*.

Pugh, D. (2019). Tides. *In Encyclopedia of Ocean Sciences*.

129

Ranasinghe, R. (2016). Assessing climate change impacts on open sandy coasts: A review. *Earth-science reviews*, 160, 320-332.

Reid, I., Laronne, J. B., & Powell, D., M. (1998). Flash-flood and bedload dynamics of desert gravel-bed streams. *Hydrological Processes*, 12(4), 543-557.

Reeve, D., Chadwick, A., & Fleming, C. (2004). *Coastal engineering: processes, theory and design practice*. CRC Press.

Roelvink, D., & Reniers, A. (2011). *A Guide to Modelling Coastal Morphology*. *A Guide to Modelling Coastal Morphology*. World Scientific.

Romine, B. M., Fletcher, C. H., Genz, A. S., Barbee, M. M., Dyer, M., Anderson, T. R., ... & Richmond, B. M. (2011). National assessment of shoreline change: A GIS compilation of vector shorelines and associated shoreline change data for the sandy shorelines of Kauai, Oahu, and Maui; Hawaii. *US Geological Survey Open-File Report*, 1009.

Schlacher, T. A., Dugan, J., Schoeman, D. S., Lastra, M., Jones, A., Scapini, F., ... & Defeo, O. (2007). Sandy beaches at the brink. *Diversity and Distributions*, *13*(5), 556-560.

Shepard, F.P. (1973). Submarine Geology. *New York: Harper and Row*, 519p.

Short, A., D. (1999). *Beach and Shoreface Morphodynamics*. John Wiley and Sons, Chichester.

Short, A. D. (Ed.). (2012). *Coastal Processes and Beaches*. Nature Education

Knowledge 3(10):15 Retrieved from: https://www.nature.com/scitable/

knowledge/library/coastal-processes-and-beaches-26276621/

Smagorinsky, J. (1963). General Experiment with the Primitive Equations.

Monthly Weather Review, 91, No. 3, 99 – 164.

Study Page (2022). *Ocean Currents*. Retrieved from: https://www.studypage.

in/geography/ocean-currents

Study Smarter (2022). Coastal Management. Retrieved from: https://www.

studysmarter.us/explanations/geography/coastsgeography/coastal-

management/

Sona, G., Pinto, L., Pagliari, D., Passoni, D., & Gini, R. (2014). Experimental

analysis of different software packages for orientation and digital

surface modelling from UAV images. *Earth Science Informatics*, *7*(2),

97–107.

Spehar, R., Cormier, S. & Taylor, D. (Ed.). (2007). *Candidate Causes.*

Sediments. In: Causal Analysis, Diagnosis Decision Information

System, USEPA. U.S. Environmental Protection Agency, Washington,

DC, EPA/600/R-08/022, 2007.

Tappan, G. G., Cushing, M.W., Cotillon, S. E., Hutchinson, J.A., Pengra, B.,

Alfari, I., Botoni, E., Soulé, A., … & Hermann, S. M. (2016).

Landscapes of West Africa: A window on a changing world. United

States Geological Survey Garretson, SD

Temmerman, S., Bouma, G., Govers, T. J., Wang, Z. B., De Vries, M. B., &

Herman, P. M. (2005). Impact of vegetation on flow routing and

131

sedimentation patterns: Three-dimensional Modelling for a Tidal Marsh. *Journal of Geophysical Research,* 110, F04019.

Tessler, Z. D., Vörösmarty, C. J., Grossberg, M., Gladkova, I., Eisenman, H., Syvitski, J.P.M., & Foufoula-Georgiou, E. (2015). Profiling risk and sustainability in coastal deltas of the world. *Sciences,* 349, 638 – 643.

Thornton, E. B., & Guza, R. T. (1983). Transformation of wave height distribution. *Journal of Geophysical Research: Oceans*, 88(C10), 5925-5938.

Udden, J. A. (1898). *The mechanical composition of wind deposits* (No.1). Lutheran Augustana book concern, printers.

United Nations Ocean Conference (2017). *Ocean Facts Sheet* United Nations. Retrieved from: https://www.un.org/sustainabledevelopment/wpcontent/uploads/2017/05/ Ocean-fact-sheet-package.pdf

USGS-West Africa (2022). *Coastal erosion in northwest Guinea Bissau.* Retrieved from: https://eros.usgs.gov/westafrica/case-study/coastal-erosion-northwestern-guineabissau#:~:text=Coastal%20erosion% 20is%20a%20major%20environmental%20problem%20throughout,in %20the%20past%2040%20years%20%28see%20inset%20above%29.

Van Rijn, L. C. (1984). Sediment transport, part II: suspended load transport. *Journal of Hydraulic Engineering*, 110(11), 1613-1641.

Vassie, J. M., Woodworth, P. L., & Holt, M. W. (2004). An example of North Atlantic deep-ocean swell impacting ascension and St. Helena Islands in the central South Atlantic. *Journal of Atmospheric and Oceanic Technology*, 21(7), 1095-1103.

Ville-Levinson, A. (Ed.). (2010). *Contemporary issues in estuarine physics*. Cambridge University Press.

Vousdoukas, M. I., Ranasinghe, R., Mentaschi, L., Plomaritis, T. A., Athanasiou, P., Luijendijk, A., & Feyen, L. (2020). Sandy coastlines under threat of erosion. *Nature climate change*, 10(3), 260-263.

Webb, P. (2022a). *Introduction to Oceanography: Beaches*. Pressbooks. Retrieved from: https://rwu.pressbooks.pub/webboceanography/chapter/13-1-beaches/

Webb, P. (2022b). *Introduction to Oceanography: Classifying sediments*. Pressbooks. Retrieved from: https://rwu.pressbooks.pub/webboceanography/chapter/12-1-classifying-sediments/

Wellens-Mensah, J. Armah, A.K. Amlalo, D.S., & Tetteh, K., (2002). Ghana National Report Phase 1: *Integrated Problem Analysis. Accra, Ghana: GEF MSP Sub-Saharan Africa Project (*GF/6010-0016): Development and Protection of the Coastal and Marine Environment in Sub-Saharan Africa. Accra, Ghana.

Wentworth, C. K. (1922). A scale of grade and class terms for clastic sediments. *The Journal of Geology*, *30*(5), 377-392.

Wetzel, R. G. (2001). *Limnology: lake and river ecosystems*. Gulf Professional Publishing.

Wheaton, J. M., Brasington, J., Darby, S. E., & Sear, D. A. (2010*).* Accounting for uncertainty in DEMs from repeat topographic surveys: improved sediment budgets. Earth surface processes and landforms: *The Journal of the British Geomorphological Research Group*, *35*(2), 136-156.

Wolf, P., DeWitt, B., & Wilkinson, B. (2000). *Elements of Photogrammetry with Applications in GIS*. Columbus, OH, USA: McGraw-Hill Higher Education.

Woodroffe, C. D., Nicholls, R. J., Saito, Y., Chen, Z., & Goodbred, S. L. (2006). Landscape variability and the response of Asian megadeltas to environmental change. *Global change and integrated coastal management*: The Asian-Pacific Region 277-314.

Wu, Y., Chaffey, J., Greenberg, D. A., Colbo, K., & Smith, P. C. (2011). Tidally-induced sediment transport patterns in the upper Bay of Fundy: a numerical study. *Continental Shelf Research*, *31*(19-20), 2041-2053.

Xorse, T. M. S (2013). *Impact of Wave Dynamics on the coast of Ghana*. (MPhil Thesis – University of Ghana) Retrieved from: https://ugspace. ug.edu.gh/bitstream/handle/123456789/8788/10203247_TMSX_DMF S_(Thesis).pdf

Yankson, K. (2000). Aspects of conchological features of Anadara senilis in relation to the nature of subtratum. *Journal of the Ghana Science Association*, 2(3), 123-128.

Yidana, S.M. & Chegbeleh, L.P. (2013). The hydraulic conductivity field and groundwater flow in the unconfined aquifer system of the Keta Strip, Ghana. *Journal of African Earth Sciences*, 86, 45–52.

APPENDICES

Appendix A: XYZ coordinates for GCPs

Linear Unit: Metres

Angular Unit: DMS

Projection: GHANA-TM

Datum: WGS 1984

Time Zone: GMT Standard Time

Table A.1: Elevations for Ground Control Points at Fuveme Beach
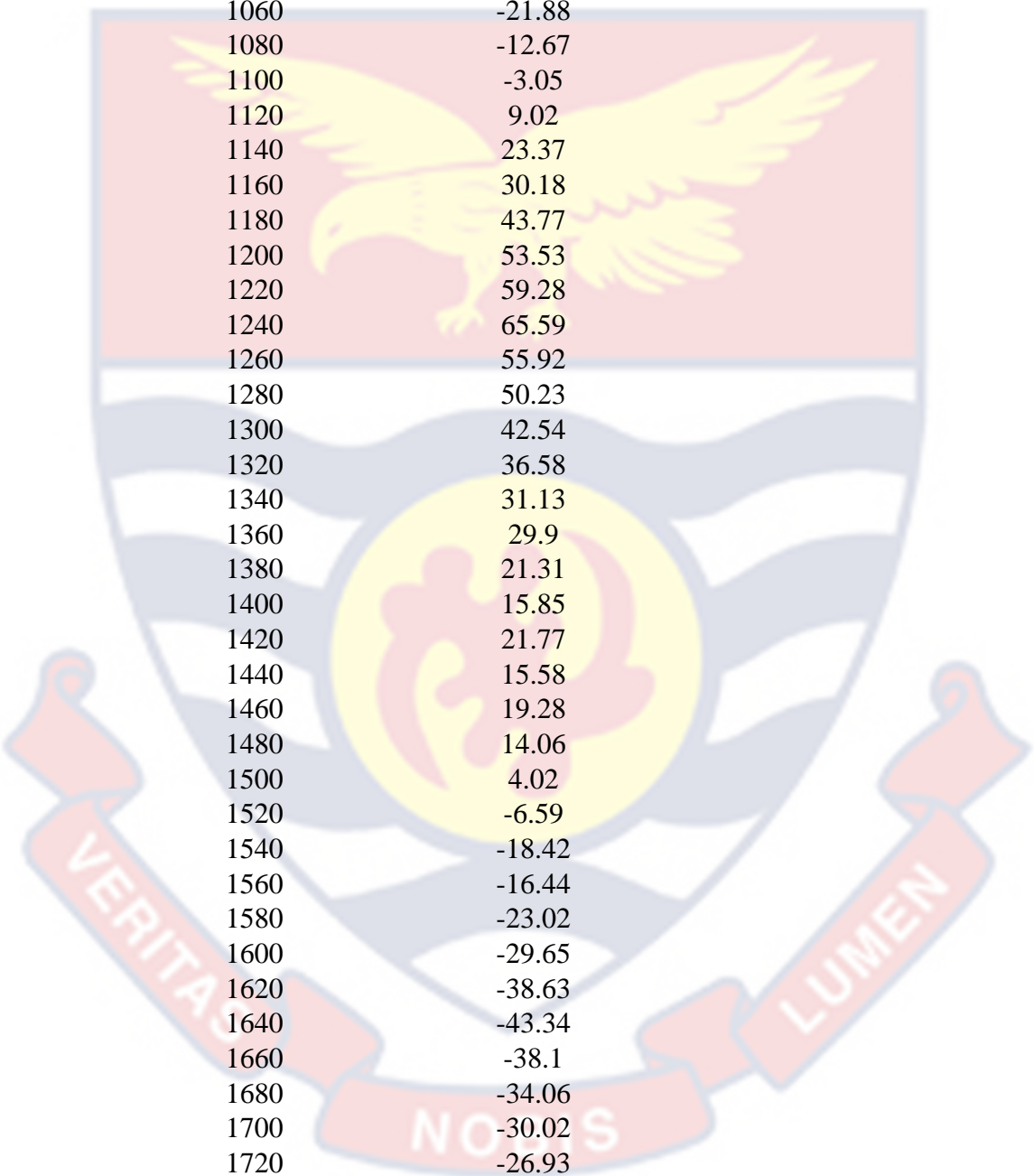
	FUVEME		
NAME	GRID EASTING (X) / m	GRID NORTHING (Y) / m	ELEVATION (Z) / m
UCC-1	462657.6028	122433.0568	4.1633
UCC-2	462567.0922	122467.5328	1.0189
UCC-3	462452.3534	122466.1045	3.2920
UCC-4	462341.4485	122501.5875	0.5683
UCC-5	462198.3654	122499.7307	4.4878
UCC-6	462062.1932	122528.4314	4.0860
UCC-7	461918.9334	122536.0281	4.3480
UCC-8	461667.0043	122485.3056	2.4803
UCC-9	461378.9983	122451.3604	4.9047
UCC-10	461194.8775	122498.5534	5.2759
UCC-11	461050.6523	122518.4386	5.0999
UCC-12	460945.6331	122531.4428	3.6825

135

Appendix B: NSM and EPR values for the period

Table B.1: NSM Values for Oct 2022- May 2022

Transect Cast Distance (TCD)	NSM
80	-35.3
100	-38.03
120	-43.73
140	-51.02
160	-43.15
180	-42.48
200	-41.69
220	-39.49
240	-40.75
260	-40.24
280	-45.56
300	-52.24
320	-53.62
340	-52.14
360	-56.58
380	-59.04
400	-60.48
420	-57.14
440	-50.81
460	-49.56
480	-50.08
500	-46.98
520	-46.03
540	-52.61
560	-54.88
580	-59.36
600	-62.2
620	-62.83
640	-67.03
660	-64.18
680	-66.55
700	-64.08
720	-67.67
740	-66.28
760	-65.73
780	-71.33
800	-77.15
820	-79.25
840	-81.72
860	-76.3
880	-68.35
900	-62.35

136
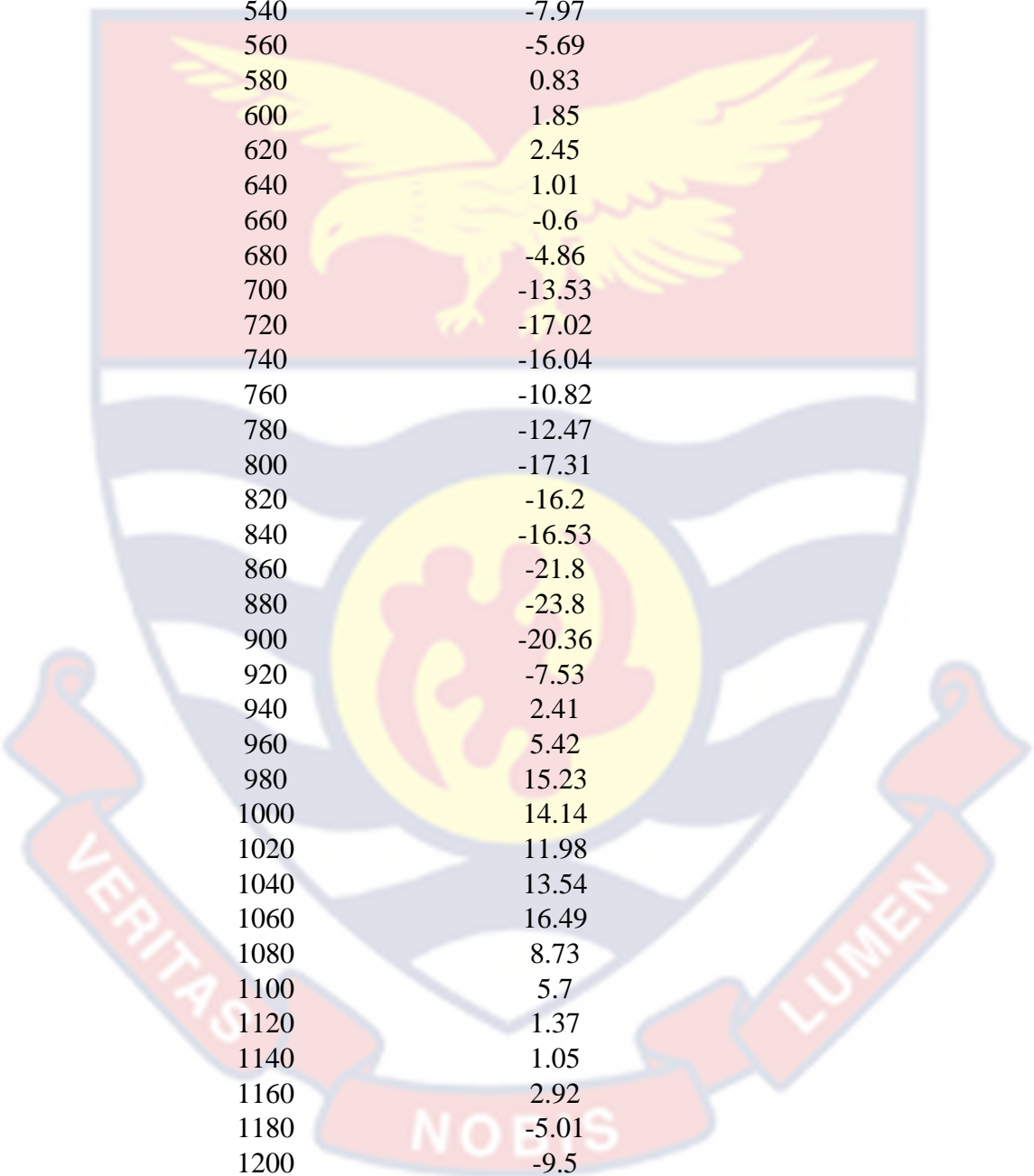
920	-61.83
940	-65.13
960	-64.85
980	-56.25
1000	-49.83
1020	-39.03
1040	-27.75
1060	-21.88
1080	-12.67
1100	-3.05
1120	9.02
1140	23.37
1160	30.18
1180	43.77
1200	53.53
1220	59.28
1240	65.59
1260	55.92
1280	50.23
1300	42.54
1320	36.58
1340	31.13
1360	29.9
1380	21.31
1400	15.85
1420	21.77
1440	15.58
1460	19.28
1480	14.06
1500	4.02
1520	-6.59
1540	-18.42
1560	-16.44
1580	-23.02
1600	-29.65
1620	-38.63
1640	-43.34
1660	-38.1
1680	-34.06
1700	-30.02
1720	-26.93
1740	-21.07
1760	-4.92
1780	-3.88
1800	-3.41
1820	-1.96
1840	7.07
1860	7.57

1880	5.96
1900	11.67
1920	18.47
1940	24.59
1960	14.66
1980	6.72
2000	1.32
2020	3.37
2040	-0.91
2060	-7.58
2080	-8.36
2100	-11.4
2120	-13.01
2140	-11.74
2160	-20.65
2180	-14.35
2200	-17.98
2220	-23.68
2240	-16.53
2260	-19.98
2280	-19.95
2300	-24.3
2320	-15.55
2340	-23.15
2360	-21.57

NSM VALUES FOR JULY – OCT 2022

Table B.2: NSM values for July 2022 – Oct 2022

TCD	NSM
80	-10.67
100	-15
120	-18.73
140	-14.81
160	-14.2
180	-12.18
200	-6.28
220	-4.85
240	-4.77
260	-3.99
280	-3.12
300	-1.94
320	-6.76
340	-7.98
360	-0.16
380	-4.92

138

400	-4.5
420	-4.2
440	-2.75
460	-1.76
480	-0.62
500	-1.3
520	0.63
540	-7.97
560	-5.69
580	0.83
600	1.85
620	2.45
640	1.01
660	-0.6
680	-4.86
700	-13.53
720	-17.02
740	-16.04
760	-10.82
780	-12.47
800	-17.31
820	-16.2
840	-16.53
860	-21.8
880	-23.8
900	-20.36
920	-7.53
940	2.41
960	5.42
980	15.23
1000	14.14
1020	11.98
1040	13.54
1060	16.49
1080	8.73
1100	5.7
1120	1.37
1140	1.05
1160	2.92
1180	-5.01
1200	-9.5
1220	-5.78
1240	-0.32
1260	8.71
1280	3.1
1300	15.98
1320	20.37
1340	27.16

139
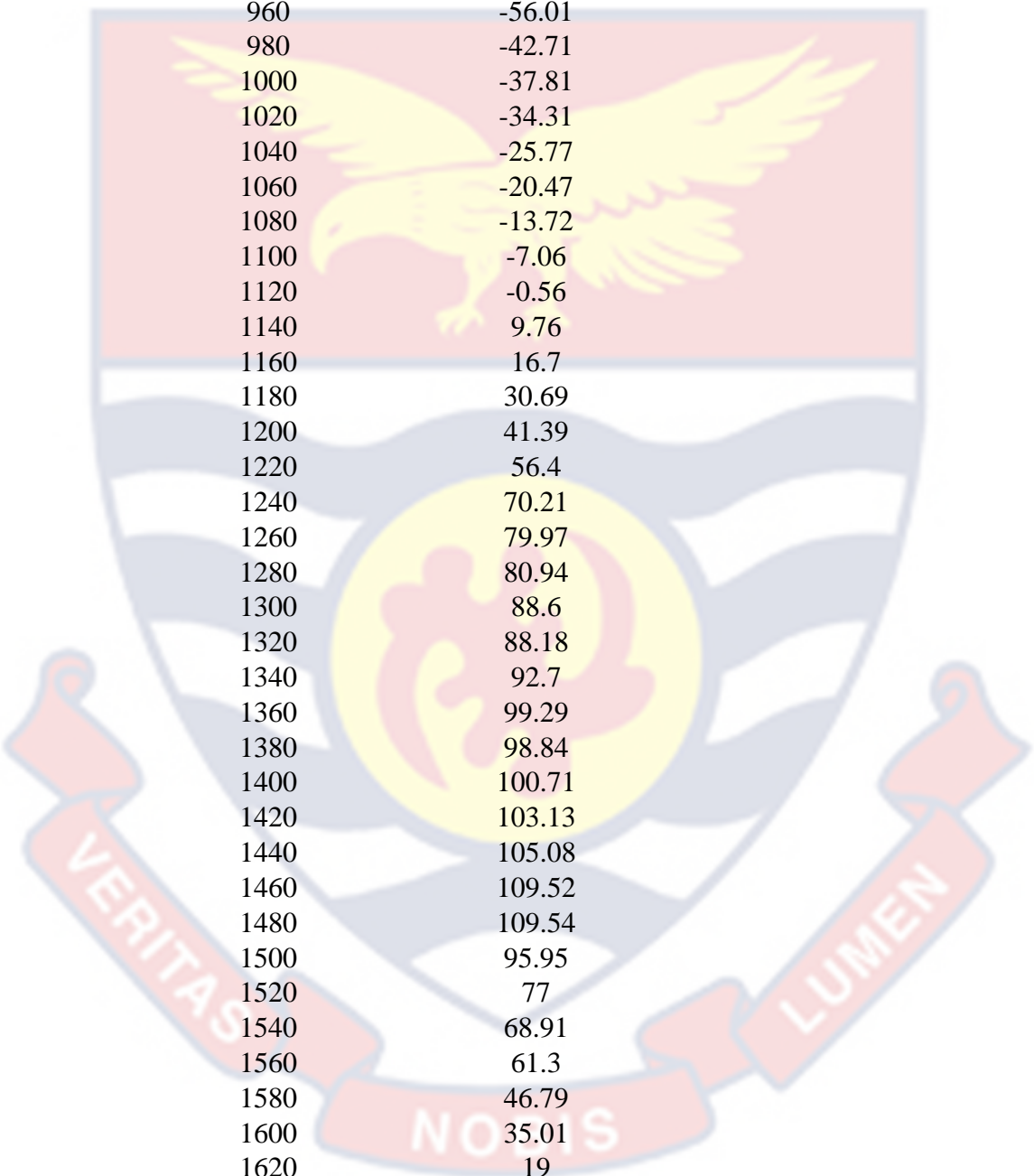
1360	40.55
1380	41.07
1400	51.51
1420	48.59
1440	60.97
1460	56.74
1480	73.12
1500	65.83
1520	75.46
1540	68.87
1560	74.88
1580	59.72
1600	61.48
1620	58.29
1640	48.37
1660	50.69
1680	43.99
1700	38.83
1720	33.03
1740	24.62
1760	24.99
1780	10.72
1800	11.15
1820	10.49
1840	7.03
1860	2
1880	3.01
1900	2.99
1920	6.93
1940	6.58
1960	-2.91
1980	-9.52
2000	-10.45
2020	-18.73
2040	-22.4
2060	-19.63
2080	-23.18
2100	-37.75
2120	-53.02
2140	-49.69
2160	-56.29
2180	-11.78
2200	-1.5
2220	-3.91
2240	6.59
2260	-10.3
2280	-2.69
2300	1.34

140

TCD	NSM
2320	3.94
2340	10.29
2360	16.15

NSM FOR OCT 2021 – OCT 2022

Table B:3 NSM values for October 2021 -October 2022

TCD	NSM
80	-61.8
100	-62.24
120	-70.65
140	-68.79
160	-63.64
180	-60.71
200	-58.16
220	-54.65
240	-55.86
260	-50.81
280	-50.78
300	-52.16
320	-57.33
340	-58.67
360	-61.61
380	-66.02
400	-69.94
420	-68.59
440	-66.04
460	-60.34
480	-59.31
500	-61.58
520	-60.04
540	-65.86
560	-68.84
580	-68.15
600	-69.86
620	-72.49
640	-78.46
660	-80.42
680	-81.51
700	-88.46
720	-90.96
740	-91.52
760	-87.84
780	-89.87
800	-90.52

141

820	-88.71
840	-87.37
860	-84.27
880	-76.95
900	-69.72
920	-63.75
940	-59.56
960	-56.01
980	-42.71
1000	-37.81
1020	-34.31
1040	-25.77
1060	-20.47
1080	-13.72
1100	-7.06
1120	-0.56
1140	9.76
1160	16.7
1180	30.69
1200	41.39
1220	56.4
1240	70.21
1260	79.97
1280	80.94
1300	88.6
1320	88.18
1340	92.7
1360	99.29
1380	98.84
1400	100.71
1420	103.13
1440	105.08
1460	109.52
1480	109.54
1500	95.95
1520	77
1540	68.91
1560	61.3
1580	46.79
1600	35.01
1620	19
1640	6.11
1660	5.94
1680	0.8
1700	0.03
1720	-3.96
1740	-8.64

1760	-2.27
1780	-12.67
1800	-6.17
1820	-5.26
1840	-3.55
1860	-2.15
1880	-5.77
1900	-5.94
1920	1.19
1940	11.03
1960	-3.58
1980	-14.46
2000	-16.63
2020	-22.05
2040	-28.52
2060	-28.65
2080	-30.17
2100	-47.42
2120	-60.72
2140	-65.06
2160	-63.45
2180	-30.03
2200	-22.31
2220	-20.14
2240	-18.71
2260	-24.98
2280	-17.52
2300	-20.55
2320	-4.12
2340	-11.16
2360	-1.31

EPR FOR OCT 2021 – OCT 2022

Table B.3: EPR values for October 2021 – October 2022

TCD	EPR
80	-64.45
100	-64.91
120	-73.67
140	-71.74
160	-66.36
180	-63.31

143

200	-60.65
220	-56.99
240	-58.26
260	-52.99
280	-52.96
300	-54.39
320	-59.79
340	-61.18
360	-64.25
380	-68.85
400	-72.94
420	-71.53
440	-68.87
460	-62.92
480	-61.85
500	-64.22
520	-62.61
540	-68.68
560	-71.79
580	-71.07
600	-72.85
620	-75.6
640	-81.83
660	-83.86
680	-85.01
700	-92.25
720	-94.86
740	-95.44
760	-91.6

144

780	-93.72
800	-94.39
820	-92.51
840	-91.11
860	-87.88
880	-80.24
900	-72.71
920	-66.48
940	-62.11
960	-58.41
980	-44.54
1000	-39.43
1020	-35.78
1040	-26.87
1060	-21.35
1080	-14.3
1100	-7.36
1120	-0.58
1140	10.17
1160	17.41
1180	32
1200	43.16
1220	58.81
1240	73.22
1260	83.39
1280	84.4
1300	92.4
1320	91.95
1340	96.67

1360	103.55
1380	103.08
1400	105.02
1420	107.55
1440	109.58
1460	114.22
1480	114.23
1500	100.06
1520	80.3
1540	71.86
1560	63.93
1580	48.79
1600	36.51
1620	19.81
1640	6.37
1660	6.2
1680	0.83
1700	0.03
1720	-4.13
1740	-9.01
1760	-2.36
1780	-13.22
1800	-6.43
1820	-5.49
1840	-3.7
1860	-2.25
1880	-6.02
1900	-6.2
1920	1.24

1940	11.5
1960	-3.74
1980	-15.08
2000	-17.35
2020	-23
2040	-29.74
2060	-29.88
2080	-31.46
2100	-49.45
2120	-63.32
2140	-67.84
2160	-66.16
2180	-31.31
2200	-23.26
2220	-21
2240	-19.51
2260	-26.05
2280	-18.27
2300	-21.43
2320	-4.29
2340	-11.63
2360	-1.37

147

Appendix C: Ground Control Point Markers
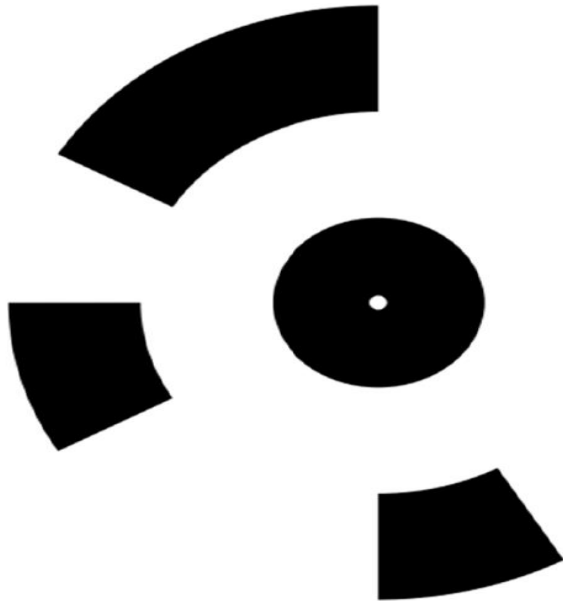
A Printed GCP Platform Sample

A GCP platform on a GCP before drone flight

148

Appendix D: Pictures taken on the field

Crossing the Volta River to Fuveme

Deploying the HOBO water logger

Beach Profile using a Dumpy Level

Bathymetry survey at Fuveme

Concrete GCPs before planting

Godfred taking some drone shots

149